Studies on Seismic Response of Buried Pipelines Induced by Soil Liquefaction(Dissertation_全文)

AUTHOR(S):

Miyajima, Masakatsu

STUDIES ON SEISMIC RESPONSE OF BURIED PIPELINES INDUCED BY SOIL LIQUEFACTION

by

Masakatsu MIYAJIMA

STUDIES ON SEISMIC RESPONSE OF BURIED PIPELINES INDUCED BY SOIL LIQUEFACTION

by

Masakatsu MIYAJIMA

SUMMARY

This dissertation is devoted to development of effective methods to analyze the response of pipelines subjected to soil liquefaction and to predict the subsequent failure of the pipelines.

Statistical analysis is conducted using actual earthquake damage data, in the 1964 Niigata Earthquake and in the 1983 Nihonkai-Chubu Earthquake, for water supply pipelines in order to clarify failure modes of buried pipelines. Based on the results obtained from the statistical analysis, model experiments, mathematical analysis and simulation are conducted. In the vibration tests, pipe strain are classified according to the mechanism of generation: i.e. vibration strains which indicate pipe vibration, and accumulated residual strains which indicate pipe bending due to uplift during liquefaction. A conceptional model of the generation factors of vibration strains is proposed. Moreover, vibration tests are conducted under several conditions, that is, experiments using a model, simulating a pipeline connected to a building and a model pipeline located through both liquefiable and non-liquefiable sandy ground.

A hybrid procedure is proposed to analyze the behavior of buried pipelines during the liquefaction process. This procedure consists of a ground response evaluation using the finite element method and a pipe response analysis using the transfer matrix method. Furthermore formulae for pipeline response due to buoyancy effects, subsidence, seismic motion in the liquefied ground, which are different from that of the neighboring ground, and liquefaction-induced permanent ground displacement are proposed and mathematical analyses for existing pipelines and ground are conducted.

ACKNOWLEDGEMENTS

The author wishes to express his sincere gratitude to Professor Kenzo Toki of the Disaster Prevention Research Institute of Kyoto University for guidance and encouragement on completing this dissertation and also for his critical reading of the manuscript. Special appreciation is extended to Professor Masaru Kitaura of Kanazawa University for his heartily support and constant encouragement during the course of this study. I am deeply indebted to Professor Toru Shibata of the Disaster Prevention Research Institute of Kyoto University for his critical reading of the manuscript and constructive criticism. Professor Tameo Kobori of Kanazawa University is acknowledged for his valuable suggestions and encouragement. Professor Hideyuki Kameda of the Urban Earthquake Hazard Research Center of Kyoto University and Professor Shiro Takada of Kobe University is also acknowledged for his helpful advise and constructive criticism. The author further wishes to thank his colleagues of Professor Kitaura's laboratory for their profitable discussions and general support.

TABLE OF CONTENTS

1. INTRODUCTION

1.1 General Remarks

Lifeline systems are networks which cover wide areas; having sources, transmission lines, storage facilities and distribution systems within themselves. These various components have different resistances to seismic disturbances and they are subjected to a variety of geotechnical hazards during earthquakes. Damage is often sustained by certain portions of a lifeline system leading to extensive loss of serviceability of the entire system, thus effective functional reliability of the total system as a network is required. Lifeline earthquake engineering, namely engineering concerned with earthquake damage to these systems, has rapidly increased since the mid-1970's. Such damage to lifeline systems has become increasingly more important in proportion to the level of urbanization in today's modern cities because of their heavy dependency on these systems. Numerous studies have been done to develop a methodology for assessment of reliability and serviceability of lifeline systems in a wide variety of conditions [1)-9)].

Great effort has been directed to clarification of response characteristics and causes of failure of the lifeline components during earthquakes in recent years [10)-18)]. It is well known that the reaction to seismic changes by underground pipelines is quite different from that of above ground structures. Seismic damage to pipelines is mainly caused by relative displacement induced by seismic waves and great changes in the composition of the soil itself, and the effect of inertia force is negligible, this force, though, is usually the most important factor for the aseismic design of above ground structures. The results of the massive amount of this research have been used effectively in the seismic design standards for gas supply pipelines in Japan [19)]. However, the present building code does not regulate the design taking into account soil malfunction such as soil liquefaction, landslides, etc. The lack of regulations is entirely due to an insufficient amount of research directed specifically to this topic. There is a certain amount of

work which deals with the reliability and risk analyses of lifeline systems, but the value of these efforts is reduced by the lack of experimental and analytical data regarding failure of pipelines caused by drastic changes in the soil conditions. There are several major problems to be solved before earthquake resistant system can be designed.

1.2 A Brief Review of Studies on Seismic Response of Pipelines

Lifeline systems have been frequently damaged. Since the 1923 Kanto Earthquake, a survey of earthquake damage to lifeline systems has been carried out by several organizations such as the Japan Society of Civil Engineers in almost all subsequent earthquakes. Some statistical approaches have been attempted to clarify the actual causes of failure of lifeline structures using actual data from each quake [20)-23)]. At the same time, field observations have continued in order to obtain response characteristics during actual earthquakes [24)-27)]. It is well known from the results of these works that causes of pipeline damage are roughly classified as either: seismic wave propagation or soil characteristics changes or a combination of the two.

The effects of seismic wave propagation have been assiduously studied. Field observations mentioned above focused on this cause. Most of the theoretical research has treated continuous or jointed pipelines both with straight configurations at the first stage [28)-37)]. The results generally agree on the following: (1) Pipe failures are dominated by the strain on the ground itself. (2) The axial strain of the pipe is predominant in comparison with the bending strain. (3) Slippage between a pipe and the surrounding soil makes the pipe strain less than the free field strain of the ground. (4) The mass effect of the pipe is negligible. Furthermore, some works have dealt with pipelines with a bend, a T-shaped portion or many branched pipes and have discussed the stress concentration in those portions in recent years [38)-40)].

Soil malfunctions are roughly classified into four categories: surface faulting, subsidence, slope instability and liquefaction. Effects

of the surface faulting have been investigated in the U.S.A. [41)-44)]. The conclusion reached is that the angle of the pipeline-fault intersection is the most critical factor affecting the pipeline behavior. Therefore, when siting a pipeline in a known faulting zone, the orientation of the pipeline with respect to the fault should be determined on the basis of the anticipated movement patterns.

Subsidence of the ground is considered to be one of the most important problems. Many buried pipelines have been damaged by the subsidence of the ground due to liquefaction and so on in past earthquakes. Experiments using a sinking sand box and analytical works using a beam theory on an elastic foundation have been carried out [45)-47)]. Moreover, design formulae and basic countermeasures of buried pipelines subjected to large ground settlement have been proposed [46)-48)]. The liquefaction-induced ground settlement is included in the category of the massive ground displacement induced by liquefaction as mentioned below.

For non-liquefaction slope instability failures, a reasonable accurate estimate of the amount of movement likely to occur during an earthquake is possible. However, not much work has been done focusing on this phenomenon. Since landslides involve many of the same deformation patterns associated with surface faulting, it is considered that pipeline behavior subjected to landslide has been investigated in the field of surface faulting.

Liquefaction is one of the most serious geotechnical hazards, particularly in Japan. Liquefaction caused heavy damage to the various types of lifeline structures during earthquakes, for example, the 1964 Niigata Earthquake in Japan, the 1971 San Fernando Earthquake in the U.S.A., the 1983 Nihonkai-Chubu Earthquake in Japan, etc. Effects of liquefaction are classified into three types as follows:

1. Loss of bearing capacity and buoyancy
2. Large dynamic response of the ground
3. Large ground displacement

The buoyancy effect is likely to be most severe at the boundary between pipelines and buildings, abutments, manholes, etc. From this point of view, some experimental research has been done. Kitaura and Miyajima focused on the pipeline-building system [49)]. Takada and Tanabe et al. [50)] and Kuribayashi and Kawamura et al. [51)] observed

pipeline-manhole systems. Sasaki and Taniguchi et al. investigated the uplift of a road which was partially buried [52]. In addition, Kennedy and Darrow et al. roughly estimated pipe displacement due to buoyancy force; solving the equation of motion of the buried pipe consisting of pipe mass inertia force, buoyancy force and drag force [53]. Furthermore, some basic countermeasures for uplift of the lifeline structures have been proposed based on the results of these works [49)-52].

Several model experiments have been carried out on the dynamic behavior of buried pipelines in liquefaction processes. The researcher concluded that the peak strain of the pipelines was caused when the liquefaction phenomena began to occur [54-55]. Moreover, the peak strain of the pipeline in an incompletely liquefied ground is greater than that present in one that is completely liquefaction [56]. Furthermore, Kitaura and Miyajima [57], [58] and Takada and Tanabe [59] proposed theoretical models. Yeh and Wang [60] and Nishio and Tsukamoto et al.[61] focused on the seismic responses of pipelines in partially liquefied ground.

Massive ground displacement induced by liquefaction is one of the most serious liquefaction hazards. Permanent ground displacement during the 1964 Niigata Earthquake, the 1971 San Fernando Earthquake and the 1983 Nihonkai-Chubu Earthquake was measured in recent years [62], [63]. Kitaura and Miyajima carried out theoretical and analytical works on pipeline damage due to permanent ground displacement [64)-67].

1.3 An Outline of the Present Dissertation

This dissertation deals with some aspects of damage to water supply pipelines due to soil liquefaction in an effort to identify some failure mechanisms and to recommend a standard for earthquake resistant design of these systems. The first chapter of this study introduces and reviews the studies on seismic response of pipelines.

Chapter 2 describes analysis of real earthquake damage to water supply pipelines using a statistical method. The relationship between ground conditions and earthquake damage to pipeline is investigated.

Particularly, influences of liquefaction and liquefaction-induced permanent ground displacement are discussed. Moreover, using a multivariate analytic approach, the most influential factor leading to pipe damage is demonstrated.

In Chapter 3, model experiments are carried out in order to clarify dynamic characteristics of pipelines during liquefaction, especially the pipe response in incompletely liquefied ground is observed. Furthermore, generation factors of vibration strains are proposed and a conceptual model of strain-occurrence in liquefaction processes is discussed.

Chapter 4 focuses on a dynamic analysis of pipelines in liquefaction processes. A hybrid procedure is proposed, which consists of a ground response evaluation using the finite element method and a pipe response analysis using the transfer matrix method. A change in response characteristics of pipelines in the liquefaction process is presented by some practical examples.

Chapter 5 deals with pipe behavior through a boundary between liquefied and non-liquefied areas. Both experimental and analytical approaches are utilized to clarify mechanisms of failure to pipelines buried at those areas. The effects of the extent of the liquefied ground and equivalent soil spring constant of the liquefied ground on pipe failure are discussed.

Chapter 6 takes up the problem of permanent ground displacement induced by liquefaction. The characteristics of liquefaction-induced permanent ground displacement are investigated through a survey of earthquake damage data and model experiments. The method for evaluation of pipeline response is proposed and pipeline failure due to permanent ground displacement is discussed based on the results of practical examples.

Finally, the results of these chapters are consolidated in Chapter 7 and recommendations are given for earthquake-resistant design of water pipeline systems along with some proposal for future studies.

References (Publications written in Japanese are so indicated; all other are in English)

1) Tamura, C. and Kawakami, E.: Seismic Risk Analysis of Underground Lifeline Systems by Use of Monte Carlo Method, Proceedings of Japan Soc. Civil Eng., No. 311, pp.37-48, 1981 (in Japanese).
2) Tan, R. and Shinozuka, M. : Optimization of Underground Water Transmission Network Systems under Seismic Risk, Soil Dynamics and Earthquake Engineering, Vol. 1, No. 1, pp. 30-38, 1982.
3) Shinozuka, M., Kameda, H. and Koike, T.: Ground Strain Estimation for Seismic Risk Analysis of Underground Lifelines, Proceedings of ASCE, Vol. 109, No. EM1, pp. 175-191, 1983.
4) Moghtaderizadeh, M., Wood, R. K., Kiureghian, A. D. and Barlow, R. E.: Seismic Reliability of Lifeline Networks, Proceedings of ASCE, Vol. 108, No. TC1, pp. 60-78, 1982.
5) Isoyama, R. and Katayama, T.: Reliability Evaluation Method of Large-scale Water Supply Networks During Seismic Disaster, Proceedings of Japan Soc. Civil Eng., No. 321, pp. 37-48, 1982 (in Japanese).
6) Kameda, H., Goto, H. and Kasuga, T.: System Reliability and Serviceability of Water Supply Pipelines under Seismic Environment, Proceedings of the 8th World Conference on Earthquake Engineering, Vol. 7, pp. 491-498, 1984.
7) Sato, T.: Seismic Reliability Analysis of Lifeline Networks Taking into Account Fault Extent and Local Ground Conditions, Journal of Natural Disaster Science, Vol. 6, No. 2, pp. 51-72, 1984.
8) Noda, S., Yamada, Y. and Iemura, H.: Restoration of Serviceability of a Pipeline System, Proceedings of the 2nd Specialty Conference of the Technical Council on Lifeline Earthquake Engineering, pp. 225-240, 1981.
9) Kitaura, M., Yamazaki, F. and Shinozuka, M. : Seismic Reliability Analysis of Underground Pipeline Network Systems, Proceedings of the 4th International Conference on Structural Safety and Reliability, Vol. 2, pp. 247-256, 1985.

10) Proceedings of Technical Council on Lifeline Earthquake Engineering Specialty Conference, ASCE, 1977.
11) Social and Economic Impact of Earthquakes on Utility Lifelines, Proceedings of Construction Division Specialty Conference, ASCE, 1980.
12) Proceedings of the Second Specialty Conference of the Technical Council on Lifeline Earthquake Engineering, ASCE, 1981.
13) Proceedings of 1983 International Symposium on Lifeline Earthquake Engineering, PVP-Vol. 77, ASME, 1983.
14) Advisory Notes on Lifeline Earthquake Engineering, ASCE, 1983.
15) Proceedings of the US-JAPAN Workshop on Seismic Behavior of Buried Pipelines and Telecommunications Systems, Edited by Shinozuka, M. and Iwasaki, T, 1984.
16) Proceedings of the Trilateral Seminar-Workshop on Lifeline Earthquake Engineering, Edited by Ang, A. H. S., Katayama, T. and Tan R. Y., 1985.
17) Recent Advance in Lifeline Earthquake Engineering, Computational Mechanics Publications, 1987.
18) Proceedings of the 1989 ASME Pressure Vessels and Piping Conference, ASME, 1989.
19) Japan Gas Association: Recommended Standards for Earthquake Resistant Design of Gas Pipelines, 1982 (in Japanese).
20) Kubo, K., Katayama, T. and Sato, N.: Quantitative Analysis of Seismic Damage to Buried Pipelines, Proceedings of the 3rd Japan Earthquake Engineering Symposium-1975, pp. 655-661, 1975.
21) Matsuo, M. and Horiuchi, T.: Earthquake Damage and Methodology of Design of Small Diameter Pipelines, Soils and Foundations, Japan Soc. of Soil Mecha. and Founda. Eng., Vol. 19, No. 1, pp. 23-38, 1979.
22) Ichihara, M. and Yamada, K.: Relative Degree of Risk of Water-Supply Pipes in Nagoya City During Earthquake, Proceedings of Japan Soc. Civil Eng., No. 316, pp. 51-63, 1981 (in Japanese).
23) Kitaura, M. and Miyajima, M. : Quantitative Evaluation of Damage to Buried Pipelines Induced by Soil Liquefaction, Proceedings of the 9th World Conference on Earthquake Engineering, Vol. 7, pp. 11-16, 1989.

24) Sakurai, A. and Takahashi, T.: Dynamic Stresses of Underground Pipelines During Earthquakes, Proceedings of the 4th World Conference on Earthquake Engineering, Vol. 2, pp. 81-95, 1969.
25) Nakamura, M., Katayama, T. and Kubo, K.: Quantitative Study on Observed Seismic Strains in Underground Structures, Proceedings of Japan Soc. Civil Eng., No. 320, pp. 35-45, 1982 (in Japanese).
26) Oishi, H. and Sekiguchi, K.: Earthquake Observation of an Underground Pipeline and Seismic Response Analysis, Proceedings of the 8th World Conference on Earthquake Engineering, Vol. 5, pp. 295-302, 1984.
27) Nishio, N.: Mechanism of Seismic Strain in Buried Pipelines Based on Field Observations and Model Experiments, Proceedings of the 5th Canadian Conference on Earthquake Engineering, pp. 637-644, 1987.
28) Goto, H., Toki, K. and Takada, S.: A Few Studies on the Vibrational Characteristics of Underground Pipe, Proceedings of Japan Soc. Civil Eng., No. 209, pp. 15-25, 1973 (in Japanese).
29) Takada, S.: Earthquake Response Characteristics of Buried Pipe Structures, Doctoral Dissertation submitted to Kyoto University, 1974 (in Japanese).
30) Anderson, J. C. and Singh, A. K.: Seismic Response of Pipelines of Friction Supports, Proceedings of ASCE, Vol. 102, No. EM2, pp. 275-291, 1975.
31) Ugai, K. : Dynamic Analysis of Underground Pipelines under the Condition of Axial Sliding, Proceedings of Japan Soc. Civil Eng., No. 272, pp. 27-37, 1978 (in Japanese).
32) Hindy, A. and Novak, M.: Pipeline Response to Random Ground Motion, Proceedings of ASCE, Vol. 106, No. EM2, pp. 339-360, 1980.
33) Kameda, H. and Shinozuka, M. : Simplified Formula for Axial Strains of Buried Pipes Induced by Propagating Seismic Waves, Memoirs of the Faculty of Engineering, Kyoto University, Vol. 44, Part 2, pp. 287-308, 1982.
34) Akiyoshi, T. and Fuchita, K.: Effect of Slippage on the Seismic Response on Buried Pipes, Proceedings of Japan Soc. Civil Eng., No. 334, pp. 25-34, 1983 (in Japanese).

35) Toki, K., Fukumori, Y. and Sato, T.: Recommended Practice for Earthquake Resistant Design of High Pressure Gas Pipelines, Proceedings of the 4th National Congress on PVP, ASME, pp. 349-356, 1983.
36) Koike, T.: Estimation of Buried Pipe Strains under Seismic Risk, Proceedings of Japan Soc. Civil Eng., No. 331, pp. 13-24, 1983 (in Japanese).
37) Sato, H. and Ishikawa, N.: Elastic-plastic Analysis of Buried Pipelines under Axial Ground Deformation, Proceedings of Japan Soc. Civil Eng., No. 338, pp. 39-48, 1983 (in Japanese).
38) Isenberg, J., Weidlinger, P., Wright, J. P. and Baron, M. L.: Underground Pipelines in a Seismic Environment, Proceedings of the Technical Council on Lifeline Earthquake Engineering, ASCE, pp. 267-281, 1977.
39) Takada, S., Tsubakimoto, T. and Hori, K.: Earthquake Response Simulations of T-shaped Portion in Ductile-Iron Pipelines and Developed of Earthquake Resistant Hot Branch Sleeve, Proceedings of 1983 International Symposium on Lifeline Earthquake Engineering, PVP-Vol. 77, ASME, pp. 357-364, 1983.
40) Takada, S., Tanabe, K. and Horinouchi, N.: Seismic Response Analyses of Buried Pipelines with Many Branch Pipes, Proceedings of the National Congress on PVP, ASME, pp. 401-406, 1987.
41) Kennedy, R. P., Chow, A. W. and Williamson, R. A.: Fault Movement Effects on Buried Oil Pipeline, Proceedings of ASCE, Vol. 103, No. TE5, pp. 617-633, 1977.
42) O'Rourke, T. D. and Trautman, C. H.: Earthquake Ground Rupture Effects on Jointed Pipe, Proceedings of the 2nd Specialty Conference of the Technical Council on Lifeline Earthquake Engineering, pp. 65-80, 1981.
43) McCaffrey, M. A. and O'Rourke, T. D.: Buried Pipeline Response to Reverse Faulting During the 1971 San Fernando Earthquake, Proceedings of 1983 International Symposium on Lifeline Earthquake Engineering, PVP-Vol. 77, ASME, pp. 151-159, 1983.
44) Ariman, T.: Buckling and Rupture Failures of Pipelines Due to Large Ground Deformations, Proceedings of the 8th World Conference on Earthquake Engineering, Vol. 8, pp. 271-278, 1984.

45) Takada, S. and Yamabe, Y.: An Experiment on a Seismic Behavior of Buried Pipelines Subjected to Large Ground Deformations Using the Sinking-soil-box, Proceedings of Japan Soc. Civil Eng., No. 323, pp. 55- 65, 1982 (in Japanese).
46) Oishi, H.: Considerations on Behaviour of Underground Pipelines Caused by Ground Settlement, Proceedings of Japan Soc. Civil Eng., No. 356, pp. 379- 386, 1985 (in Japanese).
47) Takada, S., Tanabe, K., Hazama, Y. and Irioka, H. : An experiment of Manhole-Fitting Pipes Subject to Large Ground Settlement and Development of Countermeasure Pipelines, Proceedings of Japan Soc. Civil Eng., No. 347, pp. 575-582, 1986.
48) Tanabe, K. and Takada, S.: Design Formulae of Buried Pipes Subjected to Large Ground Settlement and Its Application, Proceedings of Japan Soc. Civil Eng., No. 374, pp. 593-602, 1986 (in Japanese).
49) Kitaura, M. and Miyajima, M.: Dynamic Behaviour of a Model Pipe Fixed at One End During Liquefaction, Proceedings of Japan Soc. Civil Eng., No. 336, pp. 31-38, 1983 (in Japanese).
50) Takada, S., Tanabe, K., Yamajyo, K. and Katagiri, S. : Liquefaction Analysis for Buried Pipelines, Structure and Stochastic Methods, Developments in Geotechnical Engineering, Computational Mechanics Publications, Vol. 45, pp. 319-333, 1987.
51) Kuribayashi, E., Kawamura, M., Ieda, R., Aida, M. and Yuri, Y.: An Experimental Behavior of Buried Pipes During Liquefaction of Saturated Sandy Soil, Proceedings of the PVP Conference, ASME, Vol. 98-4, pp. 19- 24, 1985.
52) Sasaki, S. and Taniguchi, E. : Shaking Table Tests on Gravel Drains to Prevent Liquefaction of Sand Deposits, Soils and Foundations, Japan Soc. Soil Mecha. Founda. Eng., Vol. 22, No. 3, pp. 1-14, 1982.
53) Kennedy, R. P., Darrow, A. C. and Short, S. A.: General Considerations for Seismic Design of Oil Pipeline Systems, Proceedings Technical Council on Lifeline Earthquake Engineering Specialty Conference, pp. 2-17, 1977.
54) Katada, T. and Hakuno, M.: Experimental Analysis on Dynamic Behavior of Underground Structure in the Liquefaction Process,

Proceedings of Japan Soc. Civil Eng., No. 306, pp. 1-10, 1981 (in Japanese).
55) Kitaura, M. and Miyajima, M.: Experimental Study on Strain Characteristics of Underground Pipe During Liquefaction, Proceedings of Japan Soc. Civil Eng., No. 323, pp. 43-53, 1982 (in Japanese).
56) Kitaura, M. and Miyajima, M.: Dynamic Behavior of Buried Model Pipe During Incomplete Liquefaction, Journal of Structural Engineering, Japan Soc. Civil Eng., Vol. 31A, pp. 421-426, 1985 (in Japanese).
57) Kitaura, M. and Miyajima, M.: Analytical and Experimental Study on Behavior of Pipelines Subjected to Soil Liquefaction, Proceedings of the 2nd International Conference on Soil Dynamics and Earthquake Engineering, pp. 3.33-3.42, 1985.
58) Kitaura, M. and Miyajima, M. : Response Analysis of Buried Pipelines Considering Rise of Ground Water Table in Liquefaction Processes, Proceedings of Japan Soc. Civil Eng., No. 380, pp. 173-180, 1987.
59) Takada, S. and Tanabe, K.: Dynamic Behaviors of Underground Structures Subjected to Liquefaction, Proceedings of the 18th JSCE Earthquake Engineering Symposium-1985, pp. 233-236, 1985 (in Japanese).
60) Yeh, Y. H. and Wang, L. R. L.: Dynamic Response of Buried Pipelines in a Soil Liquefaction Environment During Earthquake, Proceedings of the 5th International Conference on Numerical Methods in Geomechanics, Vol. 3, pp. 1409-1423, 1985.
61) Nishio, N., Tsukamoto, K. and Hamura, A.: Model Experiment on the Seismic Behavior of Buried Pipeline in Partially Liquefied Ground, Proceedings of Japan Soc. Civil Eng., No. 380, pp. 449-465, 1987 (in Japanese).
62) O'Rourke, T. D. and Tawfik, M. S.: Effects of Lateral Spreading on Buried Pipelines During the 1971 San Fernando Earthquake, Proceedings of 1983 International Symposium on Lifeline Earthquake Engineering, PVP-Vol. 77, ASME, pp. 124-132, 1983.
63) Hamada, M., Yasuda, S., Isoyama, R. and Emoto, K. : Study on Liquefaction-Induced Permanent Ground Displacement and

Earthquake Damage, Proceedings of Japan Soc. Civil Eng., No. 376, pp. 221-229, 1986 (in Japanese).

64) Kitaura, M. and Miyajima, M.: Effects of Lateral Spreading Due to Soil Liquefaction on Buried Pipelines, Journal of Structural Engineering, Japan Soc. Civil Eng., Vol. 32A, pp. 857-864, 1986 (in Japanese).

65) Kitaura, M., Miyajima, M. and Nomura, Y: Study on Behavior of Buried Pipelines Due to Lateral Spreading Induced by Soil Liquefaction, Journal of Structural Engineering, Japan Soc. Civil Eng., Vol. 33A, pp. 679-686, 1987 (in Japanese).

66) Kitaura, M. and Miyajima, M.: Response of Buried Pipelines Due to Liquefaction-Induced Lateral Spreading, Proceedings of the Pacific Conference on Earthquake Engineering, pp. 123-130, 1987.

67) Miyajima, M., Kitaura, M. and Nomura, Y.: Study on Response of Buried Pipelines Subjected to Liquefaction-Induced Permanent Ground Displacement, Proceedings of Japan Soc. Civil Eng., No. 404, pp. 163-172, 1989.

2. EARTHQUAKE DAMAGE TO BURIED PIPELINES INDUCED BY SOIL LIQUEFACTION

2.1 General Remarks

Reports on a survey of earthquake damage to pipelines were presented by several organizations such as Japan Society of Civil Engineers in almost all earthquakes after the 1923 Kanto Earthquake [1)-4)]. However, there are not sufficient data available to investigate the damage to pipelines quantitatively because it has been considered to be more important to repair the damage than to survey the damage just after earthquake. Kubo and Katayama et al. indicated the relationship between pipeline damage and characteristics of the surface ground layer using a damage ratio of the pipelines which was defined as a number of damages divided by the total length of pipeline. The conclusion reached was that liquefaction was a very influential factor in pipe damage [5)]. Matsuo and Horiuchi conducted a factorial analysis associated with SPT blow count of ground, material and diameter of a pipe based on field investigation data of the 1964 Niigata Earthquake. The results indicated that the pipe damage was influenced by the pipe type and SPT blow count to a depth of 5 m [6)]. Ichihara and Yamada tried to establish a prediction model of pipeline damage due to an earthquake using a multivariate analysis, which is often referred to as the "Quantification Theory I" in Japan [7)]. These research efforts, however, did not focus on pipeline damage due to liquefaction.

The purposes of this chapter are to analyze earthquake damage to water supply pipelines quantitatively using a statistical method, and to clarify failure modes of buried pipelines. In Chapter 2.2, the relationship between pipeline damage and several influential factors is described using field investigation data in Niigata City during the 1964 Niigata Earthquake, and in Noshiro City during the 1983 Nihonkai-Chubu Earthquake. In Chapter 2.3, liquefaction effects, including a permanent ground displacement, are investigated. In this paper, a "damage" refers to one specific site of damage in a pipeline.

Therefore, "number of damages" refers to the number of sites of damage in the piping under discussion. The contents of this chapter are based on material in the references 8-10.

2.2 Characteristics of Earthquake Damage to Buried Pipelines

2.2.1 Data of Past Earthquake Damage

It is necessary to collect data on earthquake damage and to define characteristics of ground in advance of the analysis. However, old documents and reports on past earthquakes contain insufficient data and inadequate qualitative descriptions. Thus the author has collected soil profiles for areas containing buried pipelines, along with maps plotting sites of the pipe damage in Niigata City and Noshiro City [11].

Figs. 2.1 and 2.2 indicate maps of Niigata City and Noshiro City.

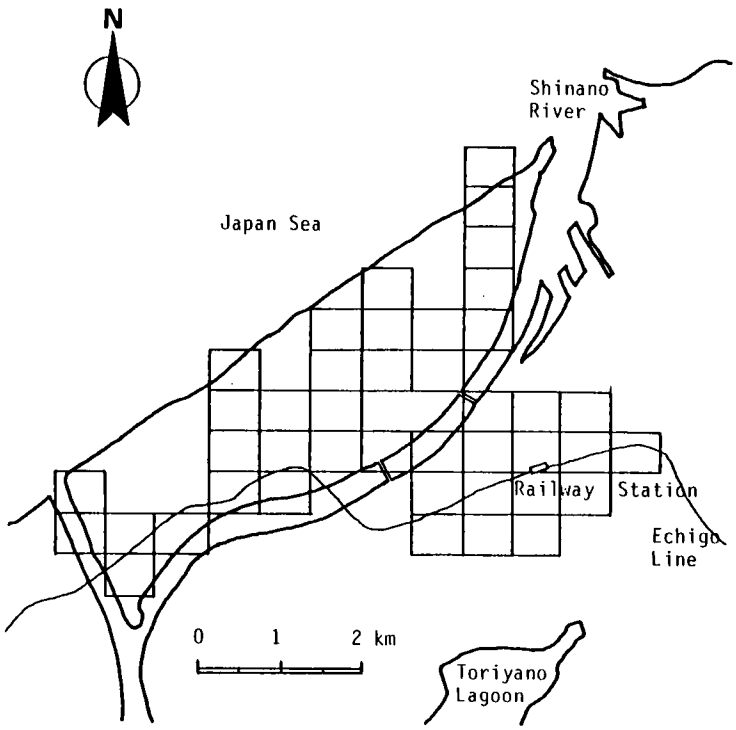

Fig. 2.1 Map of Niigata City with cells used in the analysis.

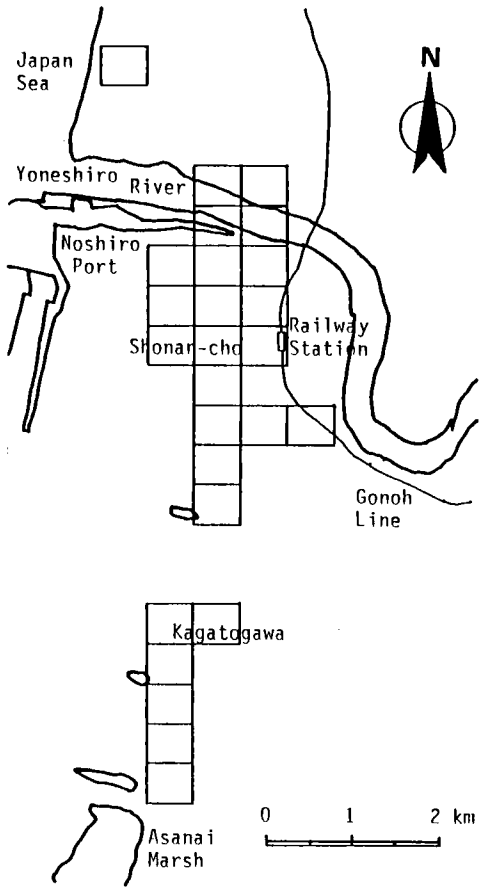

Fig. 2.2 Map of Noshiro City with cells used in the analysis.

Cells used in the present study are also shown in these figures. The smaller cell size is better to evaluate local characteristics of the ground and pipe damage. However, since pipe length in a cell decreases and a cell with no soil profiles increases with a decrease of the cell size, it is difficult to analyze the characteristics of the earthquake damage to the pipelines. In the present study, cell size is approximately 500 m x 500 m, one of 400 equal cells on a topographical map with a scale of 1:25,000 (Figs. 2.1 and 2.2).

2.2.2 Relationship between State of Ground and Earthquake Damage to Pipelines

The length of pipelines, and number of damages for each type and diameter of pipe were measured in each cell based on the pipe-

laying maps. Figs. 2.3 and 2.4 indicate the relationship between pipe diameter and damage ratio in Niigata City and Noshiro City, respectively. The damage ratio is defined as the number of pipe damages divided by the total length of a pipeline in the present study, following the method of Kubo and Katayama et al. [5]. The number of pipe damage includes damage to pipe body (breakage, bursting,

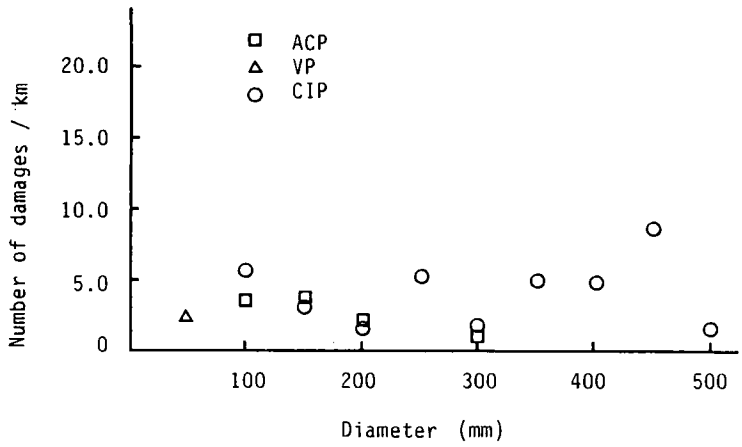

Fig. 2.3 Relationship among damage ratio of pipelines, diameter and pipe type (Niigata City).

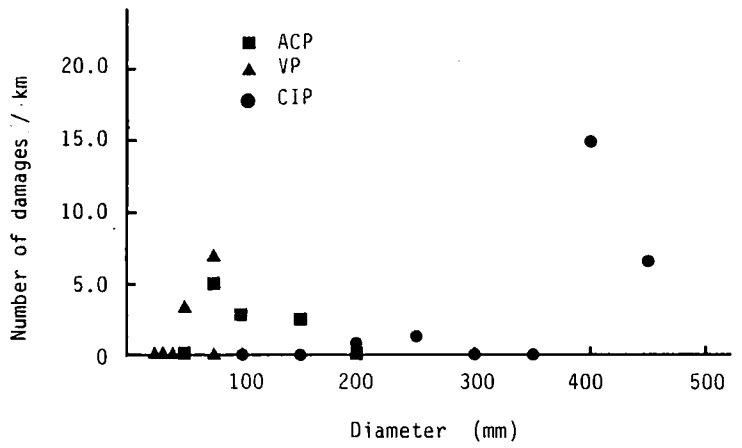

Fig. 2.4 Relationship among damage ratio of pipelines, diameter and pipe type (Noshiro City).

cracking and thrusting), and damage to joint (breakage, pull-out, and looseness). It can be seen from these figures that markedly high damage ratios are obtained for the cast iron pipe (CIP) with 400 mm and 450 mm diameters. Moreover, all of these damages occurred at joints and such damages were caused at liquefied areas near the boundary between the liquefied and non-liquefied areas according to the pipe-laying maps. The causes of those pipe damages could be explained in terms of complicated ground movements due to sharp change of the ground characteristics and buoyancy effect at the liquefied area. This will be discussed in Chapter 5 in detail. Given the fact that the pipes with the relatively small diameter of 50 mm to 150 mm were severely damaged, a great similarity can be seen in a comparison of past earthquake damage to the pipelines in which liquefaction was not present.

Fig. 2.5 shows the relationship between SPT blow count up to a depth of 5 m in Niigata City and Noshiro City, and damage ratio of pipelines during the Niigata Earthquake and during the Nihonkai-Chubu Earthquake, respectively. The damage ratios in this figure

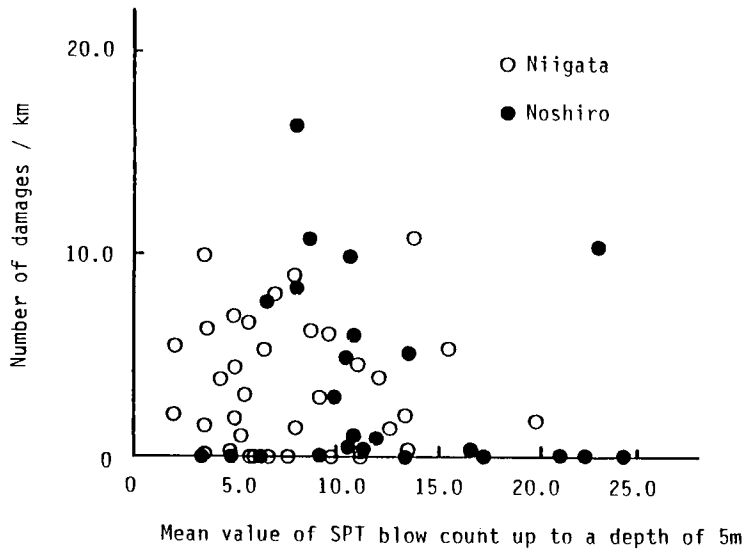

Fig. 2.5 Relationship between damage ratio of pipelines and mean value of SPT blow count up to a depth of 5 m.

indicate the average values in each cell. It can be seen from this figure that the high damage ratios appear at the sites with an SPT blow count lower than 15; however it is difficult to draw a clear conclusion, since the plots in the figure are somewhat scattered. Fig. 2.6 illustrates the relationship between the ground water table depth and damage ratio of the pipelines which were buried at a depth of about 1.5 m. This figure shows that the higher damage ratio appears at sites in which the ground water table is deeper than 1.5 m, that is, many pipe damages occurred at sites where the ground water table was lower than the buried pipelines. There appears to be several casual factors involved. One is permanent ground movement of superficial unsaturated sand layers, induced by the liquefaction of the deeper saturated sand layers below the buried pipelines. Another is the spreading of a liquefaction area from deep saturated layers to shallow unsaturated sand layers. The former will be discussed further in Chapter 6 and the latter will be studied in Chapter 4.

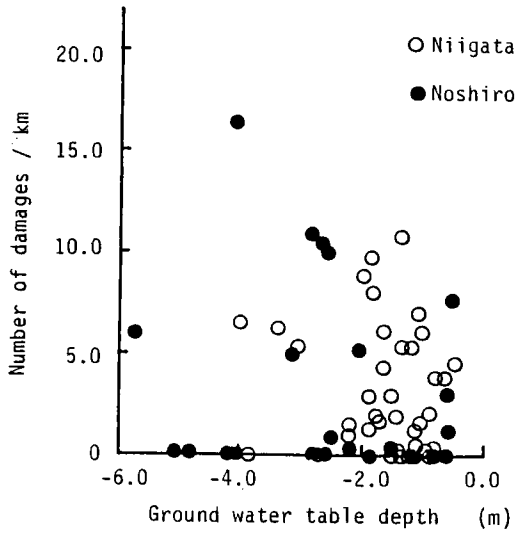

Fig. 2.6 Relationship between damage ratio of pipelines and ground water table.

As mentioned above, the correlation between the damage ratio and factors regarding ground characteristics such as SPT blow count and ground water table is not clear. It suggests that the damage of the pipelines is affected by various interrelated factors of ground characteristics. In the next section, a multivariate analysis is conducted in order to investigate the relationship between the pipe variety and ground characteristics on pipeline damage.

2.2.3 Multivariate Analysis

The relative degree of influence of pipe and ground on pipeline damages is quantitatively investigated here, employing a multivariate analysis known as the "Quantification Theory I". The factors for piping consist of material and diameter. The ground factors consist of SPT blow count and soil type up to a depth of 5 m, ground water table depth and so on, which are obtained from results of standard penetration tests. In addition to these factors, the length of piping contained in a cell is also a factor in the analysis. Pipe length has no relation to pipe damage mechanically. However, the length of piping could affect the damage ratio statistically because it is a denominator of the fraction indicating the damage ratio. Fig. 2.7, which shows the relationship between the length of pipeline in a cell and damage ratio, reveals that plots for the short piping length are scattered. In other words, many plots for the short piping length have a zero damage ratio; however if damage occurs, there is a very high value. This means that the reliability of the damage ratio as a index of the degree of the damage decreases with shorter piping length. Therefore, the piping length was taken into consideration as a factor in the present study in order to examine the effects. While factors for ground motion are important, they are not considered in the present study for two reasons. First, the ground motion at the surface is influenced to a great extent by the ground characteristics. Another is that the base rock motion is almost the same at each cell in the present analysis because they all share a similar focal distance.

Tables 2.1 and 2.2 show results of the multivariate analysis for pipe damage in Niigata City and Noshiro City, respectively. The greatest possible multiple correlation coefficient was obtained in the analysis using the category classification shown in Tables 2.1 and 2.2.

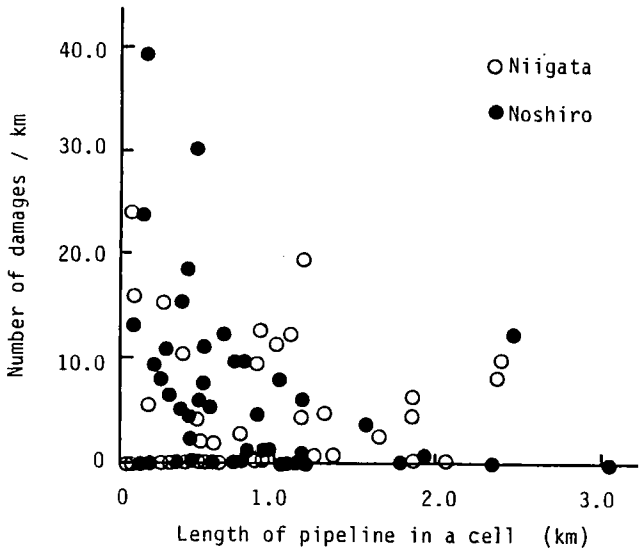

Fig. 2.7 Relationship between damage ratio of pipelines and length of pipelines in a cell.

In category classification, attention was given to the following points; equal distribution of sample data for each category and regular classification of categories. A partial correlation coefficient indicates the degree of influence of each item on the damage ratio. It can be seen from Table 2.1 that partial correlation coefficient is greatest for the items listed under ground water table, and that the soil type and SPT blow count up to a depth of 5 m are also very high. As shown in Table 2.2, the SPT blow count up to a depth of 5 m has the greatest partial correlation coefficient, followed by ground water table and soil type. It is interesting to note that all items related to ground conditions have a great influence on the damage ratio. On the other hand, the partial correlation coefficient of the pipe length in a cell is small in each of the

Table 2.1 Results of multivariate analysis in Niigata City.

Item	Category	Num.	Category weight	Partial correlation coefficient
Pipe type	A C P	57	-0.685	0.139
	V P	13	2.585	
	C I P	102	0.053	
Diameter (ϕ) mm	$\phi \leq 50$	12	-4.841	0.326
	$50 < \phi \leq 100$	59	1.134	
	$100 < \phi \leq 200$	66	-0.319	
	$200 < \phi \leq 300$	19	-0.652	
	$300 < \phi \leq 400$	8	5.714	
	$400 < \phi$	8	-2.638	
SPT blow count up to a depth of 5m (N)	$0 \leq N < 5$	59	2.057	0.403
	$5 \leq N < 10$	83	-2.428	
	$10 \leq N < 15$	26	2.993	
	$15 \leq N$	4	0.594	
Soil type	Silt	8	1.227	0.273
	Fine sand	47	1.009	
	Medium sand	109	-0.099	
	Clay	8	-5.804	
Ground water table (H) m	$0 \geq H > -1.0$	35	-2.485	0.411
	$-1.0 \geq H > -1.5$	49	-0.830	
	$-1.5 \geq H > -2.0$	59	2.217	
	$-2.0 \geq H > -2.5$	8	-5.640	
	$-2.5 \geq H > -3.0$	2	-6.437	
	$-3.0 \geq H$	19	2.885	
Total length in a mesh (l) km	$0 < l \leq 0.2$	36	1.596	0.195
	$0.2 < l \leq 0.4$	44	-0.220	
	$0.4 < l \leq 0.6$	39	-1.073	
	$0.6 < l$	53	-0.113	

Multiple correlation coefficient 0.54

Table 2.2 Results of multivariate analysis in Noshiro City.

Item	Category	Num.	Category weight	Partial correlation coefficient
Pipe type	A C P	56	0.563	0.278
	V P	27	1.295	
	C I P	29	-2.294	
Diameter (ϕ) mm	$\phi \leq 50$	17	-0.790	0.269
	$50 < \phi \leq 100$	48	-0.017	
	$100 < \phi \leq 200$	29	-1.093	
	$200 < \phi \leq 300$	10	0.384	
	$300 < \phi \leq 400$	4	3.290	
	$400 < \phi$	4	7.237	
SPT blow count up to a depth of 5m (N)	$0 \leq N \leq 9$	15	1.185	0.427
	$9 < N \leq 11$	48	3.453	
	$11 < N \leq 13$	16	-5.671	
	$13 < N$	33	-2.862	
Soil type	Silt	3	-1.306	0.289
	Fine sand	45	1.866	
	Medium sand	46	-0.953	
	Coarse sand	11	-2.722	
	Clay	7	-0.893	
Ground water table (H) m	$0 \geq H \geq -2.0$	25	-0.254	0.385
	$-2.0 > H \geq -2.5$	22	3.638	
	$-2.5 > H \geq -3.0$	22	3.251	
	$-3.0 > H \geq -4.5$	22	-2.158	
	$-4.5 > H$	21	-4.654	
Total length in a mesh (l) km	$0 < l \leq 0.1$	23	-1.322	0.150
	$0.1 < l \leq 0.3$	33	0.621	
	$0.3 < l \leq 0.5$	26	0.810	
	$0.5 < l$	30	-0.371	

Multiple correletion coefficient 0.56

cases analyzed. This certifies there is no significant relation between the pipe length in a cell and damage ratio statistically in the present analysis.

In the present analysis, the multiple correlation coefficients are 0.54 and 0.56 for Niigata City and Noshiro City, respectively. These values are too low to discuss the size of each category weight and to establish an equation for the prediction of earthquake damage. In the following section, liquefaction and permanent ground displacement induced by liquefaction are chosen for consideration as factors of the ground characteristics.

2.3 Earthquake Damage to Buried Pipelines Induced by Soil Liquefaction

2.3.1 Influence of Liquefaction

Liquefied areas in Noshiro City during the 1983 Nihonkai-Chubu Earthquake were identified by some researchers [12)-14)]. Based on liquefaction maps indicated by Tohno and Shamoto [13)], we indicate the number of pipe damage in liquefied areas and that in non-liquefied areas in Fig. 2.8. This figure also shows the failure modes of the pipelines in accordance with those illustrated in Fig. 2.9, which are taken from Noshiro City Gas and Waterworks Bureau [15)]. Since the data in this figure are not taken from the pipe-laying maps but from reference 15, the damage of ductile cast iron pipes (DCIP) is also shown. It is evident from Fig. 2.8 that roughly half of the damage of asbestos cement pipes (ACP) and polyvinyl chloride pipes (VP) were caused in the liquefied areas irrespective of the failure modes. Furthermore, it is very interesting to note that almost all of the damage of cast iron pipes (CIP) and ductile cast iron pipes (DCIP) were caused at joints of a pipe in the liquefied areas. These facts suggest that earthquake damage to the pipelines is strongly related to soil liquefaction.

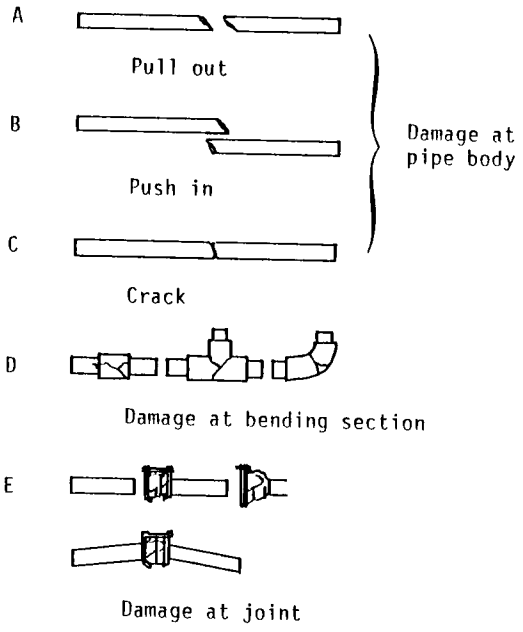

Fig. 2.9
Failure modes of pipeline (from Noshiro City Gas and Waterworks Bureau, 1983).

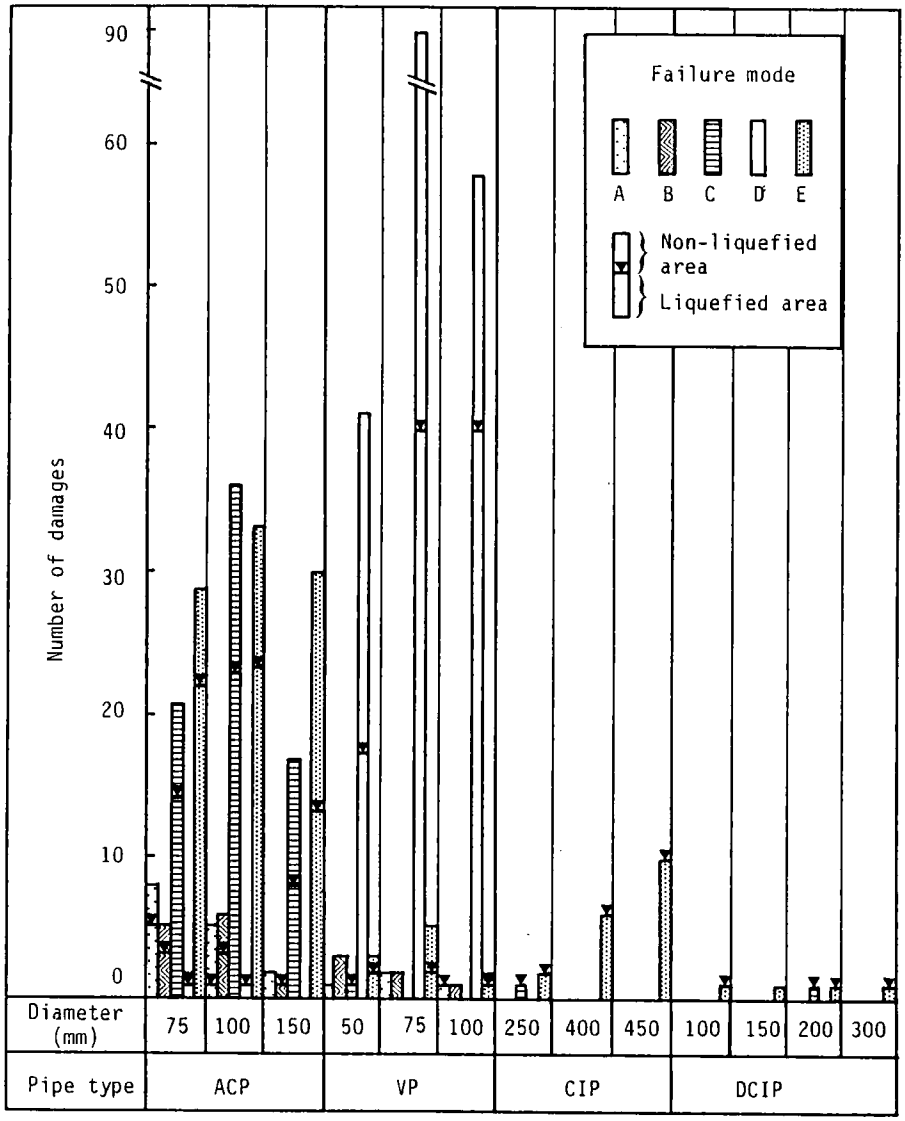

Fig. 2.8 Relationship among number of damages, ground condition, pipe type and failure mode during the 1983 Nihonkai-Chubu Earthquake.

2.3.2 Influence of Permanent Ground Displacement Induced by Soil Liquefaction

Hamada et al. pointed out that permanent ground displacements were induced by a liquefaction during the 1964 Niigata Earthquake and during the 1983 Nihonkai-Chubu Earthquake. Moreover, the permanent ground displacements were measured by means of aerial photographs taken before and just after the earthquake [16]. As permanent ground displacement is considered as one of the most serious liquefaction hazards, the relationship between pipe damage and permanent ground displacement induced by liquefaction is investigated in this section.

Table 2.3 shows the total number of pipe damages in Noshiro City (α), the number of pipe damages in areas where permanent ground displacement occurred (β) and the ratio between them (β/α). The failure modes in this table are in accordance with those in Fig. 2.9. It is evident from this table that more than 30 percent of the total number of damages to ACP and VP, and about 20 percent of that to CIP and DCIP, are caused in the areas where permanent ground displacement occurred.

Table 2.3 Number of damages due to permanent ground displacement in Noshiro City.

Pipe type		Failure mode					Total
		A	B	C	D	E	
ACP	(β)	4	7	37	1	38	87
	(α)	15	12	98	4	94	223
	(β)/(α)	0.27	0.58	0.38	0.25	0.40	0.39
VP	(β)	1	0	1	68	3	73
	(α)	4	6	1	189	10	210
	(β)/(α)	0.25	0	1.00	0.36	0.33	0.35
CIP	(β)	-	-	1	-	3	4
	(α)	-	-	1	-	22	23
	(β)/(α)	-	-	1.00	-	0.14	0.17
DCIP	(β)	-	-	0	-	1	1
	(α)	-	-	1	-	4	5
	(β)/(α)	-	-	0	-	0.25	0.20

(α): Total number of damages
(β): Number of damages due to permanent ground displacement

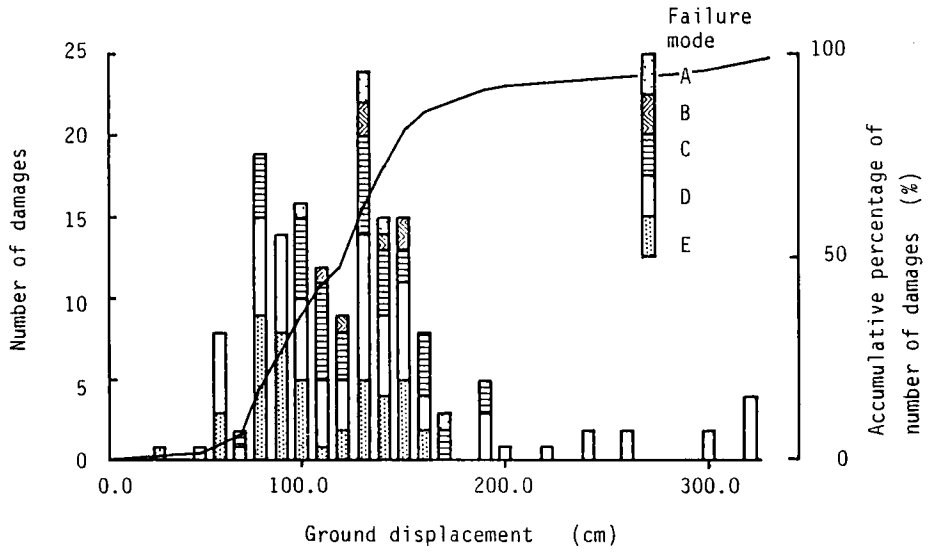

Fig. 2.10 Relationship between number of damages and permanent ground displacement (in Noshiro City).

Fig. 2.10 indicates the relationship between horizontal permanent ground displacement and the number of pipe damages. This figure suggests that many damages were caused at sites where permanent ground displacement was greater than about 1 m. However, in order to discuss the relationship between pipe damage and permanent ground displacement, it is more pertinent to observe ground strain around the buried pipelines than to observe absolute displacement. Therefore, the average ground strains for longitudinal and transverse directions of a pipe axis are evaluated using two vectors of the permanent ground displacements near the site of pipe damage. Figs. 2.11 and 2.12 indicate the relationship between the average ground strain and number of pipe damages, for longitudinal and transverse directions to the pipe axis, respectively. The minus values in Fig. 2.11 indicates a tensile strain. It can be seen from these figures that the pipe damages could be caused by an average ground strain as low as 1 percent or less. The failure modes A and B correspond with the failure due to tensile and compressive forces, respectively, as illustrated in Fig. 2.9. The failure modes in Fig. 2.11, however, do not agree with those; i.e. both modes A and B can be shown in tension and compression strain regions. This fact may

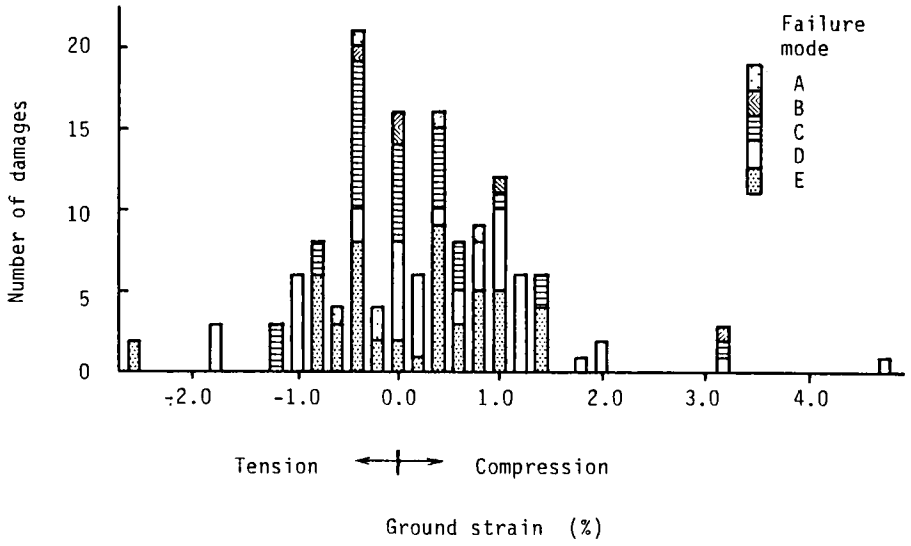

Fig. 2.11 Relationship between number of damages and average ground strain in longitudinal direction to the pipe axis (in Noshiro City).

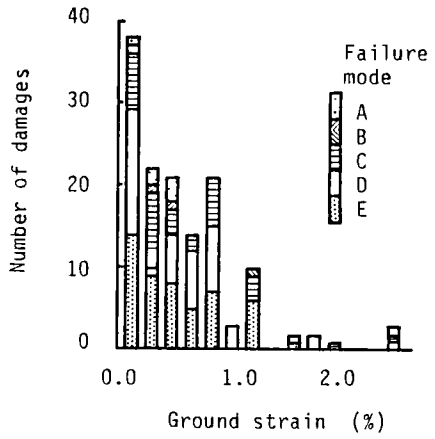

Fig. 2.12 Relationship between number of damages and average ground strain in transverse direction to the pipe axis (in Noshiro City).

be explained by following points. Since the ground movement during an earthquake is variable, it is insufficient to merely observe the residual ground deformation after an earthquake in order to discuss the relationship between the pipe damage and ground strains. Furthermore, the pipe damage may be influenced by a greater local ground strain than that evaluated in the present study.

2.3.3 Multivariate Analysis Including Liquefaction Effects

Pipe damage is revealed to be much influenced by liquefaction and permanent ground displacement due to liquefaction. In this section, a multivariate analysis including those two influences is carried out. The item of liquefaction is classified into three classes: none, light and heavy, which are determined by the size of a liquefied area in a cell based on the liquefaction map indicated by Tohno and Shamoto [13]. Similarly, permanent ground displacement is classified into four categories based on the distribution map of the permanent ground displacement indicated by Hamada et al. [16]. The analysis is carried out for the pipelines in the areas where both the liquefaction map and distribution map of the permanent ground displacement are available. The number of data, therefore, is limited but the liquefaction effects on the pipe damage seem clear.

Table 2.4 shows the results of the multivariate analysis including the liquefaction effects. The multiple correlation coefficient in this analysis is 0.56. In general, the multiple correlation coefficient decreases with a decrease in the number of items. However Table 2.4 indicates no decrease in the multiple correlation coefficient in comparison with Table 2.2, suggesting that the pipe damages are explained by liquefaction effects rather than some items of ground characteristics: SPT blow count, ground water table, etc. Moreover, the partial correlation coefficients for liquefaction and permanent ground displacement are higher in this analysis. Since the correlations for two items of liquefaction and permanent ground displacement are high, a second multivariate analysis is carried out using only the item of liquefaction and eliminating permanent ground displacement as a variable. The results are shown in Table 2.5. Since the number of items is further decreased, the multiple correlation coefficient decreases

Table 2.4 Results of multivariate analysis including liquefaction and permanent ground displacement in Noshiro City.

Item	Category	Num.	Category Weight	Partial correlation coefficient
Pipe type	A C P	46	0.024	0.155
	V P	18	-1.804	
	C I P	22	1.426	
Diameter (ϕ) mm	$\phi \leq 50$	13	1.113	0.173
	$50 < \phi \leq 75$	20	1.260	
	$75 < \phi \leq 100$	14	-0.906	
	$100 < \phi \leq 200$	22	-0.111	
	$200 < \phi \leq 300$	9	-2.985	
	$300 < \phi$	8	0.290	
Liquefaction	None	28	-2.871	0.475
	Light	27	-1.897	
	Hard	31	4.245	
Permanent ground displacement	None	16	-0.049	0.410
	Small	18	-1.049	
	Medium	22	4.340	
	Large	30	-2.568	
Total length in a mesh (l) km	$0 < l \leq 0.1$	17	-2.923	0.269
	$0.1 < l \leq 0.3$	22	1.595	
	$0.3 < l \leq 0.5$	20	0.284	
	$0.5 < l \leq 0.7$	5	0.948	
	$0.7 < l \leq 0.9$	7	-1.226	
	$0.9 < l$	15	0.850	

Multiple correlation coefficient 0.56

to 0.43. The partial correlation coefficient of liquefaction is the highest of all the items, in this result.

The above results show that liquefaction is the most influential factor in pipe damage. Although the multiple correlation coefficients of the analyses are too low to establish an equation for prediction of earthquake damage to the pipelines, the results suggest that liquefaction is more important variable for evaluating the pipe damage than individual item of the ground characteristics such as SPT blow count, ground water table, etc. It is, therefore, a crucial point in establishing a

prediction equation to determine the extent of liquefaction more precisely.

Table 2.5 Results of multivariate analysis including liquefaction in Noshiro City.

Item	Category	Num.	Category Weight	Partial correlation coefficient
Pipe type	A C P	46	0.358	0.116
	V P	18	-1.487	
	C I P	22	0.468	
Diameter (ϕ) mm	$\phi \leq 50$	13	0.970	0.198
	$50 < \phi \leq 75$	20	1.354	
	$75 < \phi \leq 100$	14	-0.672	
	$100 < \phi \leq 200$	22	-0.615	
	$200 < \phi \leq 300$	9	-3.169	
	$300 < \phi$	8	1.473	
Liquefaction	None	28	-1.661	0.318
	Light	27	-1.393	
	Hard	31	2.713	
Total length in a mesh (l) km	$0 < l \leq 0.1$	17	-2.386	0.205
	$0.1 < l \leq 0.3$	22	1.194	
	$0.3 < l \leq 0.5$	20	0.487	
	$0.5 < l \leq 0.7$	5	1.258	
	$0.7 < l \leq 0.9$	7	0.742	
	$0.9 < l$	15	-0.462	

Multiple correlation coefficient 0.43

2.4 Conclusions

Conclusions obtained from this chapter are summarized as follows:

(1) It is interesting to note that markedly high damage ratios of piping with a large diameter of 400 mm and 450 mm are present, and these pipes are located at liquefied sites near the boundary between the liquefied and non-liquefied areas. This could be explained in terms of complicated ground motion due to sharp change of the ground characteristics and buoyancy effects at the liquefied areas.

(2) Many pipe damages were caused at sites where the ground water table is lower than the buried pipelines. This suggests that permanent ground movements of unsaturated sand layers at the surface, induced by the liquefaction of deeper saturated sand layers, increases the incidence of pipe damages.

(3) Many pipe damages occurred at sites where the permanent ground displacement was greater than 1 m. Moreover, the pipe damage could be caused even by an average ground strain of less than 1 percent.

(4) The tensile and compressive failure modes of the pipelines at joints do not always agree with the direction of the permanent ground displacement. Since the ground movement during an earthquake is variable, it is insufficient to observe the residual ground deformation after an earthquake in order to assess pipe damage.

(5) Liquefaction is the most influential factor to the pipe damage. Although the multiple correlation coefficients in the analyses are too low to establish an equation for prediction of an earthquake damage to pipelines, the results suggest that liquefaction is more significant in evaluating pipe damage than such ground characteristics as SPT blow count, ground water table, etc.

Although the author has collected extensive soil profiles data and pipe-laying maps plotting the sites of pipe damage from Niigata City Waterworks Bureau and Noshiro City Gas and Waterworks Bureau, an equation for prediction of earthquake damage to pipelines is not established because of an insufficient amount of data. It is necessary to accumulate more detailed data of earthquake damage to pipelines and ground conditions.

References (Publications written in Japanese are so indicated; all others are in English)

1) Japan Society of Civil Engineers: General Report on Damage Due to the 1923 Kanto Earthquake, Vol. 2, pp. 201-238, 1927 (in Japanese).
2) Investigation Committee of the 1964 Niigata Earthquake at Japan Society of Civil Engineers: General Report on Damage Due to the 1964 Niigata Earthquake, Part 11, pp.659-739, 1966 (in Japanese).
3) Tohoku Branch of the Japan Society of Japan Water Works Association: Damage to Water Supply Installation Due to the 1968 Tokachi-oki Earthquake, and Disaster Prevention Methods, Journal of Japan Water Works Association, No. 4, 15, pp. 26-34, 1969 (in Japanese).
4) Japan Society of Civil Engineers: General Report on Damage by the 1983 Nipponkai-Chubu Earthquake, Part 8, pp. 635-710, 1986 (in Japanese).
5) Kubo, K., Katayama, T. and Sato, N.: Quantitative Analysis of Seismic Damage to Buried Pipelines, Proceedings of the 3rd Japan Earthquake Engineering Symposium-1975, pp. 655-661, 1975.
6) Matsuo, M. and Horiuchi, T.: Earthquake Damage and Methodology of Design of Small Diameter Pipelines, Soils and Foundations, Japan Soc. of Soil Mecha. and Founda. Eng., Vol. 19, No. 1, pp. 23-38, 1979.
7) Ichihara, M. and Yamada, K.: Relative Degree of Risk of Water-Supply Pipes in Nagoya City During Earthquake, Proceedings of Japan Soc. Civil Eng., No. 316, pp. 51-63, 1981 (in Japanese).
8) Kitaura, M. and Miyajima, M.: Damage and Restoration of Lifeline Systems Due to the Nipponkai-chubu Earthquake of 1983, Journal of Japanese Society for Natural Disaster Science, No. 3, Vol. 1, pp. 1-11, 1984 (in Japanese).
9) Kitaura, M. and Miyajima, M.: Damage to Pipelines Subjected to Soil Liquefaction in 1983 Nipponkai-Chubu Earthquake in Japan, Proceedings of the 8th European Conference on Earthquake Engineering, Vol. 2, pp. 25-32, 1986.

10) Kitaura, M .and Miyajima, M.: Quantitative Evaluation of Damage to Buried Pipelines Induced by Soil Liquefaction, Proceedings of the 9th World Conference on Earthquake Engineering, Vol. 7, pp. 11-16, 1989.
11) Hokuriku Construction Association: Ground Soil Chart of Niigata Plain, 1981 (in Japanese).
12) Tohno, I., Yasuda, S. and Shamoto, Y.: Site Liquefaction and Damage Caused by the Nipponkai Chubu Earthquake, TSUCHI-TO-KISO, Japan Soc. of Soil Mecha. and Founda. Eng., Vol. 31, No. 12, pp. 13-20, 1983 (in Japanese).
13) Tohno, I. and Shamoto, Y.: Liquefaction Damage to the Ground During the 1983 Nihonkai-Chubu (Japan Sea) Earthquake in Akita Prefecture, Tohoku, Japan, Natural Disaster Science, Vol. 7, No. 2, pp. 67-93, 1985.
14) OYO Corporation: Report on Survey of Damage Caused by the May 26, 1983 Nihonkai-chubu Earthquake, 1984 (in Japanese).
15) Noshiro City Gas and Waterworks Bureau: Report on the Damage to Water Supply Pipelines by the 1983 Nipponkai Chubu Earthquake, 1983 (in Japanese).
16) Hamada, M., Yasuda, S, Isoyama, R. and Emoto, K.: Observation of Permanent Ground Displacements Induced by Soil Liquefaction, Proceedings of Japan Soc. Civil Eng., No. 376, pp. 211-220, 1986 (in Japanese).
17) Kitaura, M., Miyajima, M. and Suzuki, H.: Response Analysis of Buried Pipelines Considering Rise of Ground Water Table in Liquefaction Processes, Proceedings of Japan Soc. Civil Eng., No. 380, pp. 73-80, 1987.

3. EXPERIMENTS ON BURIED PIPELINES' RESPONSE IN LIQUEFACTION PROCESSES

3.1 General Remarks

As mentioned in the previous chapter, the damage investigation of pipelines during actual earthquakes has revealed that damage ratios of pipelines have much larger values in liquefied ground compared with ones in a shaking ground without liquefaction. The damage investigation, however, does not provide specific descriptions of pipeline behavior or failure mechanisms of the pipelines during liquefaction. An experiment using a model pipe is an effective means for gaining an understanding of pipe behavior during liquefaction.

Some experimental research on buried pipeline subjected to liquefaction has been undertaken. Katada and Hakuno conducted experiments using a model pipe and concluded that bending strains of a buried pipeline in an incompletely liquefied ground are greater than those in a completely liquefied ground [1]. Takada, Tanabe et al. investigated the damage in a manhole-pipeline system due to liquefaction by experiments to which simulated a drag force, an external force and an equivalent soil spring constant [2]. Kuribayashi, Kawamura et al. observed uplifting and settlement along a manhole-pipeline system induced by liquefaction [3].

Little experimental work has been done on pipe response to liquefaction processes so far, however. The purpose of this chapter is to clarify pipe behavior in liquefaction processes. The following Chapter 3.2 describes the results of vibration tests using a rubber pipe model in a loose dry sand stratum, conducted in order to compare with pipe behavior in liquefaction processes which is discussed in Chapter 3.3. In Chapter 3.3, experiments carried out to obtain strain characteristics of the buried pipe during liquefaction and strain occurrence mechanisms are discussed. The contents of this chapter are based on references 4 and 5.

3.2 Pipeline Response in Dry Sand Stratum

3.2.1 Testing Procedure

A general view of experimental apparatus is shown in Fig. 3.1. The model sand stratum was 500 mm in width, 1500 mm in length and 250 mm in height. The model buried pipe was simulated by a rubber rod with 20 mm in diameter and 1000 mm in length. Its elastic modulus was 810 kg/cm^2 (79.4 MPa) and its weight per unit volume was 1.14 g/cm^3 (11.2 kN/m^3). Strain gauges were utilized at the center (distance from either end of the model pipe is 500 mm) and 125 mm from the end of the pipe. Two accelerometers were buried just under the lower strain gauges. River sand was used in the experiments. Table 3.1 lists its material properties and Fig. 3.2 shows the grain size accumulation curve of the sand. The procedure for making a loose sand layer was as follows: sand was poured into a sand box through a slit in a bucket which was placed on the sand box (See Fig. 3.3). Then the sand layer was vibrated by harmonic wave of 100 gal.

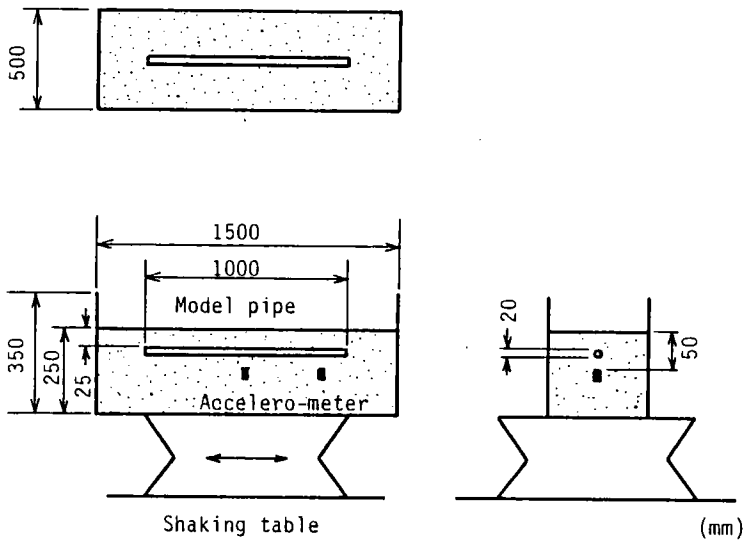

Fig. 3.1 General view of experimental apparatus.

Table 3.1 Physical properties of sand.

Specific gravity	2.67
Uniformity coefficient	2.96
Maximum void ratio (e_{max})	0.982
Minimum void ratio (e_{min})	0.717
Coefficient of permeability for e_{min}	0.0157
(cm/s) for e_{max}	0.0176

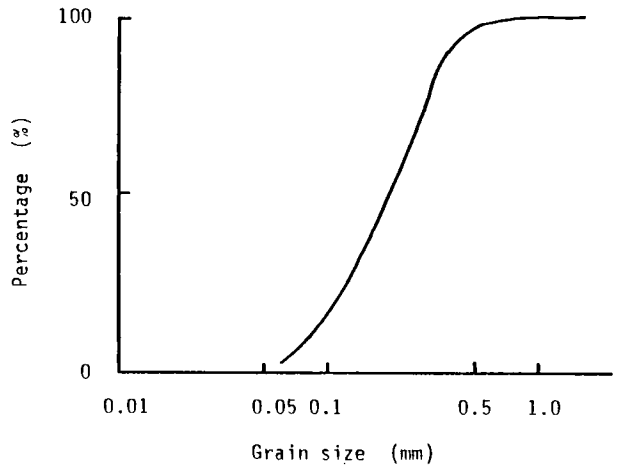

Fig. 3.2 Grain size accumulation curve of sand.

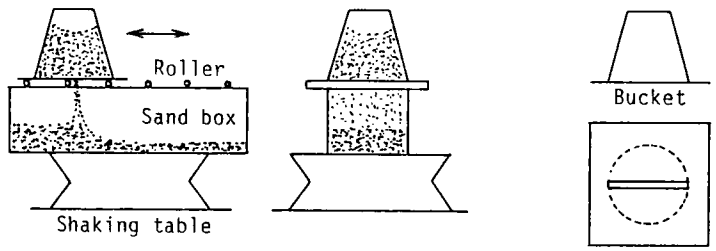

Fig. 3.3 Schematic diagrams of equipment for making homogeneous, loose sand layers.

The strains on the buried pipe, excess pore water pressure and acceleration of the model ground were recorded during 30 seconds of shaking. In a series of experiments, the model pipe which was buried at 25 mm in depth was vibrated by stationary harmonic waves of 5 Hz, 10 Hz, 15 Hz, 20 Hz, 25 Hz, 30 Hz, 35 Hz and 40 Hz both parallel and perpendicular to the pipe axis.

3.2.2 Strain Characteristics of Pipelines in Dry Sand Stratum

A record of pipe strain of 40 Hz excitation is shown in Fig. 3.4. The model was excited by the harmonic wave in a direction parallel to the pipe axis in this case. The upper and lower strain gauges and those of the two sides are named A, C, B and D, respectively. Suffix 1 and 2 indicate the center and end of the pipe. It can be seen from this figure

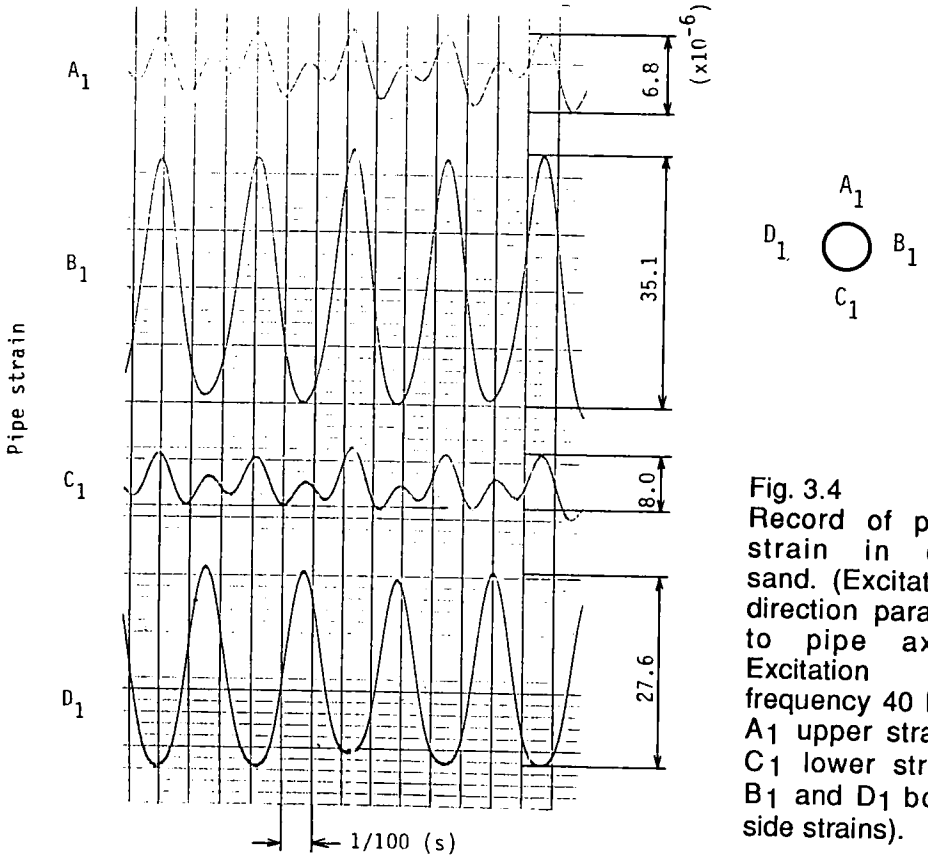

Fig. 3.4 Record of pipe strain in dry sand. (Excitation direction parallel to pipe axis, Excitation frequency 40 Hz, A_1 upper strain, C_1 lower strain B_1 and D_1 both side strains).

that the axial strains are predominant because the four strains: the upper, lower and two sides are in phase. This agrees with the results of other excitation frequencies. Figs. 3.5 (a) and (b) illustrate frequency response curves of acceleration of the model ground, and strain at the center and near the end of the model pipe, respectively. The upper curve shows the response acceleration of the sand layer and the lower four curves display the pipe strains in the stationary state. These figures reveal that the predominant frequency of the model ground is about 35 Hz and the resonance of the model ground affects the pipe strain. The maximum strain of the pipe is about 20 $x10^{-6}$ at 35 Hz excitation. On the other hand, the pipe strain near the end of the pipe rose sharply at 40 Hz. This can be explained by the partial resonance of the side walls of the sand box in the 40 Hz excitation.

Next, the model was excited by a harmonic wave perpendicular to the pipe axis. In this case, the sand box was turned in the transverse direction to the vibration axis, which was used in the former case. The degree of restraint of the sand box to shearing deformation is different in each case. The results in the both cases could not be, therefore, compared quantitatively. Fig. 3.6 indicates a record of the pipe strain at 30 Hz excitation. The pipe strains of the two sides (B_1 and D_1) are in reverse phase with one another and their frequencies are the same as that of the excitation wave. While the lower and upper strains (A_1 and C_1) are in phase, and the predominant frequency is twice as much as that of the excitation wave. This could be explained by the bending vibration of the model pipe. Fig. 3.7 is a schematic diagram of the pipe bending. It is evident from this figure that the frequency of the upper strain is twice of that of the side strain. This agrees with the results of other excitation frequencies. It can, therefore, be concluded that the bending strains are predominant in the vibration tests in this case. Fig. 3.8 indicates the frequency response curves of the pipe strain and acceleration of the model ground. The two sides strains at the center of the model pipe increase at the 35 Hz excitation because of greater pipe bending vibration due to the resonance of the model sand layer. The maximum strain of the pipe is about 20 $x10^{-6}$ in this case.

Generally speaking, axial strain predominates in a seismic response of buried pipelines. The experimental results, however, show that the axial strain is predominant during parallel excitation, while

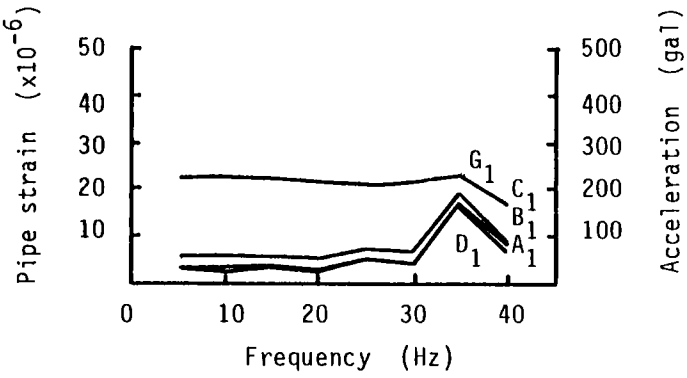

(a) At the center of the model pipe
(G_1 acceleration of ground,
A_1 upper strain, C_1 lower strain ,
B_1 and D_1 both side strains).

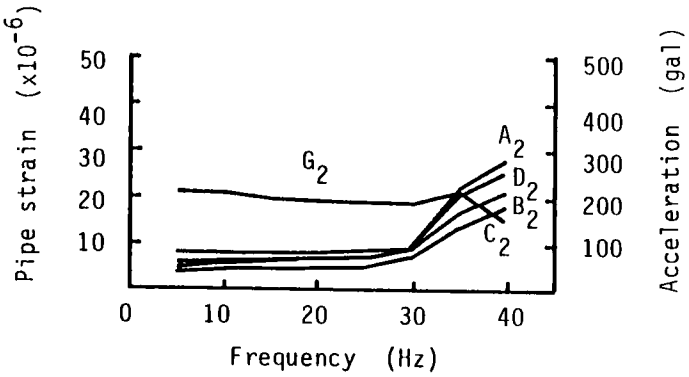

(b) Near the ends of the model pipe
(G2 acceleration of ground,
A_2 upper strain, C_2 lower strain,
B_2 and D_2 both side strains).

Fig. 3.5 Frequency response curves of pipe strain and acceleration of ground in dry sand (Excitation direction parallel to pipe axis).

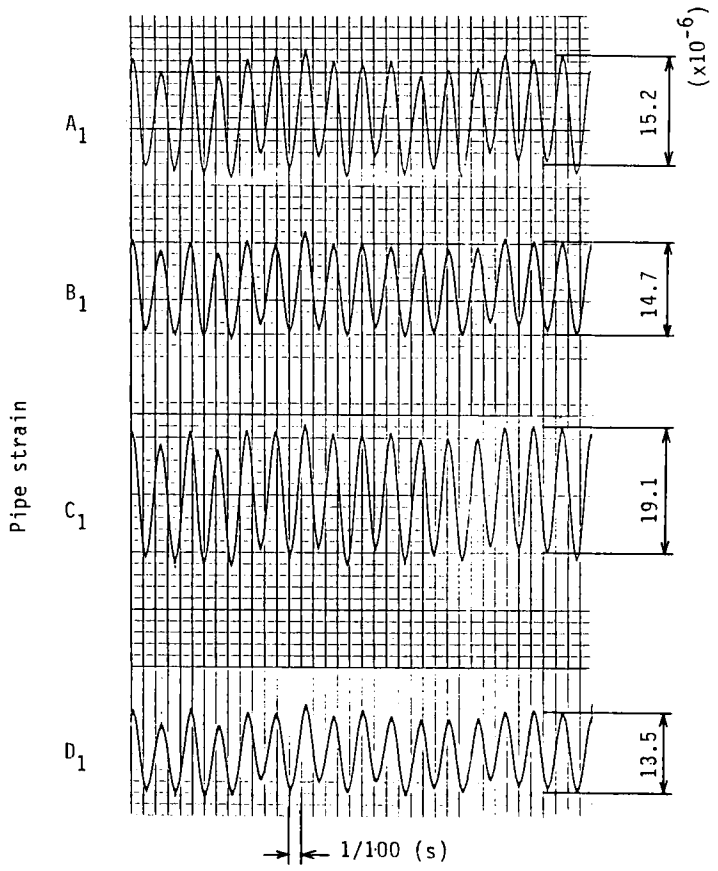

Fig. 3.6 Record of pipe strain in dry sand (Excitation direction perpendicular to pipe axis, Excitation frequency 30 Hz, A_1 upper strain, C_1 lower strain B_1 and D_1 both side strains).

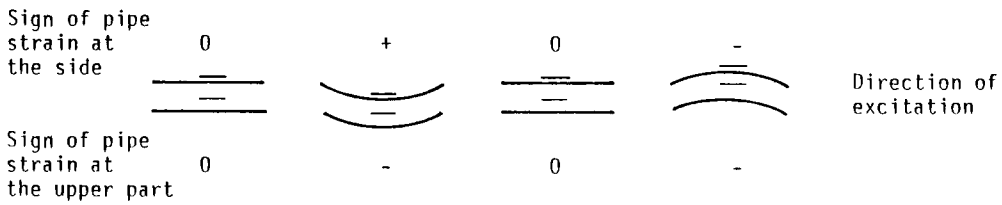

Fig. 3.7 Schematic diagram of pipe bending and strain gauge placement.

perpendicular excitation bring about a stronger bending strain. This can be explained by the difference in the resistance of the sand box to shearing deformation in each case.

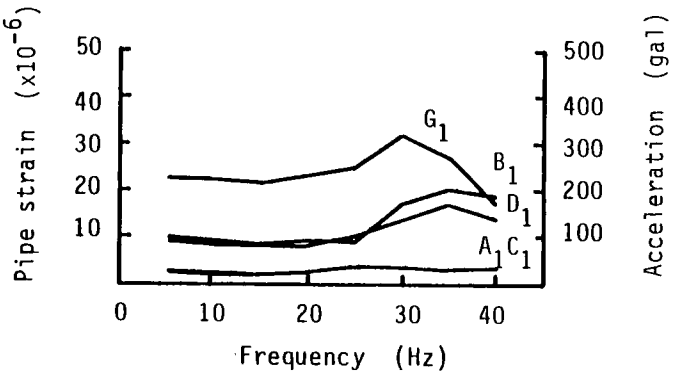

(a) At the center of the model pipe
(G_1 acceleration of ground,
A_1 upper strain, C_1 lower strain,
B_1 and D_1 both side strains).

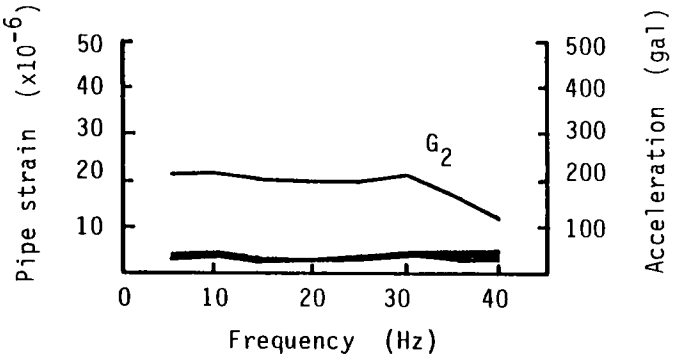

(b) Near the ends of the model pipe
(G_2 acceleration of ground,
A_2 upper strain, C_2 lower strain,
B_2 and D_2 both side strains).

Fig. 3.8 Frequency response curves of pipe strains and acceleration of ground in dry sand (Excitation direction perpendicular to pipe axis).

3.3 Pipeline Response in Saturated Sand Stratum

3.3.1 Testing Procedure

Experiments were carried out by means of the same equipment as Chapter 3.2. The strain gauges and accelerometer were waterproofed. In addition, a manometer was embedded at the same depth as that of the model pipe in order to measure the excess pore water pressure during liquefaction. This manometer is a miniature pressure transducer using a semiconductor. It is able to measure pressure in a transient state with accuracy because its predominant frequency is very high, 8 kHz. The procedure for making the loose saturated sand layer was as follows: a polyvinyl pipe, joined to the hose from the water source was inserted into the bottom of the sand stratum. Water was poured into the sand stratum. This operation was repeated for 10 to 20 times. Then the excess water on the surface of the sand stratum was soaked up with a sponge. As a result, the water table was level with the surface of the sand stratum.

The strain at the center of the buried pipe, excess pore water pressure and acceleration of the model ground were measured during 30 seconds of shaking. The model sand stratum was vibrated in stationary and transient harmonic waves with a frequency of 5 Hz, because liquefaction is attained easily at this frequency.

3.3.2 Experimental Results of Harmonic Wave Excitation

Fig. 3.9 shows records of the excess pore water pressure and pipe strains at the center during excitation in the direction parallel to the pipe axis. Input acceleration was about 150 gal. Burial depth of the pipe was 25 mm. As the excess pore water pressure rose, the higher strains of the pipe were caused by an increase in flexibility of the vibrating system consisted of the pipe and surrounding sand. The neutral axis in the records of the upper and lower strains (A_1 and C_1) moved because the pipe floated as the surrounding sand liquefied. It is interesting to note that the upper and lower strain gauges respectively indicate tension and compression during liquefaction. This suggests that the central portion of the pipe floated first due to a buoyancy effect which was induced by liquefaction, and the deformation of the pipe was retained after the dissipation of the excess pore water pressure.

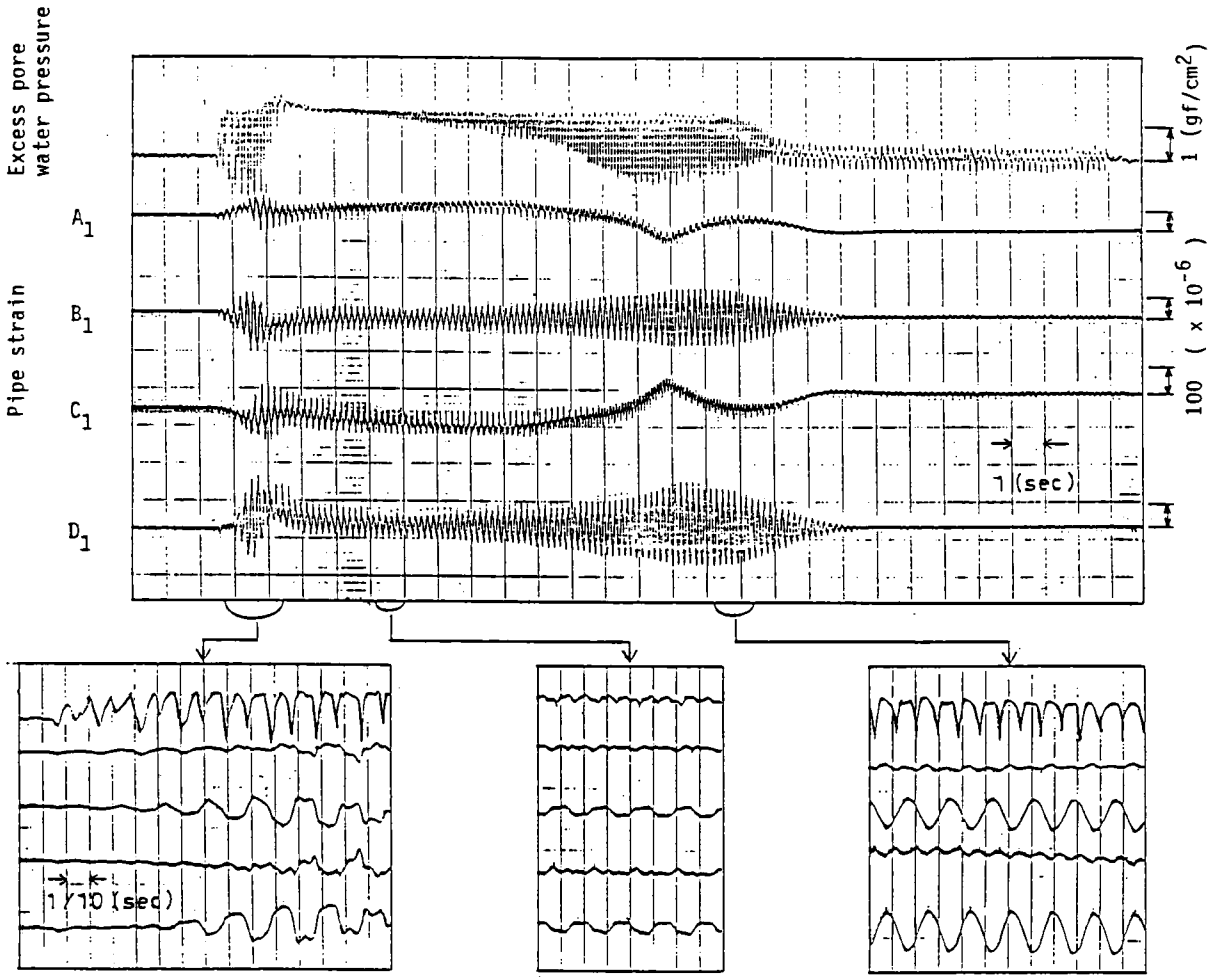

Fig. 3.9 Record of excess pore water pressure and pipe strain in saturated sand (Excitation direction parallel to pipe axis, A_1 upper strain, C_1 lower strain B_1 and D_1 both side strains).

Vibration and accumulated residual strains are defined in the present study as follows. The accumulated residual strain is defined as the drift of the neutral axis in the strain record. The vibration strain is defined as the vibration strain amplitude. The former strain is due to pipe bending and the latter is due to pipe vibration. Fig. 3.10 shows a graphic rearrangement of the records in Fig. 3.9. The change rate of the accumulated residual strain is expressed by the value of change in the accumulated residual strain for the preceding one second. It provides a kind of index of the deforming velocity of the pipe during liquefaction processes. It is very interesting to note that strain increased in value as the excess pore water pressure rose and fell; that is, the peak strain occurred during incomplete liquefaction rather than

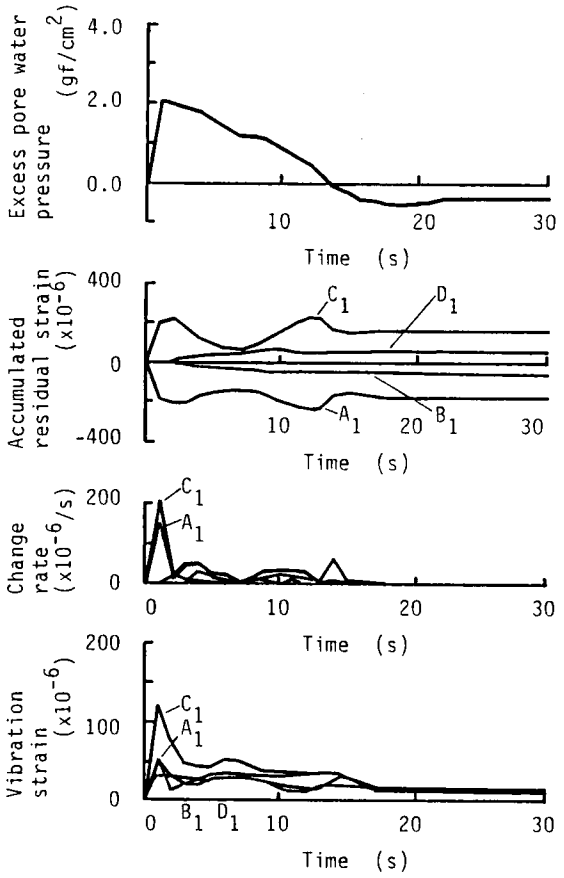

Fig. 3.10
Time histories of excess pore water pressure and pipe strain in saturated sand (Excitation direction parallel to pipe axis, Burial depth 25 mm).

in complete liquefaction. This will be discussed later in detail. Fig. 3.11 shows the results of further experimentation. In this case, the burial depth was 50 mm, deeper than in the former experiments. The results agree roughly with Fig. 3.10.

As mentioned above, the vibration strain and change rate of the accumulated residual strain were maximum at the same stage. The mechanics of generation are, however, different in each case. It is considered that generation factors of the vibration strains are dynamic characteristics of the system and the degree of transmission of the ground vibration to the pipe; while the accumulated residual strains, which indicate the degree of pipe bending, have relation to the degree of the liquefaction of the surrounding sand and to the volume of the liquefied ground.

As concerns the maximum value, the accumulated residual and vibration strains were about 240 $x10^{-6}$ and 120 $x10^{-6}$, respectively, as shown in Fig. 3.10 which were obtained at a burial depth of 25 mm. On the other hand, the strain at a burial depth of 50 mm as shown in Fig. 3.11 was about 80 $x10^{-6}$. This means that the pipe strain decreases as the burial depth of the pipe is increased. These strains are 4 to 12 times as large as the maximum pipe strains in the dry sand stratum. As concerns the phase of the strains in Fig. 3.9, the four strains were in phase when the model ground was incompletely liquefied. This suggests that axial strain dominates. It can be seen from this figure, however, that the bending strain dominates in complete liquefaction because the upper and lower strains are in reverse phase. The reason is considered to be as follows: At the first stage of liquefaction, the center of the pipe floated where surrounding soil was liquefied most easily, followed by the other parts whose surrounding soil was liquefied easily. Since the pipe did not uniformly float, the incident angle of input wave to the pipe was not perpendicular to the pipe axis. The bending strains, therefore, dominated when the ground was completely liquefied.

Fig. 3.12 provides the records of the excess pore water pressure and pipe strains at the center during excitation in a direction perpendicular to the pipe axis. In this case, the sand box was turned in a transverse direction to the vibration axis, which was used in the former case. The experimental conditions were otherwise the same as in the former case. Fig. 3.13 shows a graphic rearrangement of the

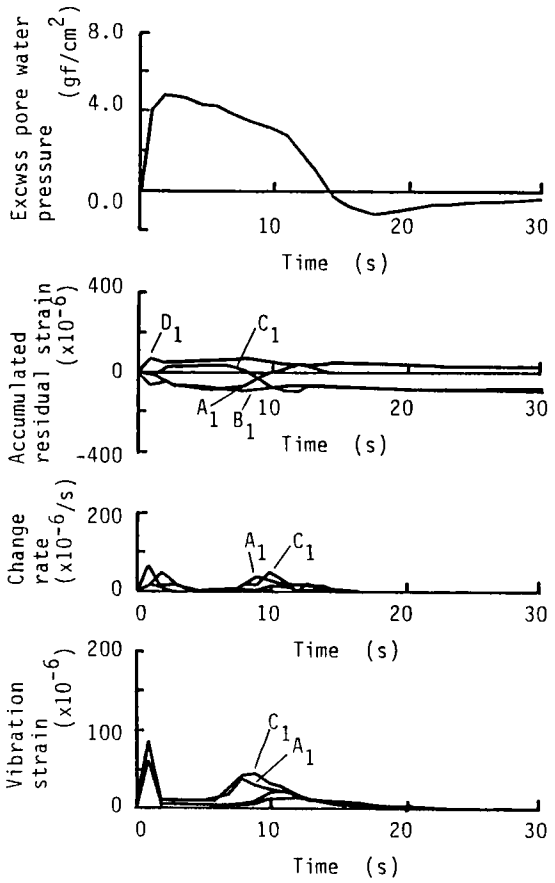

Fig. 3.11
Time histories of excess pore water pressure and pipe strain in saturated sand (Excitation direction parallel to pipe axis,Burial depth 50 mm).

data in Fig. 3.12. It can be seen from this figure that the accumulated residual strain of A_1 and C_1 and the vibration strain of B_1 and D_1 dominate. The strains took the peak value as the excess pore water pressure rose and fell. This agrees with the results of the former cases. As concerns the maximum value, the accumulated residual and vibration strains are about 120 $x10^{-6}$ and 130 $x10^{-6}$, respectively. These values are 6 to 7 times as large as the maximum strain of the pipe in the dry sand stratum. As concerns the phase of the strains in Fig. 3.12, the upper and lower strains (A_1 and C_1) are in phase and two side strains (B_1 and D_1) are in reverse phase when the excess pore water pressure rises. This suggests that the lateral bending strain dominates.

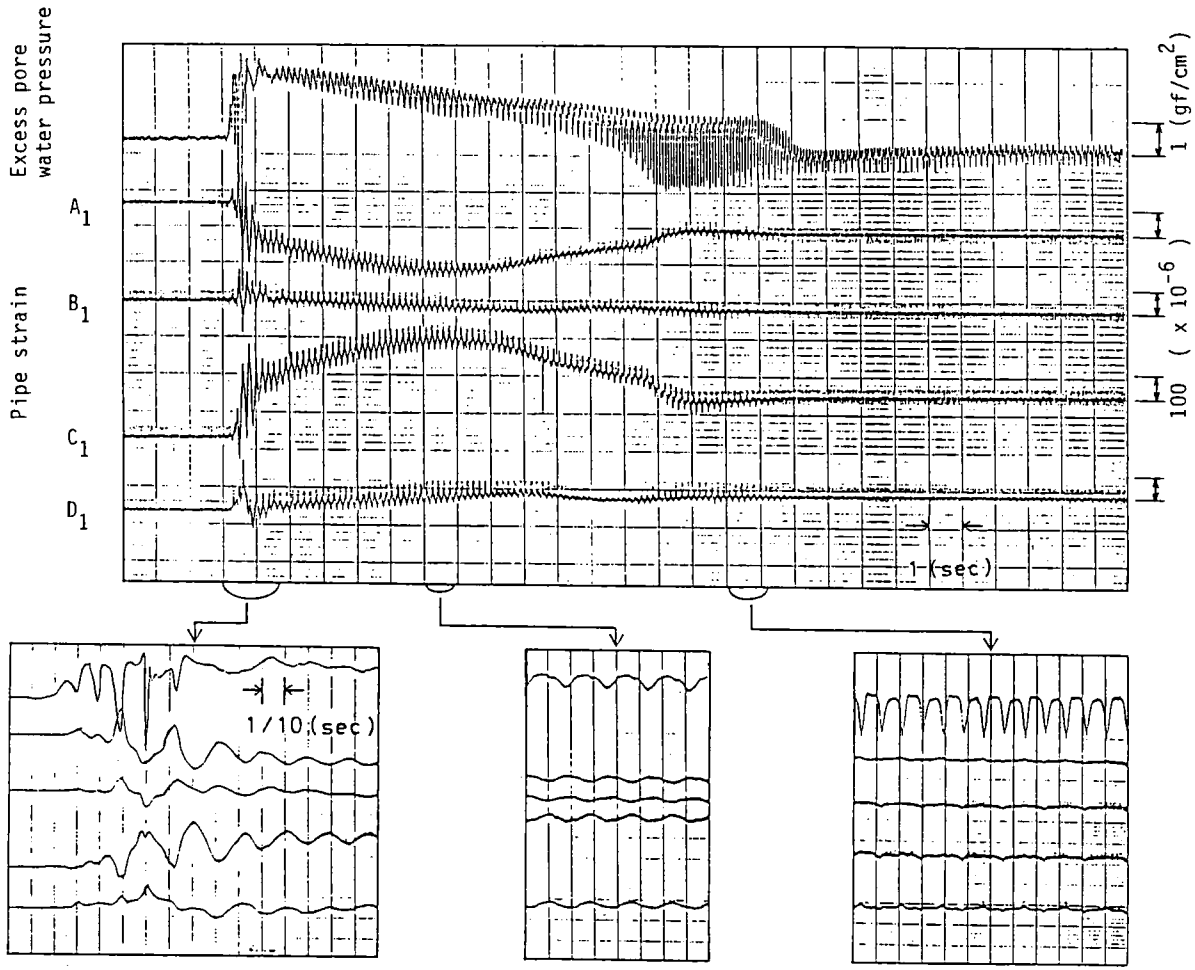

Fig. 3.12 Record of excess pore water pressure and pipe strain in saturated sand (Excitation direction perpendicular to pipe axis, A_1 upper strain, C_1 lower strain B_1 and D_1 both side strains).

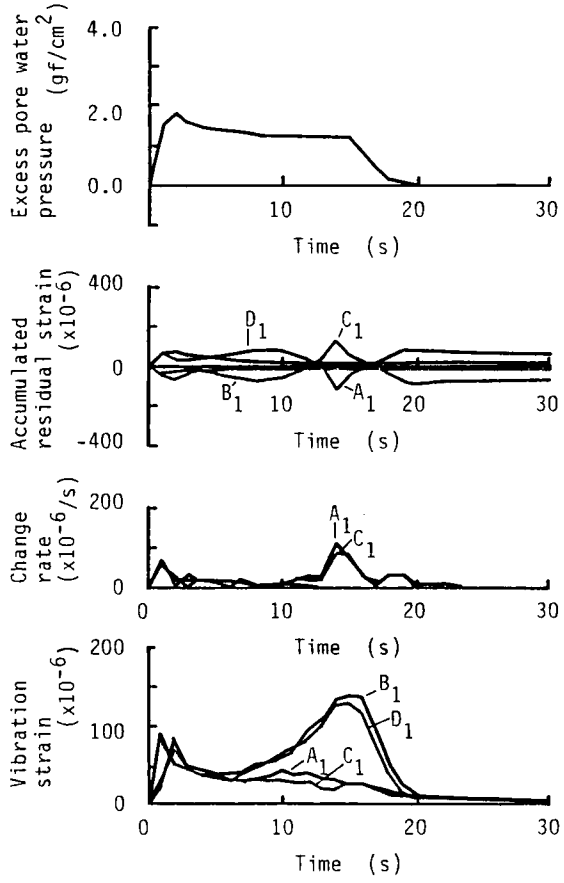

Fig. 3.13
Time histories of excess pore water pressure and pipe strain in saturated sand (Excitation direction perpendicular to pipe axis, Burial depth 25 mm).

While the upper and lower strains are in reverse phase in complete liquefaction. The reason for this could be similar to the former cases in which the buried pipe is excited in the direction parallel to the pipe axis. It is also noted that the upper and lower strains are smaller than two side strains. Therefore the bending strain dominates laterally. These results are similar to those obtained from the experiments using a dry sand stratum.

3.3.3 Experimental Results of Transient Harmonic Wave Excitation

The model sand stratum was vibrated by a transient harmonic wave with a frequency of 5 Hz, as shown in Fig. 3.14. Fifteen strain gauges were attached to the model pipe as shown in Fig. 3.15 in order to investigate the distribution of strain. Fig. 3.16 shows records of the excess pore water pressure, acceleration of the shaking table, acceleration of the model ground and pipe strains at gauges 1, 4, 7 and 10. The acceleration varying time was 50 seconds in this case. The excess pore water pressure increased after 25 seconds of shaking, kept a constant value for about 10 seconds, and then decreased. The maximum

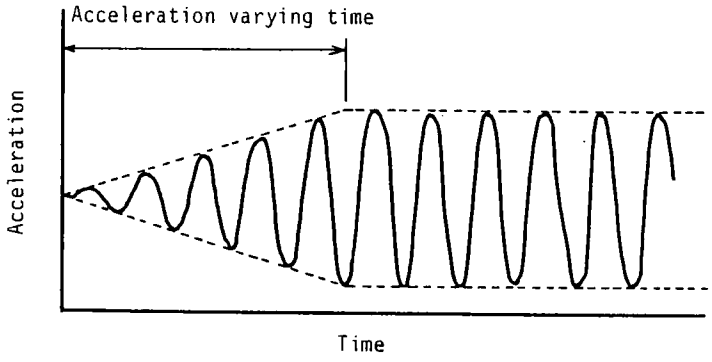

Fig. 3.14 Input transient harmonic wave.

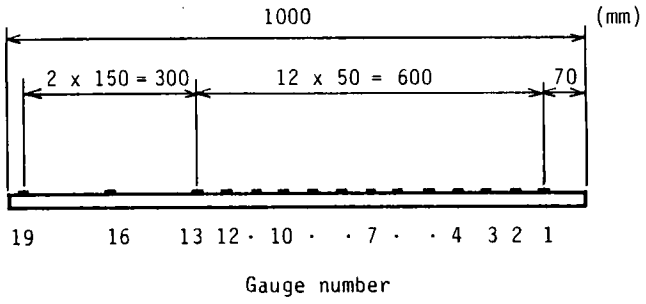

Fig. 3.15 Model pipe and strain gauge placement.

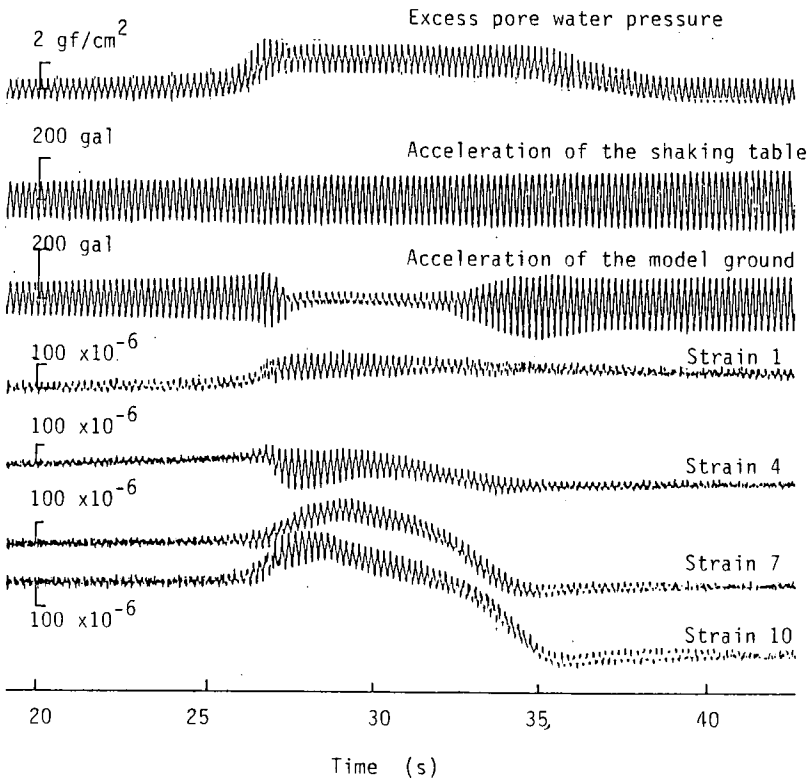

Fig. 3.16 Record of excess pore water pressure, acceleration of shaking table, acceleration of model ground and pipe strain .

value of the excess pore water pressure was about 2 gf/cm^2 (196 Pa). This figure indicates that the state of incomplete liquefaction remained for about 10 seconds because the excess pore water pressure ratio was about 0.6 at that stage. The ratio is derived from the value of the excess pore water pressure divided by the initial vertical effective stress. The acceleration of the model ground rose as the excess pore water pressure began to accumulate. Furthermore the vibration strains remained high value during incomplete liquefaction. It can be seen from this figure that the neutral axis of the strain records moved during incomplete liquefaction, especially at gauges 7 and 10. That could be explained in terms of the buoyancy effect on the incomplete liquefied ground at this stage.

Fig. 3.17 shows the relationship between the excess pore water pressure ratio and vibration strains at the gauge 10, which was attached to the center of the pipe. Each line in this figure indicates the experimental results in the acceleration varying times of 3 sec, 20 sec, 50 sec and 70 sec, respectively. The arrows in this figure refer to the process of time, and the interval between two points indicates a time lapse of 0.5 sec. The experimental result in the acceleration varying time of 3 sec shows that the model ground completely liquefied because the maximum value of the excess pore water pressure ratio reached 1.0. While the others indicate the model ground did not liquefy completely

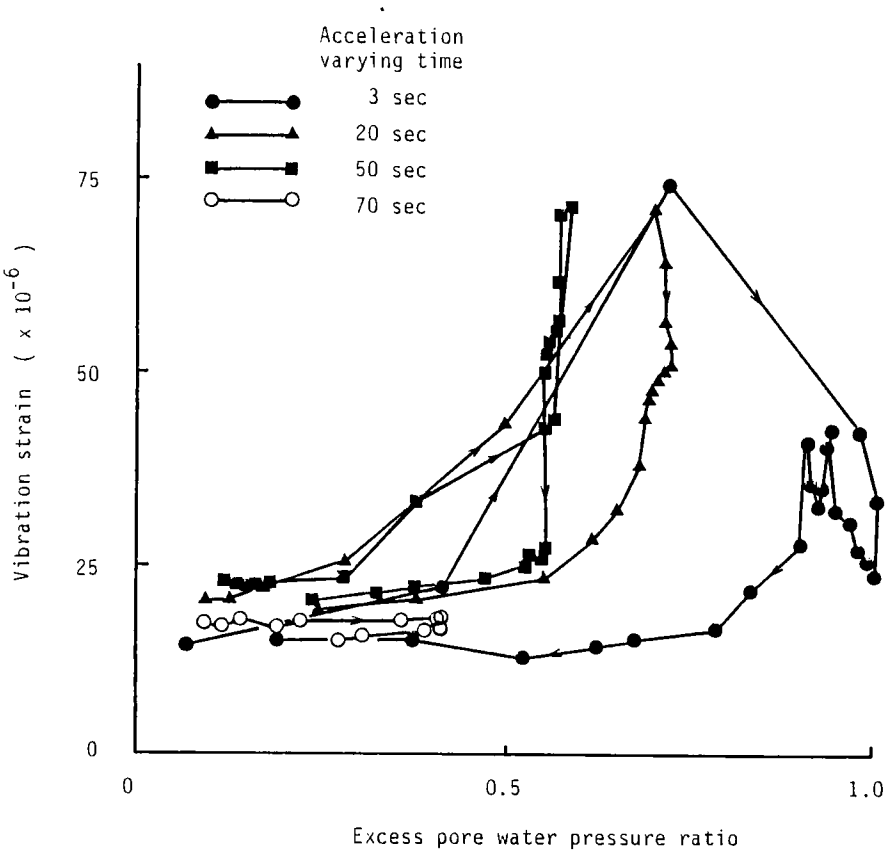

Fig. 3.17 Relationship between excess pore water pressure ratio and vibrating strain.

because the maximum values of that were 0.71, 0.59 and 0.43, respectively. The vibration strains took the maximum value when the excess pore water pressure ratio was 0.5 to 0.9. The periods when the vibration strains became more than 50 $x10^{-6}$ were about 8 sec in duration when there were the acceleration varying times of 20 sec and 50 sec. While the line of the acceleration varying time of 3 sec was about 1 sec in duration. The value of 50 $x10^{-6}$ means relatively great vibration strain in these experiments. Fig. 3.17 suggests that the period when the vibration strains become great coincides with that when the excess pore water pressure ratio is 0.5 to 0.9, that is, when the model ground incompletely liquefies. These results confirm that the longer the period of the incomplete liquefaction of the ground, the longer the period of great vibration strains.

3.3.4 Strain Characteristics of Pipelines in Saturated Sand Stratum

The experimental results described above revealed that high pipe strains occur when the excess pore water pressure rises and falls; that is, the model ground is incompletely liquefied. It has been reported that the great dynamic response of a buried structure is temporarily caused during liquefaction by reduction of strength of the sand stratum and the resonance of a buried structure [1), 6)]. It is, however, important to consider the effects of slippage between the buried pipe and the surrounding soil. Three generation factors of vibration strains are considered here:

(1) Degree of transmission of ground vibration through a model ground.
(2) Degree of transmission of ground strains to a pipe.
(3) Flexibility of a system consisting of a pipe and surrounding ground.

Ground vibration can not be almost transmitted in completely liquefied ground because the model ground responds just like liquid. This effect is considered in factor (1). The slippage between the buried pipe and surrounding soil is considered in factor (2). In factor (3), the change in the flexibility of the system during softening the ground and resonance of the system are considered.

At first, changes in the natural frequency of model ground in the liquefaction process were investigated in order to consider the

resonance of the system. The dynamic amplitude of the excess pore water pressure shown in Fig. 3.18 was observed in cases of various excitation frequencies, because it indicated the degree of the shearing deformation of the model ground in the dissipating process of liquefaction. Fig. 3.19 shows the relationship between the excitation frequency and excess pore water pressure ratio, when the dynamic amplitude of the excess pore water pressure is at maximum in each excitation frequency. Only the dissipating process of liquefaction is taken up in Fig. 3.19. It can be seen from this graph that the excess pore water pressure ratio increases with a decrease in the excitation

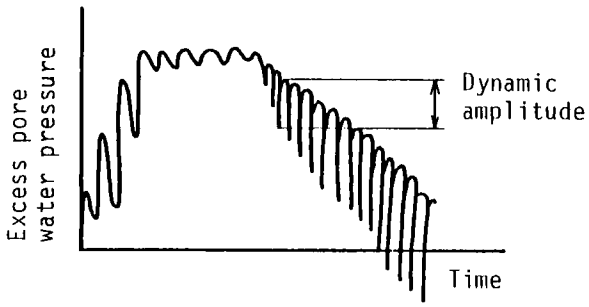

Fig. 3.18 Schematic diagram of record of excess pore water pressure.

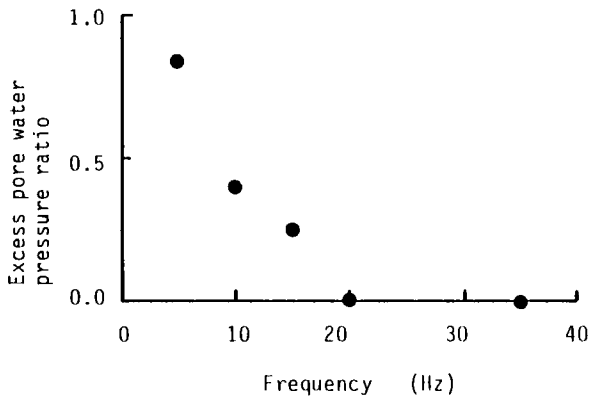

Fig. 3.19 Relationship between predominant frequency of model ground and excess pore water pressure ratio.

frequency except for the region near to 0 Hz.. This suggests that the natural frequency of the model ground decreases as the excess pore water pressure ratio increases, and it becomes less than 5 Hz upon complete liquefaction. The relationship between the dynamic amplitude of the excess pore water pressure and shearing deformation of the model ground at the stage of rising excess pore water pressure is not clear; however it is conceivable that the natural frequency of the model ground could decrease as the excess pore water pressure ratio increases in all stages of the liquefaction process.

If coefficient of friction is constant, the frictional force between the pipe and surrounding soil is approximately in proportion to the effective stress in the liquefaction process. Since the degree of transmission of ground strains to the pipe is proportional to the frictional force, the degree of transmission of ground strains to the pipe is approximately in proportion to the value of $(1 - r)$, r denotes the excess pore water pressure ratio. Providing that the degree of the transmission of the ground strains to the pipe is 1.0 before excitation, the generation factor of the vibration strains (2) can be assumed as shown in Fig. 3.20 (a). Generation factor (1) tends to correspond to Fig. 3.20 (b), on the assumption that the degree of the transmission of the ground vibration through the model ground is in proportion to the effective stress. Generation factor (3), in Fig. 3.20 (c) shows how the flexibility of the system is proportional to the degree of liquefaction. The resonance of the system, however, is not considered in Fig. 3.20 (c). It is described later.

The relationship between the degree of the excess pore water pressure ratio and degree of the pipe strains is shown in Fig. 3.20 (d) on the assumption that the degree of the vibration strain during liquefaction can be obtained as the product of the three factors (1), (2) and (3) as mentioned at the beginning of Chapter 3.3.4. This figure agrees with the experimental finding that peak vibration strains occur when the excess pore water pressure rises and falls. However, according to Fig. 3.17 the vibration strain rose to the maximum value at an excess pore water pressure ratio between 0.5 and 0.9; that does not agree with Fig. 3.20 (d) which indicates the maximum at that of 0.33. This may be explained in terms of resonance of the system. As shown in Fig. 3.19, the natural frequency of the model ground seems to

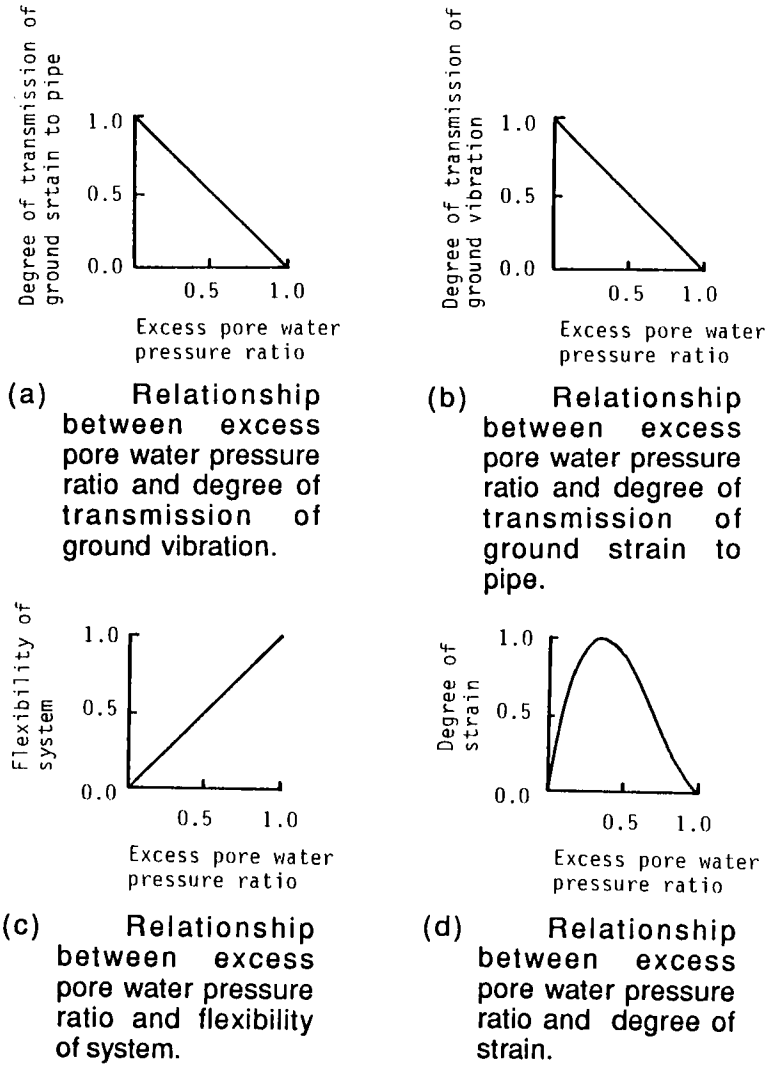

(a) Relationship between excess pore water pressure ratio and degree of transmission of ground vibration.

(b) Relationship between excess pore water pressure ratio and degree of transmission of ground strain to pipe.

(c) Relationship between excess pore water pressure ratio and flexibility of system.

(d) Relationship between excess pore water pressure ratio and degree of strain.

Fig. 3.20 Relationships between degree of strains and excess pore water pressure ratio.

coincide with 5 Hz when the excess pore water pressure ratio is about 0.8. Therefore, the degree of strain could be larger at the excess pore water pressure ratio of 0.5 to 0.9 than that at the ratio of 0.33. The pipe reaches its most vulnerable state when the excitation frequency coincides with the natural frequency of the model ground at an excess pore water pressure ratio of 0.33, which corresponds with that of the

maximum degree of strain in Fig. 3.20 (d). The natural frequency corresponding with the excess pore water pressure of 0.33 is about 10 Hz in Fig. 3.19. The pipe, therefore, becomes most vulnerable when it is excited by a wave of about 10 Hz in this case. This qualitatively agrees with the experimental results; however clarification of the quantitative relationship between excess pore water pressure ratio and three generation factors awaits future research.

3.4 Conclusions

From the results of the experiments in this chapter, the following conclusions have been derived

(1) Peak strains are caused when the excess pore water pressure rises and falls.

(2) The pipe strains should be classified according to the mechanism of generation: vibration strains which indicate pipe vibration, and accumulated residual strains which indicate the pipe bending due to uplift. Modes of pipe failure induced by the former is different from the latter.

(3) The vibration strain peaks when the excess pore water pressure ratio is between 0.5 and 0.9 during liquefaction process. The longer the period of incomplete liquefaction remains, the longer that of great vibration strain is.

(4) A conceptual model of the generation factors should include not only the resonance of the system by an external exciting force, but also the degree of transmission of the ground vibration through the model ground, the degree of transmission of ground strain to the pipe, and flexibility of the system.

(5) On the assumption that the degree of the vibration strain during liquefaction could be obtained as the product of these factors, the experimental results in this chapter can be well accounted for.

Finally, although some fundamental characteristics of pipe behavior were described in this chapter, they were not evaluated quantitatively in comparison with the behavior of pipeline prototypes. It is in importance to provide evidence of a valid coherence between experimental models and prototypes of the pipeline and ground, though

complete satisfaction is of course almost impossible to attain [7]. However, different approaches such as theoretical work and field observations should be carried out in addition.

References (Publications written in Japanese are so indicated; all others are in English)

1) Katada, T. and Hakuno, M. : Experimental Analysis on the Dynamic Behavior of Underground Structures in the Liquefaction Process, Proceedings of Japan Soc. Civil Eng., No. 306, pp. 1-10, 1981 (in Japanese).
2) Takada, S., Tanabe, K., Yamajyo, K. and Katagiri, S. : Liquefaction Analysis for Buried Pipelines, Structure and Stochastic Methods, Developments in Geotechnical Engineering, Computational Mechanics Publications, Vol. 45, pp. 319-333, 1987.
3) Kuribayashi, E., Kawamura, M., Ieda, R., Aida, M. and Yuri, Y.: An Experimental Behavior of Buried Pipes During Liquefaction of Saturated Sandy Soil, Proceedings. of the PVP Conference, ASME, Vol. 98-4, pp. 19-24, 1985.
4) Kitaura, M. and Miyajima, M. : Experimental Study on Strain Characteristics of Underground Pipe During Liquefaction, Proceedings of Japan Soc. Civil Eng., No. 323, pp. 43-53, 1982 (in Japanese).
5) Kitaura, M., Miyajima, M. and Yoshioka, M.: Dynamic Behavior of Buried Model Pipe During Incomplete Liquefaction, Journal of Structural Engineering, Japan Soc. Civil Eng., Vol. 31A, pp. 421-426, 1985 (in Japanese).
6) Yoshida, T. and Uematsu, M.: Dynamic Behavior of a Pile in Liquefaction Sand, Proceedings of the 5th Japan Earthquake Engineering Symposium-1987, pp. 657-663, 1987 (in Japanese)
7) Yoshimi, Y. and Tokimatsu, K.: Liquefaction of Sand near Structures During Earthquakes, Proceedings of the 4th Japan Earthquake Engineering Symposium-1975, pp. 439-446, 1975 (in Japanese).

4. ANALYSIS OF BURIED PIPELINES' RESPONSE IN PROCESS OF LIQUEFACTION

4.1 General Remarks

A survey of the damage following the 1983 Nihonkai-Chubu Earthquake revealed that a high damage ratio appeared in the areas where the ground water table was 2 m to 4 m in depth as mentioned in Chapter 2. Generally, the burial depths of water supply pipelines are 1.2 m to 1.5 m. The facts suggest that the pipelines buried in an unsaturated sand layer before the earthquake were damaged due to soil liquefaction as a result of that earthquake. It is, therefore, important to evaluate the response of such pipelines in process of liquefaction, including the rise of the ground water table. As mentioned in the previous chapters, the factors of the pipe failures are considered as follows: (1) Transient large displacement of the ground surrounding the pipelines when the sand layer under or near the pipelines is incompletely liquefied (the excess pore water pressure ratio is near 1.0). (2) Buoyancy effect when the surrounding ground is completely liquefied (the excess pore water pressure ratio is 1.0). (3) Liquefaction-induced permanent ground displacement. The effects of factors (1) and (2) are investigated in this chapter. Factor (3) will be described in Chapters 5 and 6.

Two different approaches have been taken regarding dissipation of the excess pore water pressure. One is based on a use of the Terzaghi's consolidation equation [1), 2)]. The other is based on the Biot theory for a consolidation and a energy balance equation [3), 4)]. Both approaches, however, do not allow for a seepage of the pore water to previously unsaturated areas. On the other hand, many analytical works on the embedded pipe response have been accomplished [5)-8)]. Only recently research has begun that deals with liquefaction-induced damage to pipelines [9)-11)].

In this chapter, a hybrid procedure is proposed to analyze the behavior of the buried pipelines in process of liquefaction. This

procedure consists of a ground response evaluation using the finite element method and a pipe response analysis using the transfer matrix method. In the following Chapter 4.2, a procedure is introduced to analyze ground response considering a rise of the ground water table induced by dissipation of excess pore water pressure. A procedure to analyze pipeline response is described in Chapter 4.3. Practical application of these formulae to existing ground shows that an unsaturated sand layer around the pipelines liquefies due to the rise of the ground water table and subsequent accumulation of the excess pore water pressure. Using the results of the ground response evaluation, a response simulation of embedded pipelines is carried out in Chapter 4.4. The contents of this chapter were based on material found in references 12-15.

4.2 A Procedure to Analyze Seismic Ground Response Considering Rise in Ground Water Table

4.2.1 Dissipation of Excess Pore Water Pressure Considering Permeation to Unsaturated Areas

The equations of seepage in saturated-unsaturated porous media are given in Reference. 16. Applying the equation of motion concerning a system of solid, liquid and gaseous phases and neglecting the gaseous phase, the conservation of mass in the field of the fluid is then given by the following equation [16]:

$$\text{div}\, q_r + n \frac{\partial S_r}{\partial t} + \kappa_w \theta \frac{\partial U_w}{\partial t} + S_r \frac{\partial \varepsilon}{\partial t} = 0 \tag{4.1}$$

in which q_r represents the relative specific volume discharge of liquid phase to solid phase, n = porosity, S_r = degree of saturation, θ = volumetric moisture content, κ_w = water compressibility, U_w = pore water pressure, ε = volumetric strain, t = time. The left hand side's first term represents the transfer of excess pore water and the second, third and fourth terms explain the storage due to the change of the degree of saturation, water compressibility and volume change of soil, respectively. Neglecting the compressibility of the pore water and the

soil, also the change in soil volume and applying Darcy's law to the systems, the equations of seepage in saturated-unsaturated porous media are:

$$\frac{\partial h_p}{\partial t} = \frac{1}{\alpha\ \gamma_w} \{ \frac{\partial}{\partial x} (k_x \frac{\partial h}{\partial x}) + \frac{\partial}{\partial y} (k_y \frac{\partial h}{\partial y}) + \frac{\partial}{\partial z} (k_z \frac{\partial h}{\partial z}) \} \tag{4.2}$$

$$\frac{\partial h_p}{\partial t} = \frac{1}{c} \{ \frac{\partial}{\partial x} (k_x{}^* \frac{\partial h}{\partial x}) + \frac{\partial}{\partial y} (k_y{}^* \frac{\partial h}{\partial y}) + \frac{\partial}{\partial z} (k_z{}^* \frac{\partial h}{\partial z}) \} \tag{4.3}$$

in which h = total head, h_p= pressure head, $k_{x,y,z}$ = coefficients of permeability in the saturated region, $k^*_{x,y,z}$ = coefficients of permeability in the unsaturated region, α = soil compressibility, c = specific moisture capacity, γ_w= unit weight of water. Subscripts x, y and z denote Cartesian coordinates. The specific moisture capacity and coefficient of permeability in the unsaturated region are indicated as follows by Brooks and Corey [17].

$$\frac{k^*}{k} = (\frac{P_b}{S})^{3\lambda + 2} \tag{4.4}$$

$$c = \frac{\partial \theta}{\partial h_p} = \lambda (n - \theta_r) \frac{P_b{}^{\lambda}}{S^{\lambda + 1}} \tag{4.5}$$

Here θ_r = volumetric moisture content in the state of constant water content, P_b, = bubbling pressure, S = suction, λ = pore size distribution index.

4.2.2 Accumulation of Excess Pore Water Pressure

The model of the pore water pressure generated during an earthquake proposed by Martin, Finn and Seed [18] is used in the present study. The rise of the pore water pressure Δu , caused in a cycle of shear strain during test of an undrained soil sample is given by

$$\Delta u = \overline{E_r}\ \Delta \varepsilon_{vd} \tag{4.6}$$

n which $\overline{E_r}$ is the one dimensional rebound modulus of the sand at an effective stress σ_v' and $\Delta \varepsilon_{vd}$ = the potential volumetric strain change associated with γ. The relationship between the total accumulated volumetric strain $\Delta \varepsilon_{vd}$ and the shear strain amplitude γ. has been demonstrated by Martin, Finn and Seed [18].

$$\Delta \varepsilon_{vd} = c_1 \left(\gamma - c_2 \varepsilon_{vd} \right) + \frac{c_3 \varepsilon_{vd}^2}{\gamma + c_4 \varepsilon_{vd}} \tag{4.7}$$

For crystal silica sand with a relative density $D_r = 45\%$, $c_1 = 0.80$, $c_2 = 0.79$, $c_3 = 0.45$ and $c_4 = 0.73$ and $\Delta \varepsilon_{vd}$, ε_{vd}, γ expressed in percentages, the volume change at another relative density is obtained from

$$\Delta \varepsilon_{vd} \mid_{D_r = \alpha} = \Delta \varepsilon_{vd} \mid_{D_r = 45} R \tag{4.8}$$

$$R = 0.0003 \left(100 - \alpha \right)^2 + 0.062 \tag{4.9}$$

in which D_r indicates the relative density and $\Delta \varepsilon_{vd} \mid_{D_r = \alpha}$ is the volumetric strain change in case of a relative density of α %. The rebound modulus E_r at any effective stress level σ_v' is given by the next equation.

$$\overline{E_r} = \frac{\left(\sigma_v' \right)^{1-m}}{m \, k_2 \left(\sigma_{v\,0}' \right)^{n-m}} \tag{4.10}$$

in which $\sigma_{v\,0}'$ = the initial effective stress, and m, n and k_2 are experimental constants. For the crystal silica sand at $D_r = 45\%$, these values are given as follows: $k_2 = 0.0025$, $m = 0.43$ and $n = 0.62$.

4.2.3 Non-linear Model of Soil

The variation of the shear modulus due to the magnitude of strain is described by Hardin and Drnevich [19]

$$G = G_0 \frac{\gamma_m}{\gamma_m + \gamma} \tag{4.11}$$

Here G_0 = initial shear modulus, γ = shear stress and γ_m = reference strain ($\gamma_m = \tau_m / G_0$, τ_m = shear stress at failure). In the present study a hyperbolic stress-strain hysteresis curve is not used; a simplified linear stress-strain relation has been substituted because the shear modulus is constant during one cycle of deformation and then the change of the excess pore water pressure is evaluated and the shear modulus is computed by factoring Eqs. 4.12 and 4.13 into Eq. 4.11.

$$G_0 = (G_0)_{\sigma_{v0}'} \left(\frac{\sigma_v'}{\sigma_{v0}'}\right)^{\frac{1}{2}} \tag{4.12}$$

$$\gamma_m = (\gamma_m)_{\sigma_{v0}'} \left(\frac{\sigma_v'}{\sigma_{v0}'}\right)^{\frac{1}{2}} \tag{4.13}$$

In these equations σ_{v0}' = initial effective confining stress, σ_v' = effective confining stress at any cycle of shear stress. These equations mean that the shear modulus and reference strain are proportional to the root of the change ratio of the vertical confining stress [20].

Concerning damping ratios, the internal damping ratio h_h and the hysteretic damping ratio h_h are considered in this analysis. The hysteretic damping ratio is presented as follows, using the Hardin and Drnevich model.

$$h_h = h_{\max} \frac{\gamma_m}{\gamma_m + \gamma} \tag{4.14}$$

Here $h_{\max}$ is the maximum value of the hysteretic damping ratio. γ_m is calculated by Eq. 4.13. The internal damping ratio h_h is given by

$$\begin{aligned} h_h &= 0.0002\, V_s + 0.017 \\ &= 0.0002 \sqrt{\frac{G}{\rho}} + 0.017 \end{aligned} \tag{4.15}$$

in Eq. 4.15 V_s = velocity of the shear wave (m/s) and ρ = density of the ground [21]. G is shear modulus calculated by Eq. 4.11. In order to control the stability of the calculation, it is assumed that the shear modulus is not less than 1% of the initial value [22].

4.2.4 Procedure for Computing Ground Response

Fig. 4.1 shows the flow chart of the response analysis presented herein. The analysis of the ground response is performed using the finite element method. The procedure for evaluating generation and dissipation of the pore water pressure is as follows:

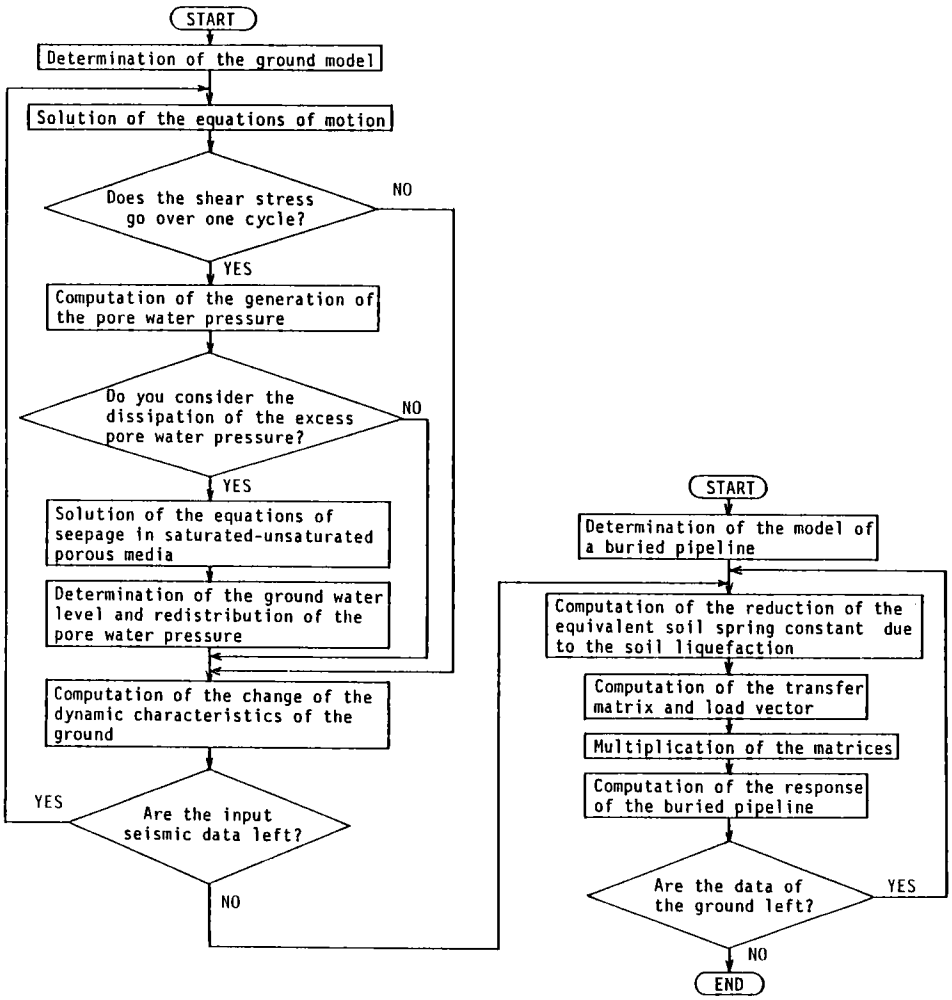

Fig. 4.1 Simulation flow chart.

1. Compute generation of he pore water pressure by means of the equations used by Martin, Finn and Seed.
2. Evaluate dissipation of the pore water pressure by using the equations of seepage in saturated-unsaturated porous media (Eqs. 4.2 and 4.3).
3. Determine the pore water pressure at any depth combining 1. and 2.
4. Determine the ground water table. The depth where the pore water pressure is zero is the ground water table.
5. Based on the ground water table, determine the distribution of the excess pore water pressure at the respective time interval.

This process is repeated at each cycle of shear strain. A procedure to analyze pipeline response in this figure is described in the following Chapter 4.3.

4.3 A Procedure to Analyze Pipeline Response

4.3.1 Analytical Model for Buried Pipelines

Analytical models are constructed under the following assumptions:

(1) Quasi-static analysis can be applied, i.e. the effects of inertia force and damping are assumed to be negligible.
(2) Buried pipelines are treated as a series of beams constructed of a material that has an elastic nature. These beams are connected longitudinally with joints which function as a spring for both axial and bending motions.
(3) Seismic forces, generated by soil deformation relative to the pipe motion, act on the pipe body through the soil spring and buoyancy effect due to liquefaction acting directly on the pipe body
(4) The pipe motion is analyzed within a two dimensional horizontal plane, and a perfect elastic behavior is assumed for the pipe material.

Fig. 4.2 shows a analytical model of buried pipelines. Let u and v be the longitudinal and transverse displacements of the pipe, and U and V be those of the free field, respectively. Then, the basic differential equations governing the motion of a buried pipe can be established as follows:

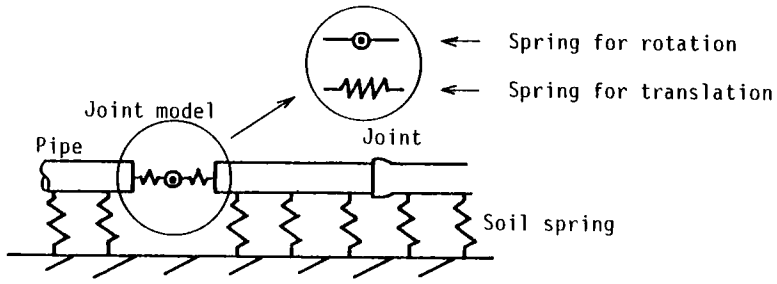

Fig. 4.2 Analytical model.

$$-EA\ \frac{d^2u}{dx^2} = K_u\ (U - u) \tag{4.16}$$

$$EI\ \frac{d^4v}{dx^4} = K_v\ (V - v) + F \tag{4.17}$$

where E = Young's modulus of the pipe material, A = cross-sectional area of the pipe, I = area moment of inertia of the pipe, K_u , K_v = equivalent spring constants for the longitudinal and transverse motions, which reflect the soil-structure interaction, F = a force caused by the buoyancy effect and groundwater flow during soil liquefaction, respectively.

4.3.2 A Modified Transfer Matrix Method for Analyzing Response of Buried Pipelines

In order to solve the basic differential equations, a modified transfer matrix method which improves round off errors presented by Nakamura [23] is employed here. This method is mentioned briefly in this section.

In this method, the relationship of physical quantities between two points is transferred. There are an even number of physical quantities (2n) at each point. They are divided into two vectors of n members; y, z. The following equation is formed in relation to y and z.

$$\begin{aligned} \vec{\alpha}\ \vec{y} + \vec{\beta}\ \vec{z} &= \vec{\gamma} \\ \leftarrow\quad \leftarrow\quad \leftarrow & \\ \alpha\ y + \beta\ z &= \gamma \end{aligned} \tag{4.18}$$

In these equations, α , β are matrices of n x n and γ is vector of n. $\leftarrow$ denotes transfer from the right side to the left side and $\rightarrow$ means transfer in the reverse direction.

Simply stated, the technique is described by using a differential equation as follows:

$$\frac{dY}{dx} = A\ Y + Q\ (x\ ) \tag{4.19}$$

Here Y is an unknown vector of physical quantity (2n), A is a coefficient matrix (2n x 2n) and Q is a load vector (2n). A general solution of Eq. 4.19 can be expressed as:

$$Y\ (x\ ) = e^{Ax}\ Y\ (0) + e^{Ax} \int_0^x e^{-As}\ Q\ (s\ )\ ds \tag{4.20}$$

The recurrence formula of Eq. 4.20 can be expressed as:

$$Y(x + \Delta x\ ) = e^{A\Delta x} Y\ (x\ ) + e^{A\Delta x} \int_0^{\Delta x} e^{-As}\ Q\ (x + s\ )\ ds \tag{4.21}$$

New relationships defined by the following equations are introduced here:

$$Y = \left\{ \begin{matrix} y \\ z \end{matrix} \right\} \tag{4.22}$$

$$e^{A\Delta x} = \left[\begin{matrix} A\ (\Delta x\ ) & B\ (\Delta x\ ) \\ C\ (\Delta x\ ) & D\ (\Delta x\ ) \end{matrix} \right] \tag{4.23}$$

$$\int_0^{\Delta x} e^{-As}\ Q\ (x + s\ )ds = \left\{ \begin{matrix} q\ (x\ ) \\ r\ (x\ ) \end{matrix} \right\} \tag{4.24}$$

in these equations y and z are unknown vectors of physical quantity (n), $A\ (\Delta x\ )$,$B\ (\Delta x\ )$,$C\ (\Delta x\ )$ and $D\ (\Delta x\ )$ are matrices of n x n, $q(x\ )$,$r(x\ )$

are vectors of n, respectively. Eq. 4.21 is rearranged by substituting Eqs. 4.22, 23, 24 and multiplying e $A\Delta x$ on both sides.

$$\begin{bmatrix} A\ (-\Delta x\ ) & B\ (-\Delta x\ ) \\ C\ (-\Delta x\ ) & D\ (-\Delta x\ ) \end{bmatrix} \begin{Bmatrix} y\ (x+\Delta x\ ) \\ z\ (x+\Delta x\ ) \end{Bmatrix} = \begin{Bmatrix} y\ (x\ ) \\ z\ (x\ ) \end{Bmatrix} + \begin{Bmatrix} q\ (x\ ) \\ r\ (x\ ) \end{Bmatrix} \quad (4.25)$$

Eq. 4.25 is rearranged by multiplying $[\vec{\alpha}\ (x\ )\ \vec{\beta}\ (x\ )]$ on both sides. The following equations result:

$$[\ \vec{\alpha}\ (x+\Delta x)\ \vec{\beta}\ (x+\Delta x)] = [\vec{\alpha}\ (x\ )\ \vec{\beta}\ (x\ )]\ \mathrm{e}^{-A\Delta x} \quad (4.26)$$

$$\vec{\gamma}\ (x+\Delta x) = \vec{\gamma}\ (x\ ) + [\vec{\alpha}\ (x\ )\ \vec{\beta}\ (x\ )] \begin{Bmatrix} q\ (x\ ) \\ r\ (x\ ) \end{Bmatrix} \quad (4.27)$$

In a similar way, the next equations can be formed in the reverse direction.

$$[\ \overleftarrow{\alpha}\ (x-\Delta x)\ \overleftarrow{\beta}\ (x-\Delta x)] = [\overleftarrow{\alpha}\ (x\ )\ \overleftarrow{\beta}\ (x\ )]\ \mathrm{e}^{A\Delta x} \quad (4.28)$$

$$\overleftarrow{\gamma}\ (x-\Delta x) = \overleftarrow{\gamma}\ (x\ ) + [\overleftarrow{\alpha}\ (x\ )\ \overleftarrow{\beta}\ (x\ )] \begin{Bmatrix} s\ (x\ ) \\ t\ (x\ ) \end{Bmatrix} \quad (4.29)$$

where,

$$-\int_0^{\Delta x} \mathrm{e}^{As}\ Q\ (x-s\ )\mathrm{d}s = \begin{Bmatrix} s\ (x\ ) \\ t\ (x\ ) \end{Bmatrix} \quad (4.30)$$

On the other hand, the following equation is formed at each point.

$$Y_{i,R} = K_i\ Y_{i,L} + F_i \quad (4.31)$$

Here K_i is the point matrix of n x n which includes the spring constants of joints, F_i is the load vector of 2n which includes the concentrated load acting at the point and Y is a vector indicating physical quantities. Subscripts l and r mean the left hand side and the right hand side of the point, respectively.

After the transfer of α, β and γ in both directions, the following equations are solved in order to obtain all of the physical quantities.

$$\begin{bmatrix} \overrightarrow{\alpha}_{i,L} & \overrightarrow{\beta}_{i,L} \\ \alpha_{i,L} & \beta_{i,L} \end{bmatrix} \begin{Bmatrix} y_{i,L} \\ z_{i,L} \end{Bmatrix} = \begin{Bmatrix} \overrightarrow{\gamma}_{i,L} \\ \gamma_{i,L} \end{Bmatrix}$$

$$\begin{bmatrix} \overrightarrow{\alpha}_{i,R} & \overrightarrow{\beta}_{i,R} \\ \alpha_{i,R} & \beta_{i,R} \end{bmatrix} \begin{Bmatrix} y_{i,R} \\ z_{i,R} \end{Bmatrix} = \begin{Bmatrix} \overrightarrow{\gamma}_{i,R} \\ \gamma_{i,R} \end{Bmatrix} \tag{4.32}$$

This method applies to Eqs. 4.16 and 4.17. Using the notation ' = d/dx, Eq. 4.16 can be rewritten as:

$$\frac{\mathrm{d}}{\mathrm{d}x} \begin{Bmatrix} u \\ u' \end{Bmatrix} = \begin{bmatrix} 0 & 1 \\ K_u/EA & 0 \end{bmatrix} + \begin{Bmatrix} u \\ u' \end{Bmatrix} + \begin{Bmatrix} 0 \\ -K_u/EA \end{Bmatrix} \tag{4.33}$$

The recurrence formula of Eq. 4.33 can be expressed as:

$$\begin{Bmatrix} u \\ u' \end{Bmatrix}_{x+\Delta x} = \begin{bmatrix} 1 & \Delta x \\ K_u \Delta x/EA & 1 \end{bmatrix} \begin{Bmatrix} u \\ u' \end{Bmatrix}_x + \begin{bmatrix} 1 & \Delta x \\ K_u \Delta x/EA & 1 \end{bmatrix} \int_0^{\Delta x} \begin{bmatrix} 1 & s \\ -K_u s/EA & 1 \end{bmatrix} \begin{Bmatrix} 0 \\ K_u U/EA \end{Bmatrix} \mathrm{d}s \tag{4.34}$$

In a similar way, Eq. 4.17 for the transverse motion can be rewritten as:

$$\begin{Bmatrix} v \\ v' \\ v'' \\ v''' \end{Bmatrix}_{x+\Delta x} =$$

$$\begin{bmatrix} 1 & \Delta x & \Delta x^2/2 & \Delta x^3/6 \\ 0 & 1 & \Delta x & \Delta x^2/2 \\ 0 & 0 & 1 & \Delta x \\ -K_v \Delta x /EI & 0 & 0 & 1 \end{bmatrix} \begin{Bmatrix} v \\ v' \\ v'' \\ v''' \end{Bmatrix}_x +$$

$$\begin{bmatrix} 1 & \Delta x & \Delta x^2/2 & \Delta x^3/6 \\ 0 & 1 & \Delta x & \Delta x^2/2 \\ 0 & 0 & 1 & \Delta x \\ -K_v \Delta x /EI & 0 & 0 & 1 \end{bmatrix}$$

$$\int_0^{dx} \begin{bmatrix} 1 & -s & -s^2/2 & -s^3/6 \\ 0 & 1 & -s & -s^2/2 \\ 0 & 0 & 1 & -s \\ -K_v s /EI & 0 & 0 & 1 \end{bmatrix} \begin{Bmatrix} 0 \\ 0 \\ 0 \\ (K_v V + F) /EI \end{Bmatrix} ds \tag{4.35}$$

The following equations are obtained by referring to Eqs. 4.34 and 4.35.

$$M = \begin{bmatrix} 1 & 0 & 0 & -DC & 0 & 0 \\ 0 & 1 & -D & 0 & D^2B/2 & D^3B/6 \\ 0 & 0 & 1 & 0 & -DB & -D^2B/2 \\ -DK_v & 0 & 0 & 1 & 0 & 0 \\ 0 & 0 & 0 & 0 & 1 & D \\ 0 & -DK_u & 0 & 0 & 0 & 1 \end{bmatrix} \tag{4.36}$$

Here $B = EI /E_0 I_0$, $C = EA /E_0 A_0$ and $D = dx /l_0$, K_v and K_u are non-dimensional equivalent soil spring constants, respectively. Suffix 0 denotes a standard value in each variable. M corresponds to e $A\Delta x$ shown in Eq. 4.21.

Here the buried pipelines are assumed to be connected by springs for both translational and rotational movements at the joints (See Fig. 4.2). The equilibrium equations governing the deformations and forces at the joints are also indicated in Fig. 4.3. The point matrix P corresponding to the situation defined in Fig. 4.3 can be obtained as:

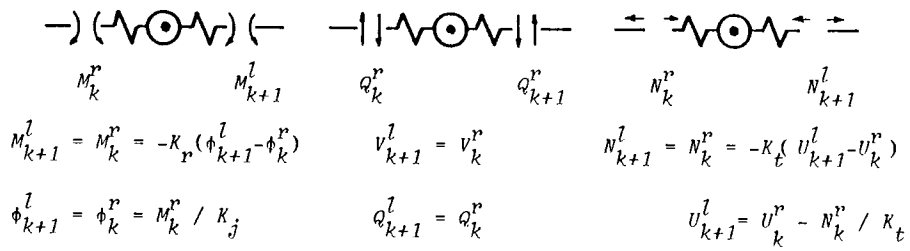

Fig. 4.3 Equilibrium equations at joint.

$$\boldsymbol{P} = \begin{bmatrix} 1 & 0 & 0 & -1/K_t & 0 & 0 \\ 0 & 1 & 0 & 0 & 0 & 0 \\ 0 & 0 & 1 & 0 & -1/K_j & 0 \\ 0 & 0 & 0 & 1 & 0 & 0 \\ 0 & 0 & 0 & 0 & 1 & 1 \\ 0 & 0 & 0 & 0 & 0 & 1 \end{bmatrix} \tag{4.37}$$

An equivalent soil spring constant in liquefaction process was proposed by Yoshida and Uematsu, Kitaura and Miyajima, Takada et al. and Yasuda et al. recently [24)-27)], however, it has not yet been established. The following empirical equation presented by Yoshida and Uematsu [24)] is used herein:

$$j = 2.81 + 528.1 / (100\, r - 291.1) \tag{4.38}$$

in which j = reduction rate of a reaction force of sand ground and r = excess pore water pressure ratio. The simulation flow chart of the pipelines is also indicated in Fig. 4.1.

4.4 Practical Application of These Formulae to Existing Ground and Pipelines

The sand deposit shown in Table 4.1 and Fig. 4.4 (model ground 1) was analyzed employing the method presented in the previous sections. The base rock motion consists of the first 30 seconds of the Taft E-W component, 1952, scaled at a maximum acceleration of 45 gal as shown in Fig. 4.5. Fig. 4.6 shows the time histories of the excess

Table 4.1 Physical properties of model ground 1.

Depth (m)	Layer number	Unit weight (tf/m^3)	Initial effective stress (kgf/cm^2)	Initial shear modulus (kgf/cm^2)	Maximum value of damping ratio	Relative density (%)	Coefficient of permeability (cm/sec)	Poisson ratio	Reference shear strain
1.0	1	1.3	0.06	690	0.20	42.1	1.0×10^{-2}	0.4	4.2×10^{-4}
2.0	2	1.3	0.19	520	0.20	42.1	1.0×10^{-2}	0.4	4.2×10^{-4}
3.5	3	1.8	0.31	460	0.20	42.1	1.0×10^{-2}	0.4	4.2×10^{-4}
5.0	4	1.8	0.43	460	0.20	52.9	1.0×10^{-2}	0.4	4.2×10^{-4}
6.5	5	1.9	0.55	1200	0.20	47.1	1.0×10^{-2}	0.4	4.2×10^{-4}
8.0	6	1.9	0.68	1500	0.20	39.4	1.0×10^{-2}	0.4	4.2×10^{-4}
10.0	7	1.9	0.84	1500	0.20	40.8	1.0×10^{-2}	0.4	4.2×10^{-4}
12.0	8	1.9	1.02	1500	0.20	80.0	1.0×10^{-2}	0.4	4.2×10^{-4}
14.0	9	1.9	1.20	1500	0.20	80.0	1.0×10^{-2}	0.4	4.2×10^{-4}
18.0	10	2.0	1.48	3200	0.25	80.0	1.0×10^{-2}	0.4	4.2×10^{-4}
20.0	11	2.1	1.78	4300	0.25	80.0	1.0×10^{-2}	0.4	4.2×10^{-4}
24.0	12	2.1	2.11	4300	0.25	80.0	1.0×10^{-2}	0.4	4.2×10^{-4}
27.0	13	2.1	2.48	4800	0.25	80.0	1.0×10^{-2}	0.4	4.2×10^{-4}
30.0	14	2.1	2.81	6400	0.25	80.0	1.0×10^{-2}	0.4	4.2×10^{-4}

($1tf/m^3 = 9.8kN/m^3$, $1kgf/cm^2 = 98kPa$)

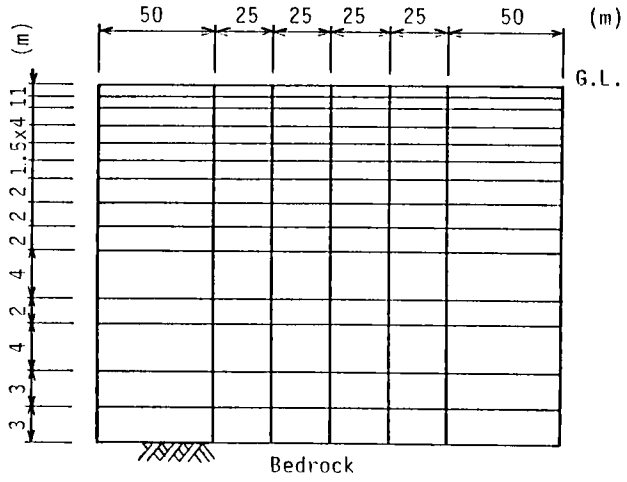

Fig. 4.4 Finite elements of the ground.

pore water pressure at the 2nd, 3rd and 4th sand layers. Fig. 4.7 illustrates the vertical distribution of the excess pore water pressure every 4 seconds of the first 20 seconds of shaking. The water table coincides with the ground surface in this case. It can be seen from these figures that the 4th layer liquefies after 13 seconds of shaking and the excess pore water pressure at the 4th layer dissipates after that. Fig. 4.8 reflects the response acceleration and response displacement at the site between the 3rd and 4th layers. The response acceleration decreases, the response displacement increases and the periods of both become long as the excess pore water pressure at the 4th layer becomes high. This agrees with the dynamic characteristics of the liquefied ground, which have been obtained from the model experiments described in Chapter 3.

Fig. 4.9 shows the response of the buried pipelines. The ductile iron pipelines with a diameter of 529 mm consisting of 20 pipes connected by 19 corresponding joints were calculated herein. These pipelines are used as a main pipeline for water supply service. The two ends of a pipeline are assumed to be fixed to buildings. The burial depth is 1.5 m. The pipeline is, therefore, buried at the 2nd layer in Fig. 4.4. The shaking direction is assumed to be parallel to the axis of

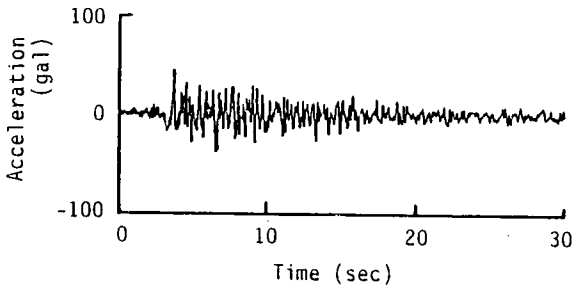

Fig. 4.5 Base motion acceleration.

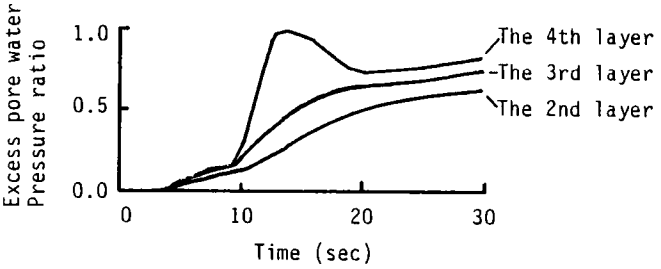

Fig. 4.6 Time histories of the excess pore water pressure
(Model ground 1 with the ground water table of 0 m).

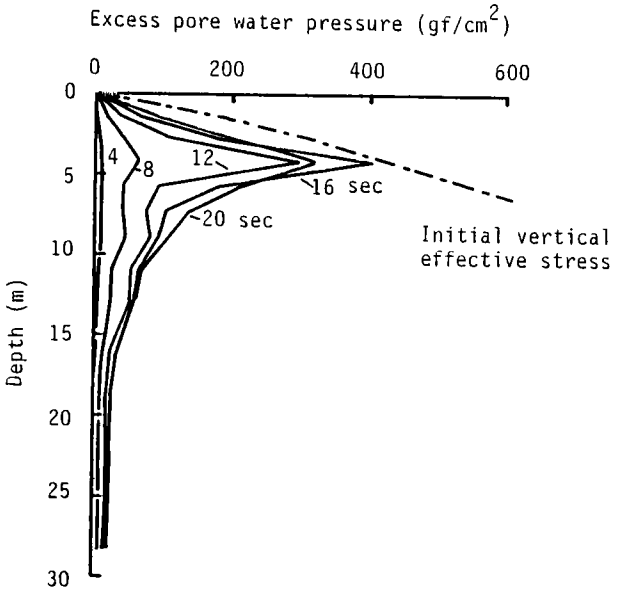

Fig. 4.7 Vertical distribution of the excess pore water pressure
(Model ground 1 with the ground water table of 0 m).

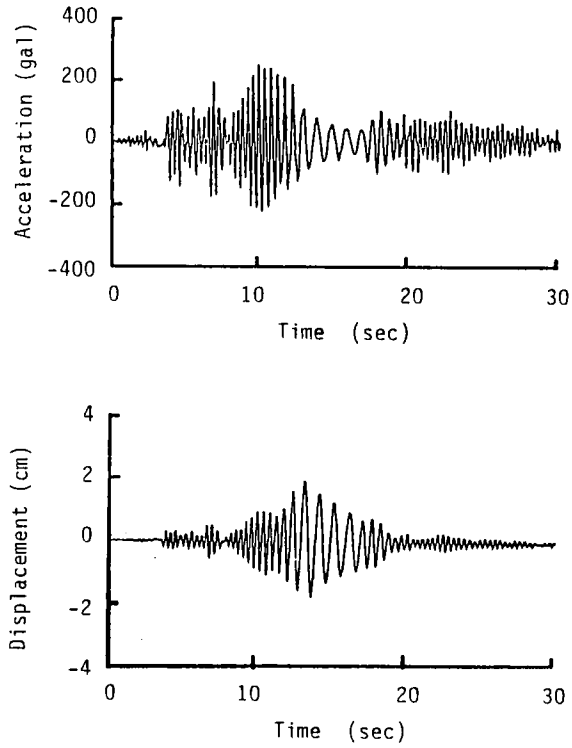

Fig. 4.8 Response ground acceleration and response ground displacement at the site between the 3rd and 4th layers.

the pipelines. Table 4.2 indicates the dimensions of the pipeline used in the analysis. Fig. 4.9 reveals that the joint displacement is large near the buildings and the maximum joint displacement is about 1.2 cm. As this value is lower than the allowable displacement of 5 cm pull-out at the joint, the pipeline does not fail at the joints. Since the surrounding soil of the pipelines did not liquefy in this example, buoyancy did not act on the pipelines.

A sand deposit which was looser than that in the previous example, shown in Table 4.3 (model ground 2) was analyzed. This

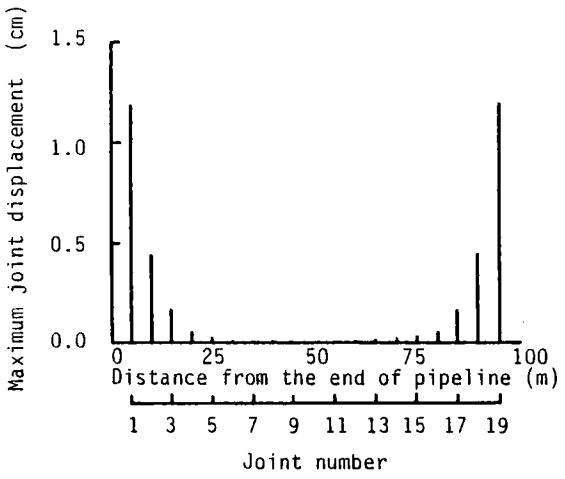

Fig. 4.9 Distribution of maximum joint displacement (Model ground 1 with ground water table of 0 m).

Table 4.2 Dimensions of the pipeline.

Ductile cast iron pipe		
Outer diameter	(mm)	529
Thickness	(mm)	9.5
Young's modulus	(kgf/cm^2)	1.6×10^6
Length	(cm)	500
Specific gravity	(gf/cm^3)	7.15
Spring constant for rotation	($kgf \cdot cm/°$)	4.9×10^5
Spring constant for translation	(kgf/cm^2)	8500

($1gf/cm^3$ =9.8kN/m^3, $1kgf/cm^2$= 98kPa)

model corresponds to the ground whose SPT blow count at the surface ground is nearly 1. Fig. 4.10 shows the time histories of the excess pore water pressure at the 2nd, 3rd and 4th sand layers. Fig. 4.11 illustrates the vertical distribution of the excess pore water pressure every 4 seconds of the first 20 seconds of shaking. These figures indicate that the 2nd and 3rd sand layers liquefy after about 5 seconds of shaking. Fig. 4.12 reflects the response acceleration and the response displacement at the site between the 1st and 2nd layers. The dynamic characteristics of the liquefied ground mentioned above

Table 4.3 Physical properties of model ground 2.

Depth (m)	Layer number	Initial shear modulus (kgf/cm^2)
1.0	1	60
2.0	2	60
3.5	3	100
5.0	4	300
6.5	5	700
8.0	6	1000

Other conditions are the same as those in Table 4.1.

($1kgf/cm^2$ = 98kPa)

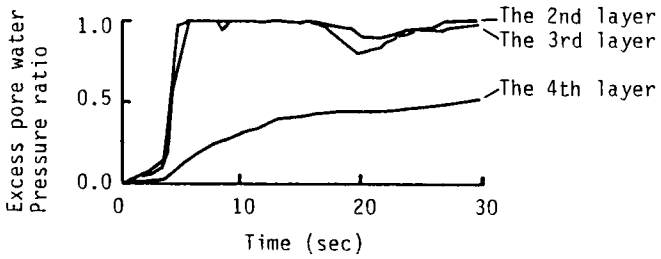

Fig. 4.10 Time histories of the excess pore water pressure (Model ground 2 with the ground water table of 0 m).

appears in this figure. Since the duration of the liquefaction is longer than that in the former example, the duration of the great response displacement and the small response acceleration are longer than those in Fig. 4.8. Fig. 4.13 shows the maximum joint displacement of the buried pipelines. This figure indicates that the tendency of the pipelines' response is similar in the former example, however, the magnitude of the response joint displacement is less than that in the former example. This can be explained in terms of the relationship between the magnitude of the response ground displacement and the soil

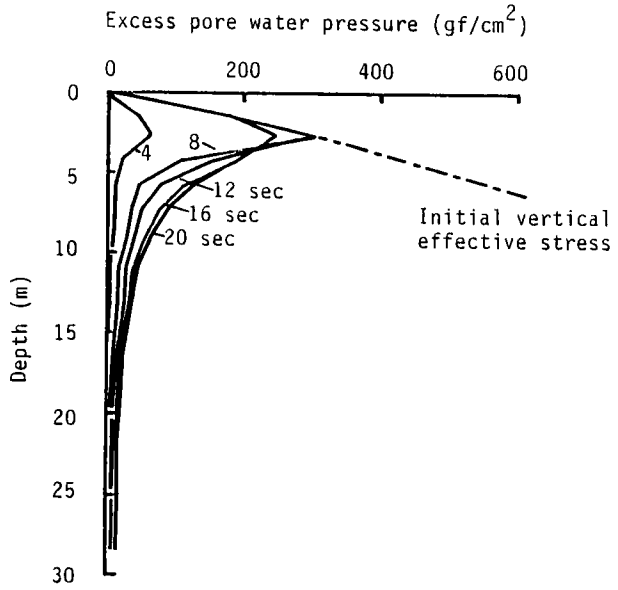

Fig. 4.11 Vertical distribution of the excess pore water pressure (Model ground 2 with the ground water table of 0 m).

spring constants. The force induced by ground vibration is estimated as the product of the response ground displacement and the soil spring constant in this study. Since the surrounding soil of the pipelines in this example is looser than that in the former example, the soil spring constant is much smaller. Therefore, the force induced by ground vibration is smaller than that in the former example despite greater response ground displacement. Fig. 4.14 illustrates the displacement angle at joints. In this case, the buoyancy acting on the pipelines caused the displacement angle at the joint because the surrounding soil was completely liquefied. This did not occur in the former example and it was one of the characteristics of pipe behavior in the liquefied ground. It can be seen from this figure that the displacement angle at joints near a building is large, with a maximum value of 0.3°. The probability of

joint failure is small in this example because the allowable displacement angle at such a joint is 7°.

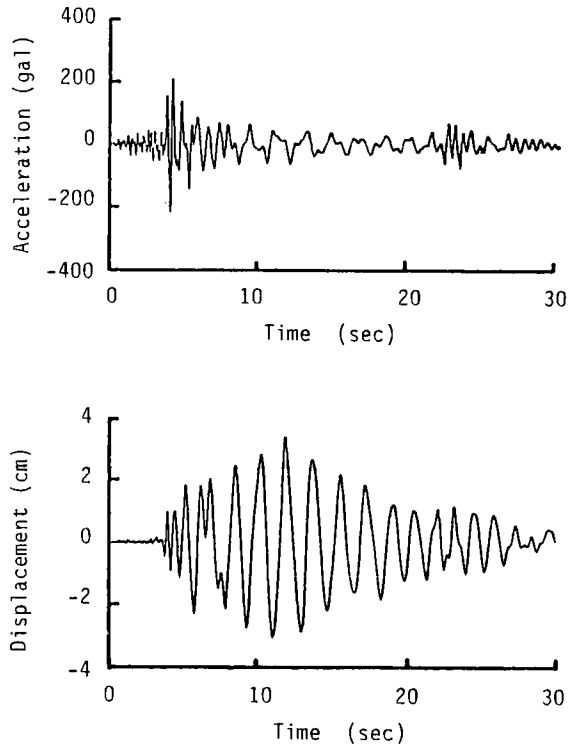

Fig. 4.12 Response ground acceleration and response ground displacement at the site between the 1st and 2nd layers.

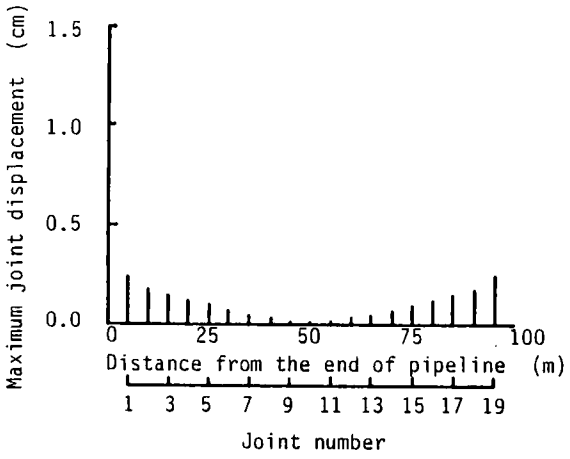

Fig. 4.13 Distribution of maximum joint displacement (Model ground 2 with the ground water table of 0 m).

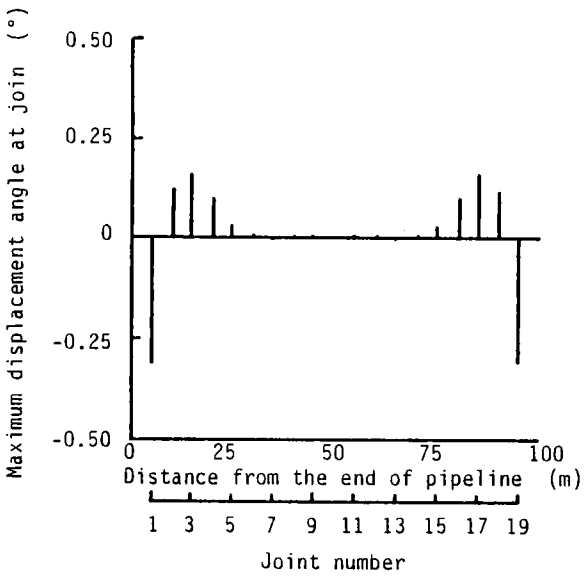

Fig. 4.14 Distribution of maximum displacement angle at joint (Model ground 2 with the ground water table of 0 m).

Next, the model ground 1 with the ground water table of 2 m was analyzed. Fig. 4.15 shows the time histories of the excess pore water pressure at the 4th sand layer, considering rise of ground water table. The results of the different methods are also shown in this figure. The excess pore water pressure ratio increases to 1.0 in the method neglecting dissipation of the pore water pressure. It is about twice as much as the results obtained when considering the dissipation. Fig. 4.16 indicates the time history of the ground water table. Figs. 4.15

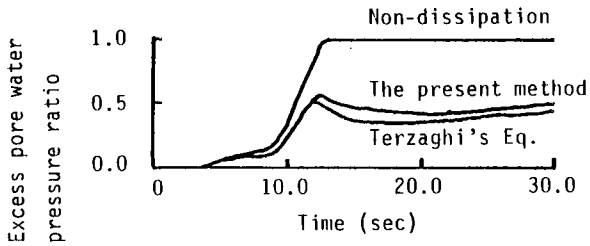

Fig. 4.16 Time history of the ground water table (Model ground 1 with the ground water table of 2 m).

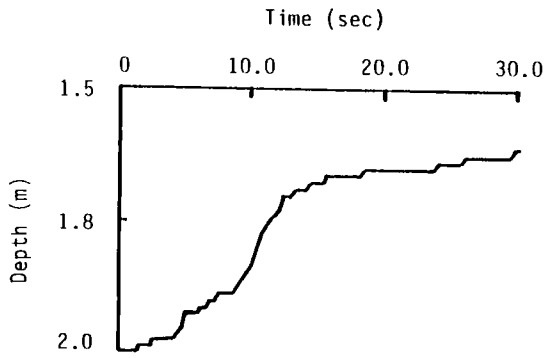

Fig. 4.15 Time histories of the excess pore water pressure.

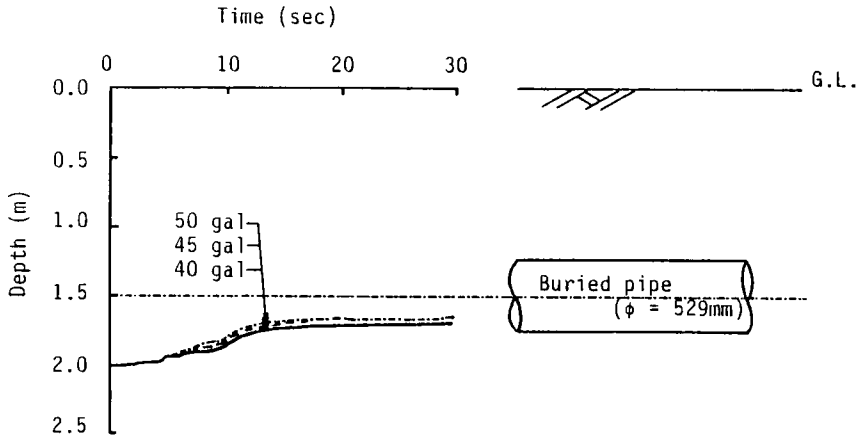

Fig. 4.17 Rise of the ground water table and location of the buried pipe (Model ground 1 with the ground water table of 2 m).

and 4.16 suggest that the ground water table rises when the excess pore water pressure rapidly increases at the 4th sand layer, located under the ground water table. Fig. 4.17 shows the time history of the ground water table in relation to the location of the embedded pipelines in case of 40 gal, 45 gal and 50 gal maximum base motion acceleration. The surrounding soil is not saturated and does not liquefy after the rise of the ground water table in these examples. Fig. 4.18 shows the response of the buried pipelines for a maximum base motion acceleration of 45 gal. This figure reveals that the joint displacement is large near the buildings and the maximum joint displacement is about 0.8 cm. Maximum joint displacement smaller than that in Fig. 4.9 can be explained in terms of smaller ground displacement because of no liquefaction in this example.

Fig. 4.19 indicates the time histories of the ground water table in relation to the location of the buried pipelines for model ground 2 with the ground water table of 2 m. This figure reveals that the surrounding soil becomes saturated due to the rise of the ground water table. The response of buried pipelines is shown in Figs. 4.20 and 4.21, for a maximum base motion acceleration of 45 gal. These figures indicate the maximum joint displacement and the maximum displacement angle at joints, respectively. Fig. 4.20 indicates the large joint displacements

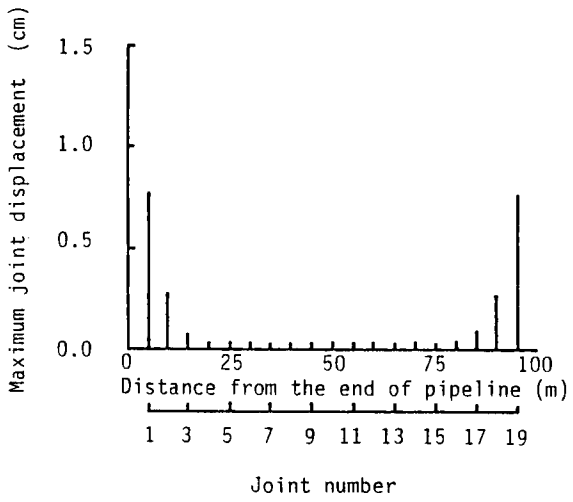

Fig. 4.18 Distribution of maximum joint displacement (Model ground 1 with the ground water table of 2 m).

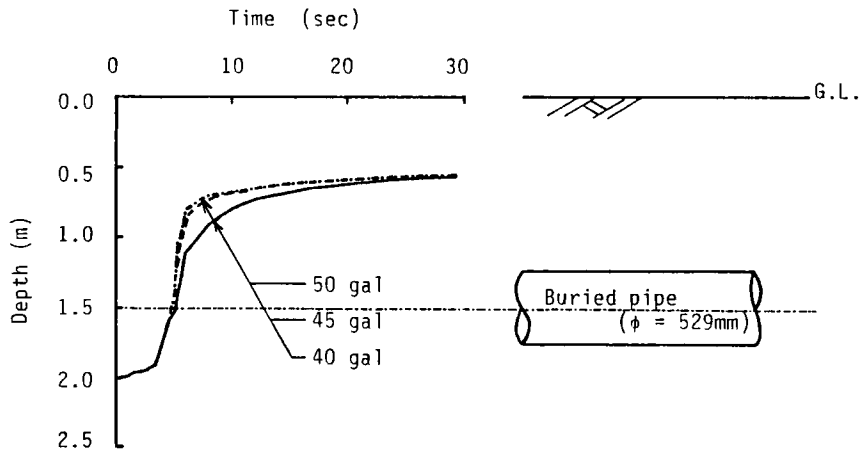

Fig. 4.19 Rise of the ground water table and location of the buried pipe (Model ground 2 with the ground water table of 2 m).

at their ends which were connected to buildings. The maximum joint displacement was, however, only about 0.5 mm. It was therefore less than that in the former example. This suggests that the higher the degree of liquefaction, the smaller the probability of the pipe's failure due to the ground vibration. While it is important to consider the buoyancy effect as the excess pore water pressure becomes high. This means that the actual cause of pipe failure changes in the liquefaction process. Therefore, countermeasures corresponding to each cause had to be provided. Fig. 4.21 indicates that the displacement angle at joints near a building is large, with a maximum value of 0.3°. The probability of joint failure is also small in this case.

According to Eq. 4.38, the soil spring constant of completely liquefied ground is 4.7 percent of the initial soil spring constant. It is, however, conceivable that the constant could be nearer to zero than that value. The equivalent soil spring constant for liquefiable ground depends on the degree of liquefaction of the soil. Takada et al., after conducting model experiments to obtain the equivalent soil spring constant of the pipeline in the liquefied ground, pointed out that the ratio of 0.1 percent to 0.3 percent seems to be an appropriate value adopted for the buried pipeline subjected to liquefaction [26]. Yasuda et al. also conducted experiments using sand box and steel pipe and concluded that critical shearing force and equivalent soil spring constant in the liquefied ground became less than 10 percent of those in the non-liquefied ground [27]. Fig. 4.22 shows the displacement of pipelines in completely liquefied ground where the soil spring constant is 0.3 percent of the initial value. The center of the pipeline almost floats to the surface of the ground. The maximum displacement angle at a joint is 2° and lower than the allowable value of 7°. The deformed pipeline as shown in this figure, however, would not be usable after an earthquake.

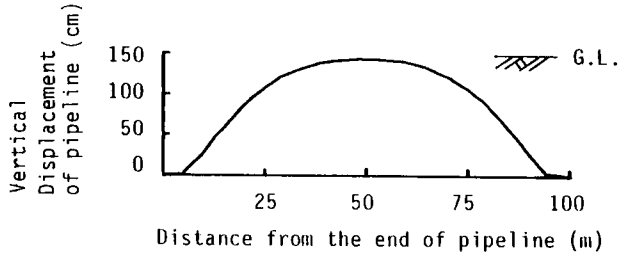

Fig. 4.22 Vertical displacement of a pipeline.

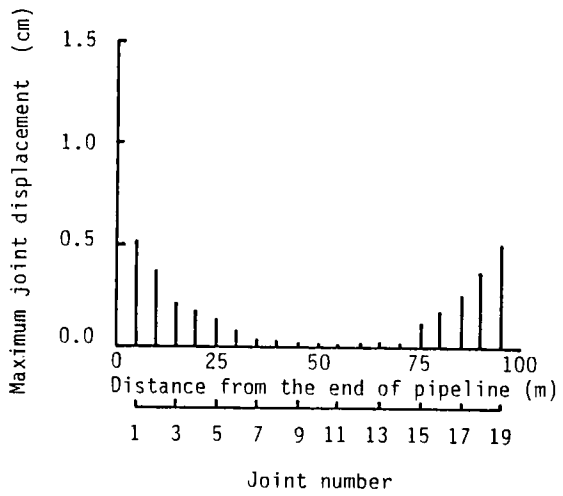

Fig. 4.20 Distribution of maximum joint displacement (Model ground 2 with the ground water table of 2 m).

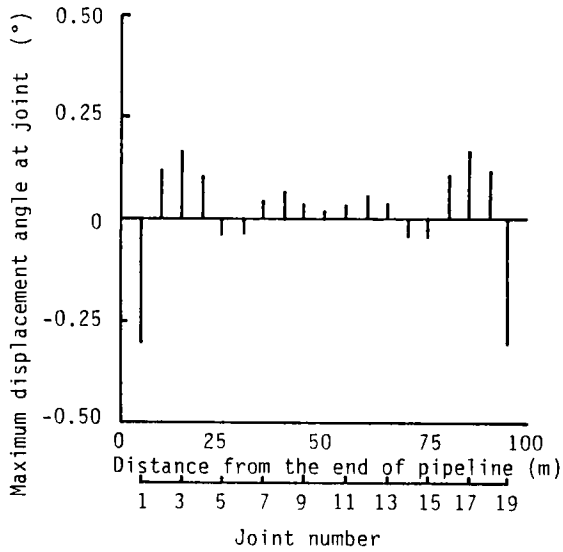

Fig. 4.21 Distribution of maximum displacement angle at joint (Model ground 2 with the ground water table of 2 m).

4.5 Conclusions

This chapter proposed a hybrid procedure to analyze the behavior of buried pipelines in process of liquefaction. Conclusions obtained from practical application to existing ground and pipelines are summarized as follows:

(1) The rise of the ground water table due to soil liquefaction can be properly evaluated by means of the method proposed in this chapter.

(2) The response of the pipelines can be investigated when the unsaturated sand layer around the pipelines liquefies, by considering the rise of the ground water table and subsequent accumulation of excess pore water pressure.

(3) It became evident from the practical application given that the response characteristics of buried pipelines change in process of liquefaction. When the excess pore water pressure is low, the effect of the ground motion on the pipelines is predominant. The higher the excess pore water pressure, the greater the buoyancy effect.

(4) It is important to assess the soil spring constant more quantitatively in order to discuss the failure of the pipelines due to the buoyancy factor present in complete liquefaction.

Finally, the failure of the pipelines to liquefaction processes could not be discussed enough in this chapter. It is explained in terms of the uniform conditions of the ground surface in these examples. For practical purposes, the dynamic response of the pipelines must be discussed on the basis of a more detailed model.

References (Publications written in Japanese are so indicated; all others are in English)

1) Finn, W. D. L., Lee, K. W. and Martin, G. R.: An Effective Stress Model for Liquefaction, Proceedings of ASCE, Vol. 103, No. GT6, pp. 517-533, 1977.
2) Seed, H. B., Martin. P, P. and Lysmer, J.: Pore-Water Pressure Changes During Soil Liquefaction, Proceedings of ASCE, Vol. 102, No. GT4, pp. 323-346, 1976.
3) Liou, C, P., Streeter, V. L. and Richart, F. E.: Numerical Model for Liquefaction, Proceedings of ASCE, Vol. 106, No. GT6, pp.589-606, 1977.
4) Oka, F., Sekiguchi, K. and Goto, H.: A Method of Analysis of Eathquake-Induced Liquefaction of Horizontally Layered Sand Deposits, Soils and Foundations, Japanese Soc. Soil Mecha. Founda. Eng., Vol. 21, No. 3, pp. 1-17, 1981.
5) Ugai, K. and Yamaguchi, H: Theoretical Research for Behavior of Buried Pipes During Earthquake, Proceedings of the Japan Earthquake Engineering Symposium-1978, pp. 433-436, 1978 (in Japanese).
6) Takada, S., Takahashi, S. and Yamabe, Y.: Seismic Response of Buried Polyvinyl Chloride Pipeline, Journal of Japan Waterworks Association, No. 547, pp. 27-39, 1980 (in Japanese).
7) Koike, T.: Estimation of Buried Pipe Strains under Seismic Risk, Proceedings of Japan Soc. Civil Eng., No. 331, pp. 13-24, 1983 (in Japanese).
8) Sato, H., Katsuki, S. and Ishikawa, N.: Elastic-Plastic Analysis of Plane Buried Pipelines under Forced Ground Deformation, Proceedings of Japan Soc. Civil Eng., No. 350, pp. 217-226, 1984 (in Japanese).
9) Kitaura, M., Miyajima, M. and Matsumura, Y.: Response Analysis of Buried Pipelines During Soil Liquefaction, Proceedings of the 17th JSCE Earthquake Engineering Symposium-1983, pp. 303-306, 1983 (in Japanese).

10) Fu-Lu, M.: Earthquake Response of Fluid-filled Pipelines Buried in Soil, Proceedings of 1983 International Symposium of Lifeline Earthquake Engineering, PVP-Vol. 77, ASME, pp. 196-201, 1983.
11) Yeh, Y. H. and Wang, L. R. L.: Dynamic Responses of Buried Pipelines in a Soil Liquefaction Environment During Earthquake, Proceedings of the 5th International Conference on Numerical Methods in Geomechanics, Vol. 3, pp. 1409-1423, 1985.
12) Kitaura, M. and Miyajima, M.: Response Simulation of Buried Pipeline During Soil Liquefaction, Memoirs of the Faculty of Technology, Kanazawa Univ., Vol. 17, No. 1, pp. 11-18, 1984.
13) Kitaura, M. and Miyajima, M.: Analytical and Experimental Study on Behavior of Pipelines Subjected to Soil Liquefaction, Proceedings of the 2nd International Conference on Soil Dynamics and Earthquake Engineering, Vol. 1, pp. 3.33-3.42, 1985.
14) Miyajima, M.: An Analytical Method of Buried Pipelines in Liquefaction Process, Proceedings of the 7th Japan Earthquake Engineering Symposium-1986, pp. 1993-1998, 1986.
15) Kitaura, M., Miyajima, M. and Suzuki, H.: Response Analysis of Buried Pipelines Considering Rise of Ground Water Table in Liquefaction Processes, Proceedings of Japan Soc. Civil Eng., No. 380, pp. 173-180, 1987.
16) Yoshikuni, H., Uno, H. and Yanagisawa, E.: Soil Mechanics (II), Gihodo-Shuppan, pp. 215-224, 1984 (in Japanese).
17) Brooks, R. H. and Corey, A. T.: Properties of Porous Media Affecting Fluid Flow, Proceedings of ASCE, Vol. 92, No. IR2, pp. 61-88, 1966.
18) Martin, G. R., Finn, W. D. L. and Seed, H. B.: Fundamentals of Liquefaction under Cyclic Loading, Proceedings of ASCE, Vol. 101, No. GT5, pp. 423-438, 1975.
19) Hardin, B. O. and Drnevich, V. P.: Shear Modulus and Damping in Soil: Design Equations and Curves, Proceedings of ASCE, Vol. 98, No. SM7, pp. 667-691, 1972.
20) Drnevich, V. P.: Undrained Cyclic Shear of Saturated Sand, Proceedings of ASCE, Vol. 98, No. SM7, pp. 807-825, 1972.
21) Toki, K.: Earthquake Resistance Analysis of Structures, Gihodo-Shuppan, pp. 77-80, 1981 (in Japanese).

22) Finn, W. D. L., Byrune, P. M. and Martin, G. R.: Seismic Response and Liquefaction of Sand, Proceedings of ASCE, Vol. 102, No. GT8, pp. 841-856, 1976.
23) Nakamura, H. : A Modified Transfer Matrix Method with Improved Round off Errors, Proceedings of Japan Soc. Civil Eng., No. 289, pp. 43-53, 1979 (in Japanese).
24) Miyajima, M. and Kitaura, M.: Experiments on Restoring Force Characteristics of Pipe-Liquefied Layer System, Memoirs of the Faculty of Technology, Kanazawa Univ., Vol. 22, No. 1, pp. 11-20, 1989.
25) Yoshida, T. and Uematsu, M.: Dynamic Behavior of a Pile in Liquefaction Sand, Proceedings of the 5th Japan Earthquake Engineering Symposium-1978, pp. 657-663, 1978 (in Japanese).
26) Takada, S., Tanabe, K., Yamajyo, K. and Katagiri, S. : Liquefaction Analysis for Buried Pipelines, Structure and Stochastic Methods, Developments in Geotechnical Engineering, Computational Mechanics Publications, Vol. 45, pp. 319-333, 1987.
27) Yasuda, S., Saito, K. and Suzuki, N.: Soil Spring Constant on Pipe in Liquefied Ground, Proceedings. of the 19th JSCE Earthquake Engineering Symposium-1987, pp. 189-192, 1987 (in Japanese).

5. RESPONSE OF PIPELINES LOCATED THROUGH BOTH LIQUEFIED AND NON-LIQUEFIED GROUND

5.1 General Remarks

One of the most striking characteristics of pipeline damage following the 1983 Nihonkai-Chubu Earthquake was that all of the damage to cast iron pipe (CIP) occurred at liquefied sites, moreover, most occurred near the boundary between the liquefied and non-liquefied sites as mentioned in Chapter 2. Fig. 5.1 shows an example of earthquake damage to a pipeline induced by the 1983 Nihonkai-Chubu Earthquake. This figure also shows failure modes of the pipelines in accordance with Fig. 2.9 (Chapter 2). Fig. 5.1 reflects that 13 failures of the cast iron pipes occur near the boundary between the liquefied and non-liquefied sites. Damage to the pipelines seems to be induced by ground movements due to sharp change of the ground characteristics,

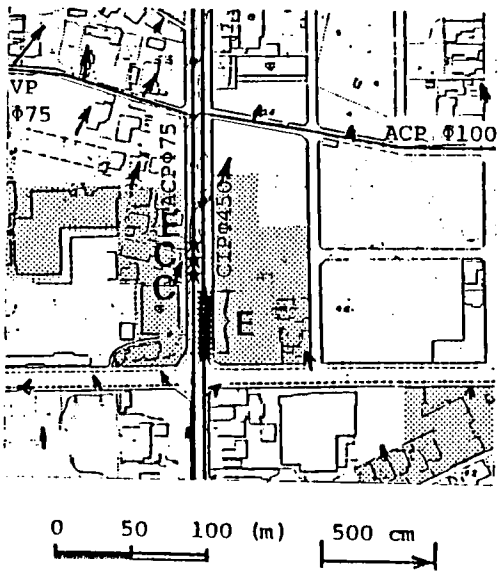

Fig. 5.1 Liquefied sites and pipe damage (Nagasaki in Noshiro).

buoyancy effect at the liquefied sites and settlement of the liquefied ground.

The purposes of this chapter are to clarify pipe behavior through a boundary between liquefied and non-liquefied sites and to discuss characteristics of the failures of the pipelines buried in such areas. In the following Chapter 5.2, vibration tests using a rubber pipe model located through both liquefied and non-liquefied ground are described. In Chapter 5.3, formulae obtained by a beam theory are presented and response analysis of pipelines is carried out as a comparison to the experimental results obtained in Chapter 5.2 and the resultant failure of pipelines is discussed. A part of this chapter is based on references 1-5.

5.2 Experiments on Response of Pipelines Located Through Both Liquefied and Non-liquefied Ground

5.2.1 Testing Procedure

In this chapter, two vibration tests were conducted. One was an experiment using a model, simulating a pipeline connected to a building. The other used a model pipeline located through both liquefiable and non-liquefiable sandy ground. Fig. 5.2 shows a general view of the experimental apparatus used in the first experiment. One end of the model pipe was fixed by a rigid arm sitting on a sand box. The model sand stratum and pipe were the same as those used in Chapter 3. Strain gauges were utilized on the model pipe as shown in Fig. 3.15 (Chapter 3). Pipe strains and excess pore water pressure were measured during a 30 second shaking period. The excitation frequency was 5 Hz, the acceleration was about 200 gals and the burial depth of the model pipe was 40 mm.

In the second test, the density of one half of the model ground was increased by vibration and the other half remained very loose as in the former case. Strain gauge number 10, which was affixed at the center of the model pipe, coincided with the boundary between liquefiable and non-liquefiable ground. All other conditions were identical for both experiments.

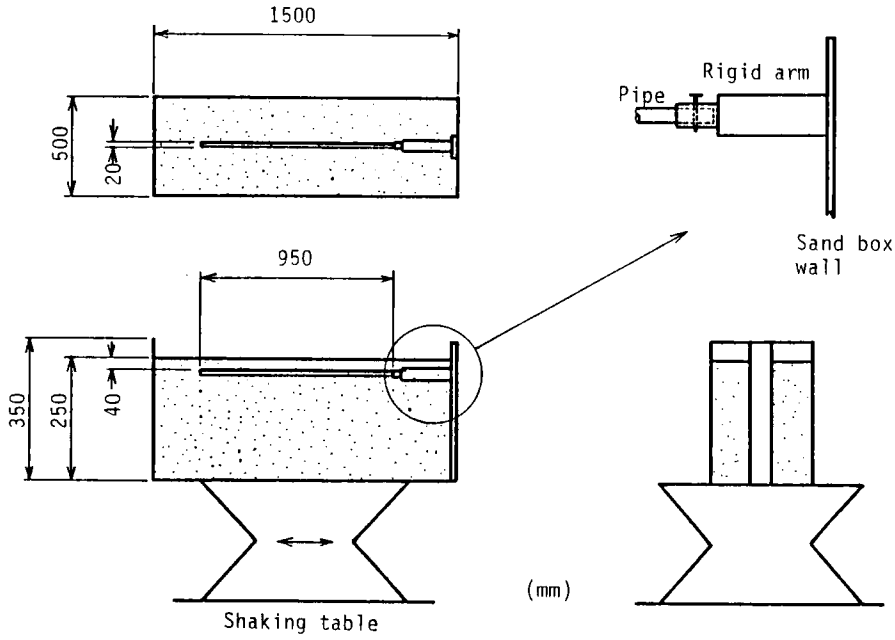

Fig. 5.2 General view of experimental apparatus.

5.2.2 Strain Characteristics of Pipelines Located Through Both Liquefied and Non-liquefied Ground

Fig. 5.3 shows the experimental results: pipe strain records at gauge numbers 1, 4, 7 and 10 and excess pore water pressure. This test situation simulated a pipeline connected to a building. In this case, a void ratio and water content of the model ground were 0.86 and 32 %, respectively. Fig. 5.4 shows the excess pore water pressure, accumulated residual strains and vibration strains prepared from Fig. 5.3. The accumulated residual strains rapidly increased during the initial 6 seconds shaking and slowly varied during the following 7 seconds of shaking. This variance of strain can be explained by Fig. 5.5 which illustrates a schematic diagram of expected deflection of the model pipe during liquefaction. The model pipe began to bend due to the buoyancy effect induced when excess pore water pressure rose. At this stage the accumulated residual strains rapidly increased. The free end of the model pipe reached the ground surface after the initial 6 seconds of shaking (see Fig. 5.5 (b)) and the pipe strains slowly varied after that. When the excess pore water pressure was dissipating after

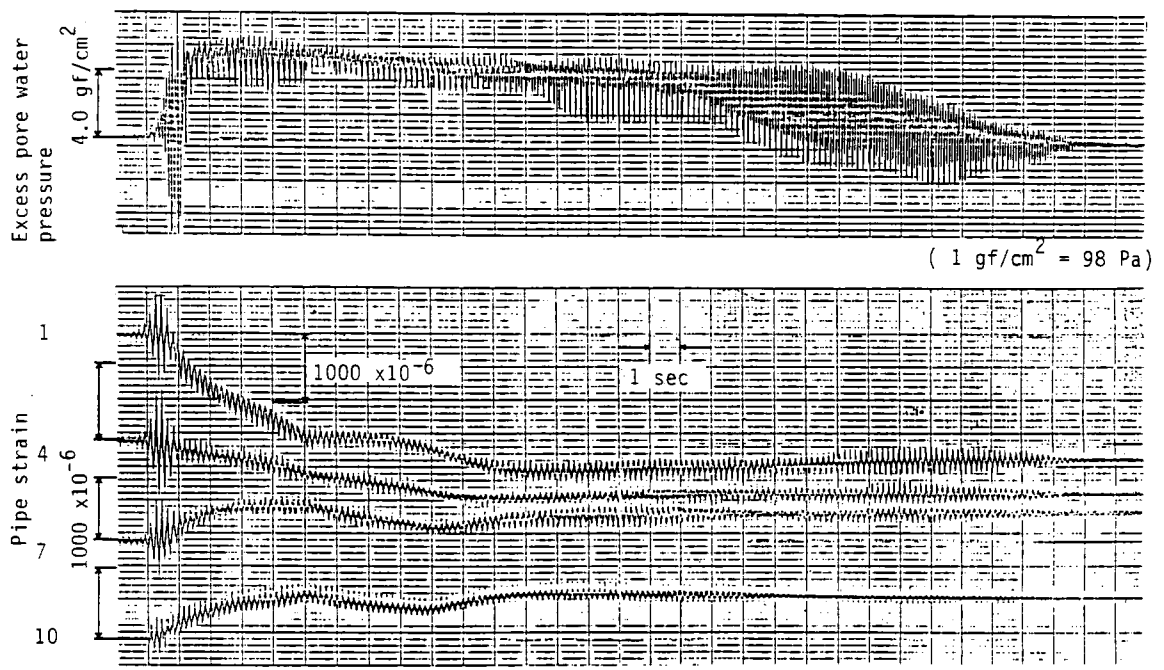

Fig. 5.3 Records of excess pore water pressure and strains of pipe.

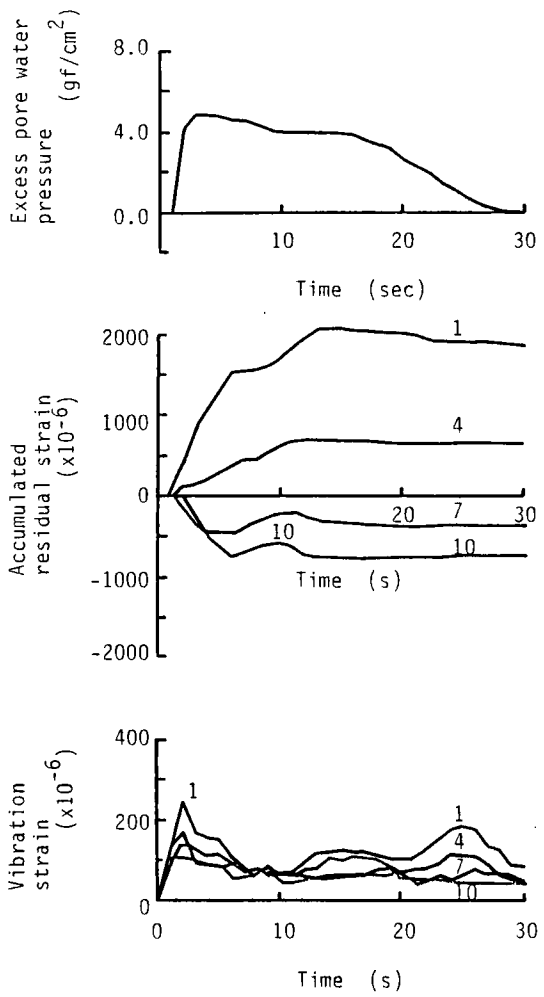

Fig. 5.4 Time histories of excess pore water pressure, accumulated residual strains and vibrating strains.

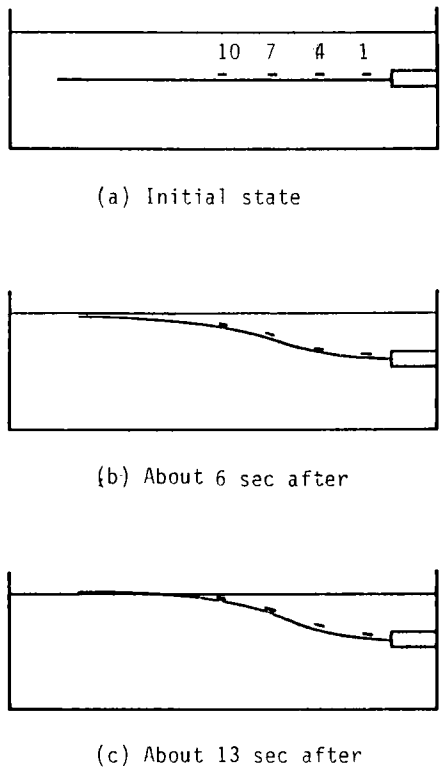

Fig. 5.5 Schematic diagram of deflection of the pipe during liquefaction.

13 seconds of shaking, the pipe deformation was retained (see Fig. 5.5(c)). The vibration strains were greatest when the excess pore water pressure rose and fell. That finding agrees with the experimental results obtained in Chapter 3.3.

Fig. 5.6 shows a distribution of the maximum accumulated residual strains. The strain gauges near the fixed end (gauge numbers 1-5) express compression and the others express tension. This result ,too,

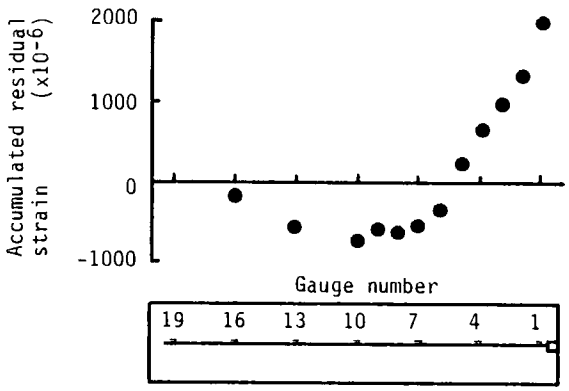

Fig. 5.6 Distribution of maximum accumulated residual strains.

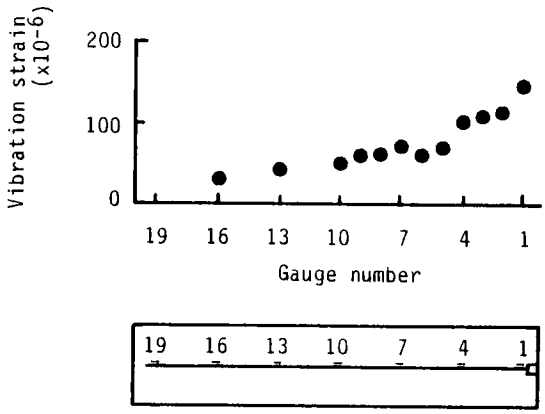

Fig. 5.7 Distribution of mean vibrating strains.

agrees with the expected deflection of the model pipe shown in Fig. 5.5. Gauge number 1 (nearest to the fixed end) recorded about 2000 x10^{-6} which was the maximum value of the accumulated residual strains in this case. Fig. 5.7 indicates a distribution of the mean vibration strains. It can be seen from this figure that the vibration strains near the fixed end registered as high values. This appears to be due to the fact that an

input wave does not transmit from the model ground to the pipe but from the fixed end of the pipe during liquefaction. The maximum vibration strain was 500 $x10^{-6}$ at gauge number 1 according to the time records shown in Fig. 5.3. As shown above, it is now apparent that the maximum accumulated residual strain is much greater than the maximum vibration strain. Therefore, the strains caused by a pipe bending due to buoyancy effect dominate those by a pipe vibrating in this case.

Fig. 5.8 shows an experimental result obtained from the vibration tests using a model, simulating pipelines located through liquefiable and non-liquefiable ground. In this case, void ratio of the loose sandy ground was 0.86 and 0.76 for more dense sandy ground. This figure indicates the input acceleration, strain records at gauges 1, 4, 7 and 10 and excess pore water pressures at both the loose and the sandy ground with a higher density. The strain gauges 1, 4 and 7 were in the sand with a higher density and strain gauge 10 coincided with the boundary ground between the two types of soil. Fig. 5.9 shows a graphic rearrangement of the records given in Fig. 5.8. According to these figures, the excess pore water pressure in the more dense sand stratum increased slightly. This suggests that the model ground near the boundary was liquefied slightly because of water seepage from the liquefied loose sand stratum. Therefore, the vibration strains at gauge number 7 and 10 were large at some instants.

Fig. 5.10 shows a distribution of the maximum accumulated residual strains. Since the strain gauges were utilized on the upper part of the pipe, the expected pipe deflection could be observed as shown in Fig. 5.11 from Fig. 5.10. The model pipe near the boundary ground was expected to bend a little due to the buoyancy effect of the liquefied ground and softening of the remaining soil. The ground softening had an effect on mitigating the accumulated residual strains concentrated at the boundary ground in comparison with the results of the former case. Maximum strain in Fig. 5.10 was about 750 $x10^{-6}$ at strain gauges 8, 9 and 13. This value was smaller than the former case shown in Fig. 5.6 (2000 $x10^{-6}$). Fig. 5.12 indicates a distribution of the mean vibration strains. The vibration strains near the boundary ground were generally large. The maximum vibration strain was about 500 $x10^{-6}$ (at gauge

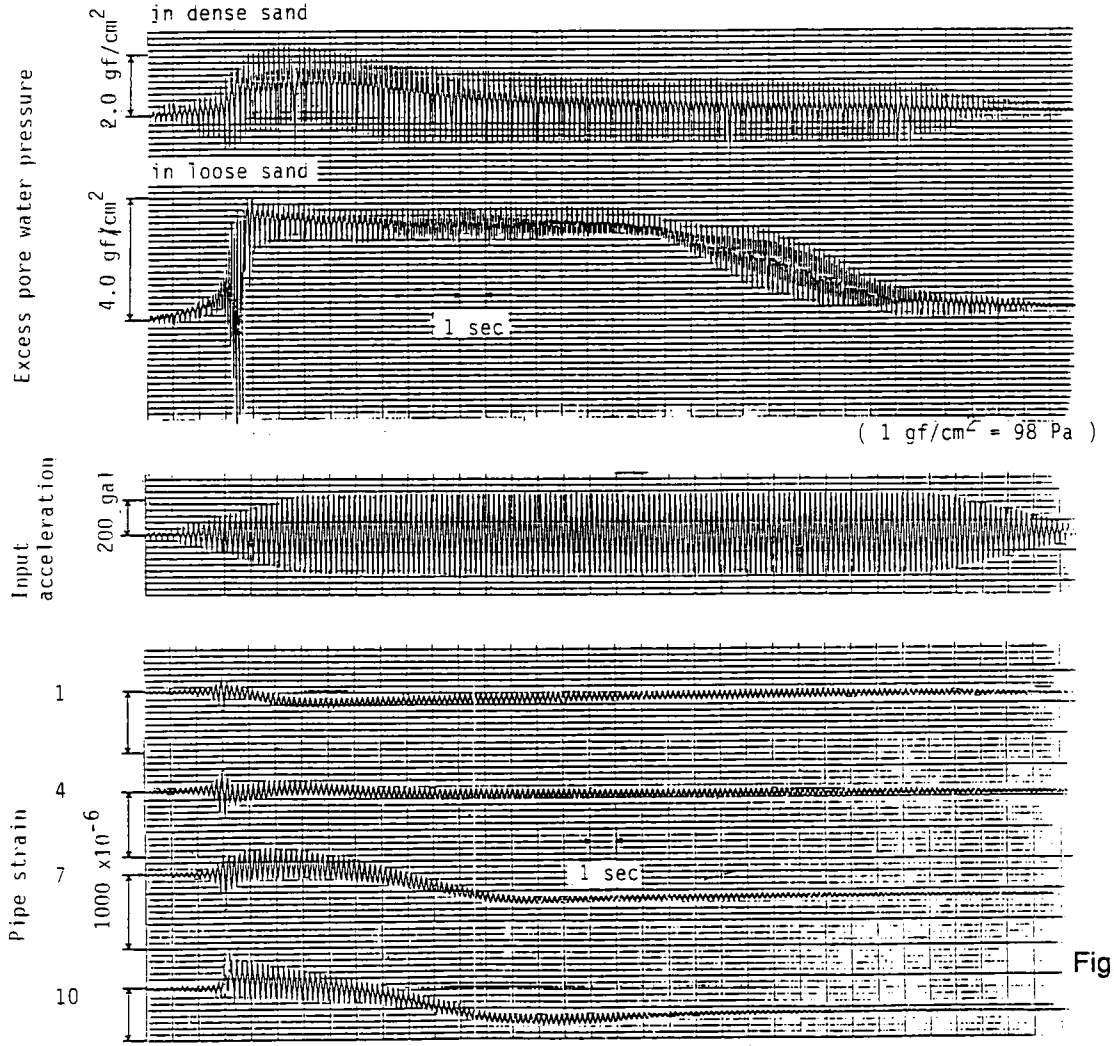

Fig. 5.8 Records of input acceleration, strains of the pipe, and excess pore water pressures.

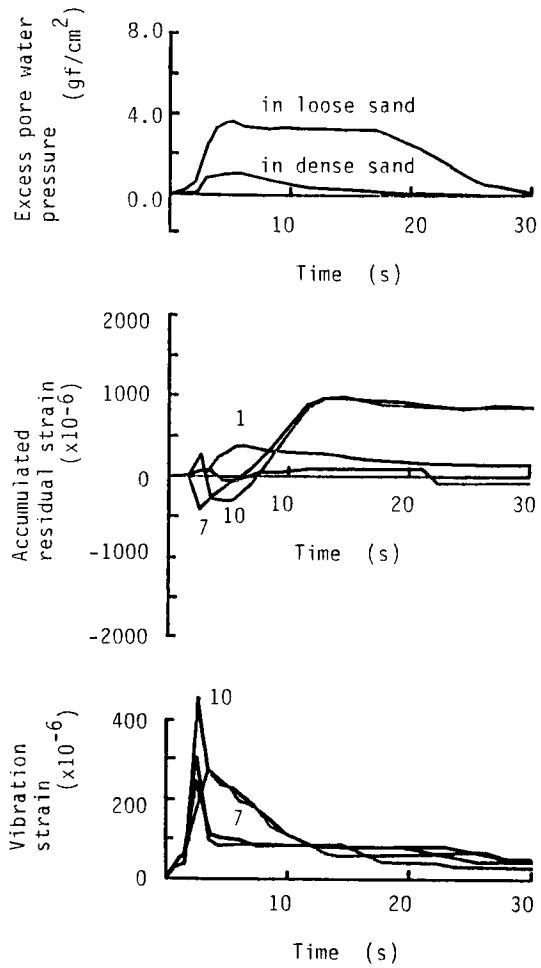

Fig. 5.9
Time histories of excess pore water pressure, accumulated residual strains and vibrating strains.

number 7) according to the time records shown in Fig. 5.8. This value is the same as in the former case.

The above experimental results seem to show that the buoyancy effect due to liquefaction is most serious to pipelines connected to a building. On the other hand, softening of the ground with a greater density reduces concentration of the accumulated residual strains at the boundary ground in the case of the pipe located through both liquefied and non-liquefied ground. However, since great vibration stain continues at some instants due to increasing softening of the soil, great consideration should be given to the dynamic behavior of pipelines.

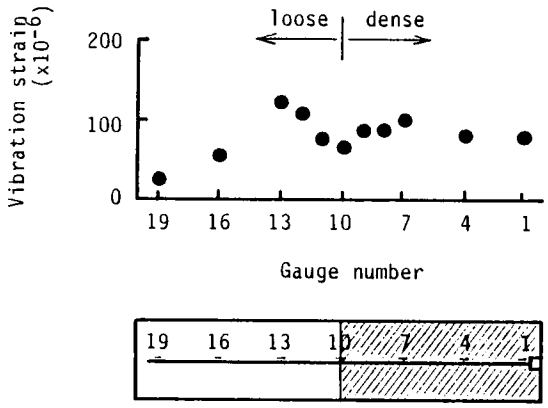

Fig. 5.10 Distribution of maximum accumulated residual strains.

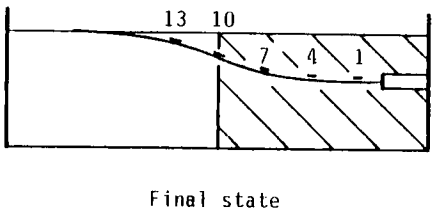

Fig. 5.11 Schematic diagram of expected pipe deflection.

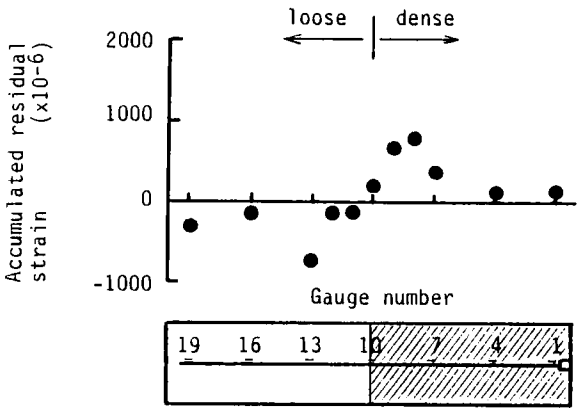

Fig. 5.12 Distribution of mean vibrating strains.

5.3 Mathematical Analysis of Response of Pipelines Located Through Both Liquefied and Non-liquefied Ground

5.3.1 A Procedure of Analysis

Fig. 5.13 shows analytical models for pipelines buried through a boundary between liquefied and non-liquefied ground. In case 1, the

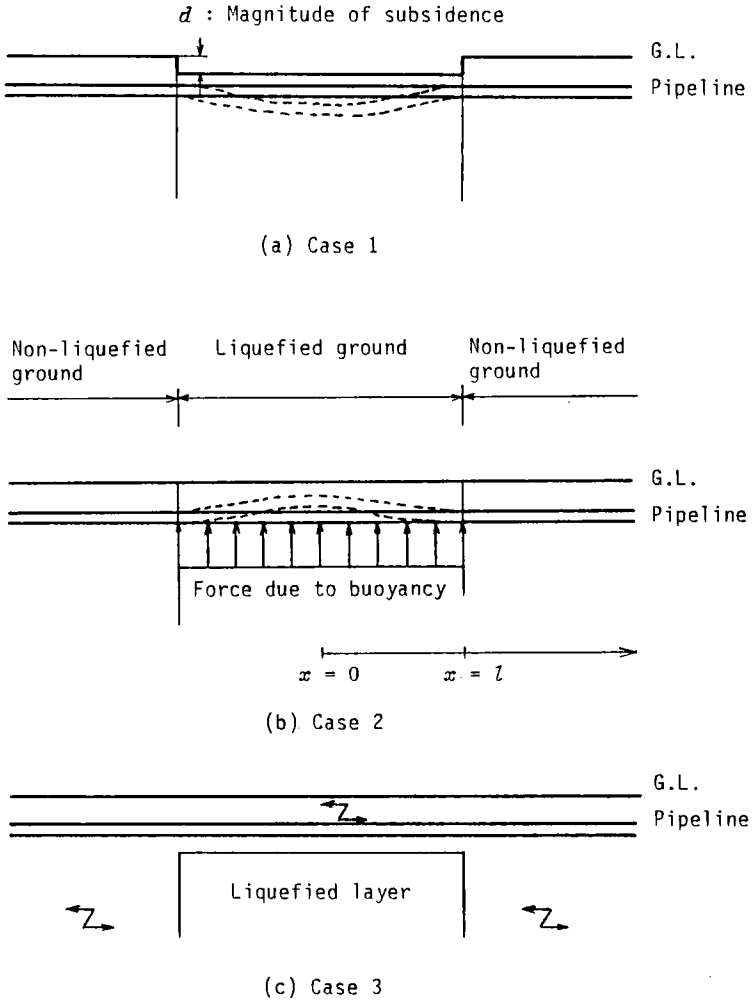

Fig. 5.13 Analytical model for buried pipelines located between liquefied and non-liquefied ground.

pipeline is assumed to be subjected to subsidence of the liquefied ground, while in case 2 buoyancy effect is a governing factor. In case 3, the pipeline is subjected to a seismic motion which is different from the motion of the neighboring zones. In this last case, the superficial layer of the ground above the liquefied layer can be regarded as a horizontally vibrating elastic plate which is subjected to a periodical driving force at both ends. These three analytical models have been constructed under the same assumptions described in Chapter 4.3. That is, the perfectly elastic behavior is assumed for the pipe material and the pipe motion is analyzed in the two-dimensional plane. Characteristics of the pipe strains are investigated using these simplified mathematical models. In this investigation, the responses of the pipelines can be estimated by solving the following differential equations with suitable boundary conditions.

(1) Case 1

According to the schematic representation of case 1, as shown in Fig. 5.13 and upon the above several assumptions, the differential equations for case 1 may be expressed as follows;

$$EI \frac{d^4 v_1}{dx^4} + K_{v1} v_1 = K_{v1} V_1 \qquad (0 < x < l) \qquad (5.1)$$

$$EI \frac{d^4 v_2}{dx^4} + K_{v2} v_2 = 0 \qquad (x > l) \qquad (5.2)$$

The boundary conditions are

$$\frac{dv_1}{dx} = 0, \quad \frac{d^3 v_1}{dx^3} = 0 \qquad (x = 0) \qquad (5.3)$$

$$v_1 = v_2, \quad \frac{dv_1}{dx} = \frac{dv_2}{dx}, \quad \frac{d^2 v_1}{dx^2} = \frac{d^2 v_2}{dx^2}, \quad \frac{d^3 v_1}{dx^3} = \frac{d^3 v_2}{dx^3}$$
$$(x = l) \qquad (5.4)$$

$$v_2 = 0, \quad \frac{dv_2}{dx} = 0 \qquad (x \to \infty) \qquad (5.5)$$

respectively.

(2) Case 2

Supposing that the transverse displacement in the pipeline depends on buoyancy effect, the governing differential equations for case 2 may be given by

$$EI \frac{d^4 v_1}{dx^4} + K_{v1} v_1 = F \qquad (0 < x < l) \qquad (5.6)$$

$$EI \frac{d^4 v_2}{dx^4} + K_{v1} v_1 = 0 \qquad (x > l) \qquad (5.7)$$

The boundary conditions Eqs. (5.3), (5.4) and (5.5) are also available for the problem of case 2. Therefore, Eqs. (5.3) through (5.5) are used to obtain the generalized analytical solutions of v_1 and v_2.

(3) Case 3

Since the schematic model of case 3 is taking account of the liquefaction in the superficial layer of the ground, including the original model presented by Nishio et al.[6], the differential equation can be written in a form of

$$EA\frac{d^2 u_1}{dx^2} - K_{u1} u_1 = - K_{u1} U_1 \qquad (0 < x < l) \qquad (5.8)$$

$$EA\frac{d^2 u_2}{dx^2} - K_{u2} u_2 = - K_{u2} U_2 \qquad (x > l) \qquad (5.9)$$

The boundary conditions are

$$\frac{du_1}{dx} = 0 \qquad (x = 0) \qquad (5.10)$$

$$u_1 = u_2, \quad \frac{du_1}{dx} = \frac{du_2}{dx} \qquad (x = l) \qquad (5.11)$$

$$\frac{du_2}{dx} = 0 \qquad (x = L) \qquad (5.12)$$

where U_1 in Eq. (5.8) and U_2 in Eq. (5.9) are expressed as follows;

$$U_1 = \frac{\cos\left(\frac{2\pi x}{cT}\right)}{\cos\left(\frac{2\pi l}{cT}\right)} U_{s0} \tag{5.13}$$

$$U_2 = U_{s0} \tag{5.14}$$

where u, v = longitudinal and transverse displacement in the pipeline, U, V = displacement in the ground, E = young's modulus of the pipe material, A = cross-sectional area of the pipe, I = area moment of inertia of the pipe, K_u , K_v = equivalent spring constant of the longitudinal and transverse motions, F = a force caused by the buoyancy effect, c = longitudinal wave velocity which is given as $c^2 = E_S/\rho$ in which E_S is Young's modulus of soil and ρ is soil density, U_{s0} = displacement amplitude in non-liquefied superficial layer, T = period of shaking, $2l$ = width of the liquefied zone and L = pipe length. Subscripts 1 and 2 respectively correspond to the two sections.

By integrating Eqs. (5.1) and (5.2) with respect to x using the boundary conditions Eqs. (5.3), (5.4) and (5.5), the analytical solutions of v_1 and v_2 for case 1 are

$$\begin{aligned} v_1(x) = {} & \exp(\beta_1 x)(A_1 \cos \beta_1 x + A_2 \sin \beta_1 x) \\ & + \exp(-\beta_1 x)(A_3 \cos \beta_1 x + A_4 \sin \beta_1 x) \\ & + \frac{F}{K_{v1}} \qquad (0 < x < l) \end{aligned} \tag{5.15}$$

$$\begin{aligned} v_2(x) = {} & \exp(-\beta_2 x)(A_5 \cos \beta_2 x + A_6 \sin \beta_2 x) \\ & (x > l) \end{aligned} \tag{5.16}$$

The solution of v_1 for case 2 is

$$\begin{aligned} v_1(x) = {} & \exp(\beta_1 x)(A_1 \cos \beta_1 x + A_2 \sin \beta_1 x) \\ & + \exp(-\beta_1 x)(A_3 \cos \beta_1 x + A_4 \sin \beta_1 x) + d \\ & (0 < x < l) \end{aligned} \tag{5.17}$$

and the solution of v_2 for case 2 may be given by Eq. (5.16). In addition, solving Eqs. (5.8) and (5.9) with the boundary conditions Eqs. (5.10) through (5.12) gives

$$u_1(x) = A_7 \cosh \lambda_1 x + \frac{U_1}{1 + \left(\frac{2\pi}{\lambda_1 cT}\right)^2} \quad (0 < x < l) \quad (5.18)$$

$$u_2(x) = A_8 \exp(\lambda_2 x) + A_9 \exp(-\lambda_2 x) + U_{s0} \quad (x > l) \quad (5.19)$$

where $\beta_1{}^4 = K_{v1} / (4EI)$, $\beta_2{}^4 = K_{v2} / (4EI)$, $\lambda_1{}^2 = K_{u1} / (EA)$, $\lambda_2{}^2 = K_{u2} / (EA)$, and d = magnitude of subsidence. A_1, A_2 ... and A_9 in the above solutions are integral constants. These constants are listed in Appendix 5.1.

5.3.2 Practical Application of Mathematical Models to Existing Pipelines

Initially, the bending pipe stresses due to subsidence of the ground induced by liquefaction are investigated in relation to the ratio of the equivalent soil spring constant K_1 / K_2 for case 1. Fig. 5.14 shows the relationship between: a) the maximum bending pipe stresses due to subsidence of the liquefied ground and, b) the width of the liquefaction zone. The pipelines used in this analysis are steel pipelines whose physical properties are listed in Table 5.1. The magnitude of subsidence of the liquefied ground is assumed to be 20 cm, and it is equivalent to a 2 % subsidence of 10 m liquefied layer. Yoshimi et al. concluded that the average vertical strain as a result of consolidation under the weight of the soil was 1 % to 3 % when a horizontal layer of loose saturated sand was liquefied to a depth of approximately 5 m to 20 m [7]. The experimental results presented by Lee et al. [8] also agree with the results indicated by Yoshimi et al. It can be seen from Fig. 5.14 that the higher the ratio of the equivalent soil spring constant is, which means smaller degree of liquefaction, the greater the maximum bending pipe stresses are. It is interesting to note that the maximum bending pipe stress for each ratio of the equivalent soil spring constant does not increase in areas of liquefied ground where the width exceeds

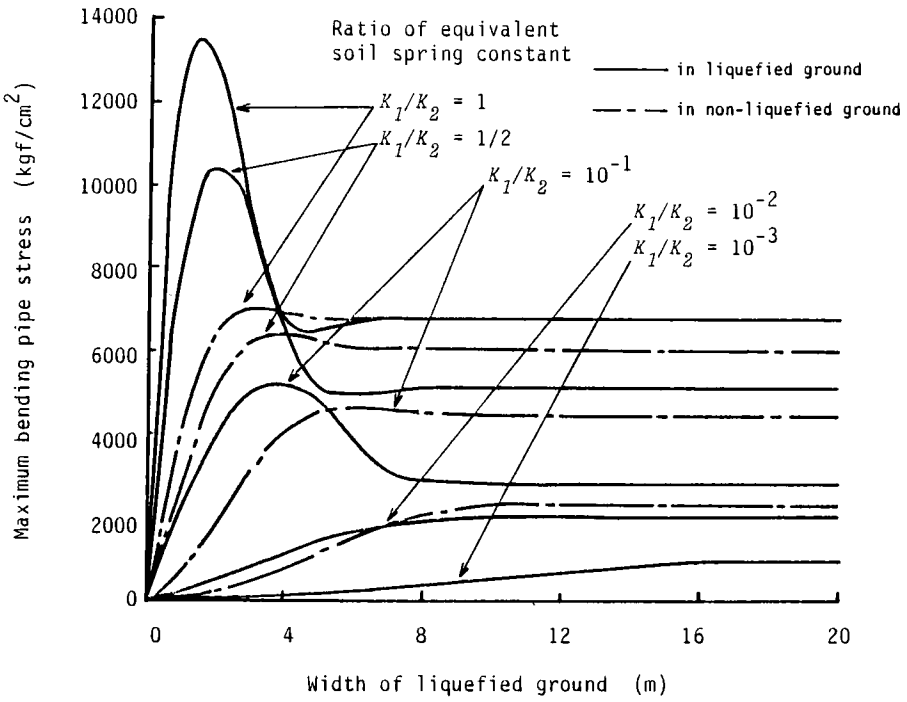

Fig. 5.14 Relationship between maximum bending pipe stress due to subsidence of liquefied ground and width of liquefied zone.

Table 5.1 Dimensions of steel pipeline.

Outer diameter	(mm)	406.4
Thickness	(mm)	6.0
Young's modulus	(kgf/cm^2)	2.1 x10^6
Specific gravity		7.85

(1 kgf/cm^2 = 98 kPa)

10 m. The maximum bending stress exceeds the allowable bending stress of steel pipe (4,200 kgf/cm2) when the ratio of the equivalent soil spring constant is greater than 0.1, particularly at a width of liquefied zone less than 5 m except for the region near 0 m. Fig. 5.15 shows the relationship between the displacement of the pipe and the width of the liquefied zone. It can be seen from this figure that for relatively

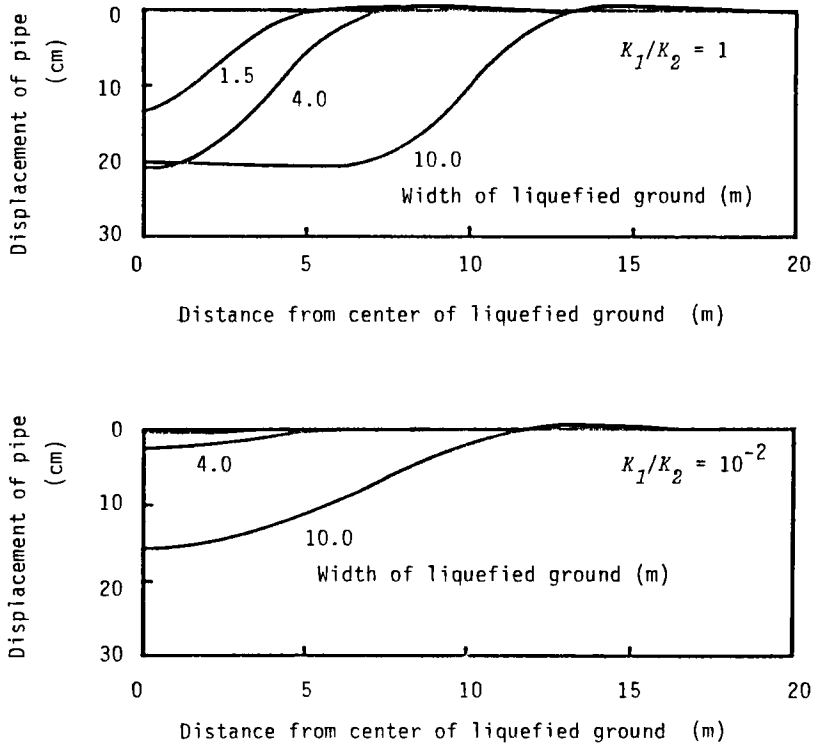

Fig. 5.15 Distribution of pipe displacement due to subsidence.

narrow width of the liquefied ground or low ratio of the equivalent soil spring constant, the relative displacement between the ground and pipe is observed. The maximum displacement of the pipe decreases because rigidity of the pipe dominates that of the ground. In case 1, the location where the maximum bending stress occurs coincides with the pipe located at the center of the liquefied zone; however, for greater width of the liquefied ground or higher ratio of the equivalent soil spring constant, the location is nearer the boundary between the liquefied and non-liquefied ground.

In Case 2, the buoyancy effects of the pipelines during liquefaction are estimated as follows: Fig. 5.16 shows the schematic diagram of forces acting on buried pipes during liquefaction processes. Let the buried pipe be regarded as a plate with the thickness represented

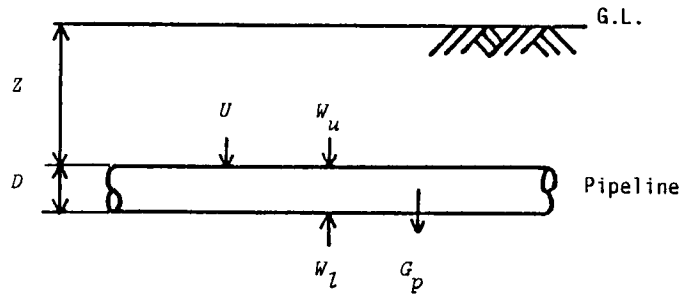

Fig. 5.16 Schematic diagram of forces acting buried pipe during liquefaction.

as D and the area of both upper and lower sides as A. The total upward force F acting on the lower side of the plate can be expressed as:

$$F = W_l - (U + W_u + G_p) \tag{5.20}$$

where W_l is water pressure acting on the lower side of the plate, which includes the accumulating excess pore water pressure, W_u is that acting on the upper surface, U is the force due to the effective confining pressure acting on the upper surface and G_p is the weight of the plate. W_l and W_u increase as the excess pore water pressure accumulates, while U decreases. Eq. 5.20 can be rewritten as:

$$F = (z + D) P_w A - (\gamma_s z + \rho_p D) A \tag{5.21}$$

where $(z + D) P_w$ is the pore water pressure in a depth of $z + D$, P_w means the pore water pressure divided by the depth, that is, P_w is a tentative unit weight of water taking into consideration the variance of the excess pore water pressure. γ_s is the submerged unit weight of the ground and rp is the unit weight of the plate. In Eq. 5.21, Z, D, A, γ_s and ρ_p are constants during the liquefaction process and P_w varies from γ_w to γ_s ; (γ_w is the unit weight of water). Therefore Eq.5.21 suggests that the upward force does not begin to act on the buried pipe as soon as the excess pore water pressure increase but it begins to act

when the excess pore water pressure accumulates to less than 1.0. When the upward force begins to act on the buried pipes the excess pore water pressure ratio depends on the dimensions of the buried pipes, the submerged unit weight of soil and the burial depth of the pipes. In this case, the upward force began to act when the excess pore water pressure ratio reached 0.88.

Fig. 5.17 shows the relationship between the maximum bending pipe stress due to buoyancy effects induced by liquefaction and the excess pore water pressure. Fig. 5.18 illustrates the relationship between the displacement of the pipe and the width of the liquefied ground. In this study, the equivalent soil spring constant of the liquefied soil is estimated by the empirical equation proposed by Yoshida and Uematsu [9] (Eq. 4.38 in Chapter 4.3). It was noted that the pipe reached the ground surface in the area where the width of liquefied ground exceeded 10 m as shown in Fig. 5.18. Therefore, the maximum bending pipe stresses disappear for great width and high excess pore water pressure in Fig. 5.17. It is evident from Fig. 5.17

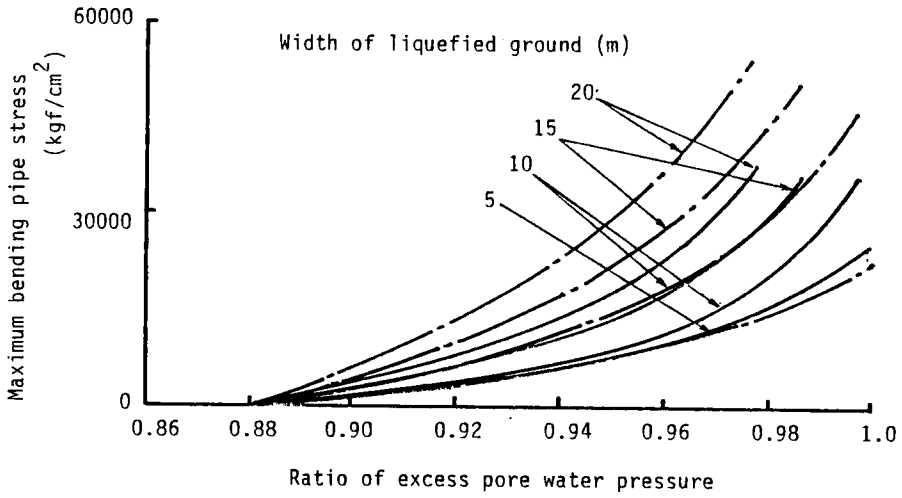

Fig. 5.17 Relationship between maximum bending pipe stress due to buoyancy effects induced by liquefaction and excess pore water pressure ratio.

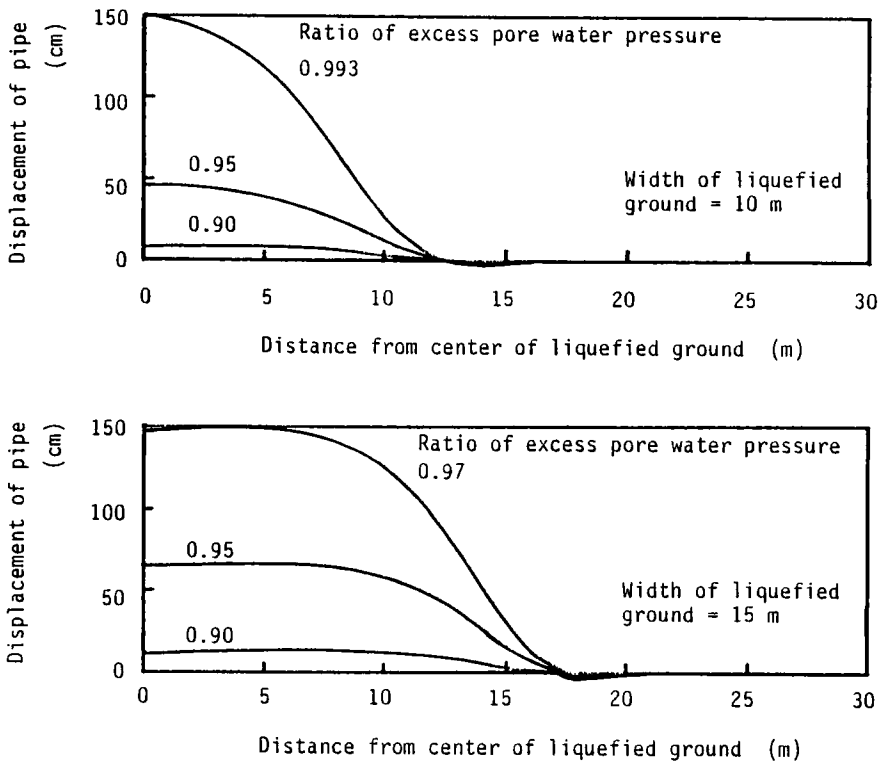

Fig. 5.18 Distribution of pipe displacement due to buoyancy effects.

that the greater the width of the liquefied ground is, the higher the maximum bending stress are, that is, the greater the probability of failure of the pipe due to buoyancy effects. It is also interesting to note that the maximum bending pipe stresses occurred in the non-liquefied ground in case of great width of the liquefied ground. In these analyses, it is assumed that the duration of the liquefaction process is lengthy enough to allow the occurrence of pipe deformation. However, since the duration of liquefaction induced by an actual earthquake depends on the local soil conditions, the above may actually not be the cases in reality. Therefore, these results may be overestimated. In order to evaluate the pipeline response due to buoyancy effects more precisely, the method described in Chapter 4 is preferable.

In case 3, the distribution of the axial pipe strain is shown in Fig. 5.19, in relation to the ratio of the equivalent soil spring constant K_1 /K_2 . Fig. 5.20 illustrates the relationship between the maximum axial pipe strain and the ratio of the equivalent soil spring constant. The conditions for the ground and the magnitude of an earthquake used in these analyses are summarized in Table 5.2. It is evident from these figures that the maximum axial strains decrease and the location where the maximum strains occurs approaches the boundary of the ground with a decrease in the ratio. During liquefaction processes, not only the equivalent soil spring constant varies but also longitudinal wave velocity c varies. Therefore, the longitudinal wave velocity is assumed to be proportional to the fourth root of (1 - r), where r is the excess pore water pressure ratio because the longitudinal wave velocity is proportional to the square root of Young's modulus of soil, and the shear modulus of the soil is proportional to the square root of (1 - r). Moreover, Young's modulus is proportional to the shear modulus of the soil. Fig. 5.21 shows the distribution of the axial pipe strain in relation to the excess pore water pressure ratio. Fig. 5.22 illustrates the relationship between the maximum axial pipe strain and the excess pore water pressure ratio. Excess pore water pressure higher than 0.9 is not included in this analysis because the longitudinal wave cannot be transmitted in such soft ground. It is evident from these figures that the maximum axial pipe strain occurs at the liquefied ground near the boundary between the liquefied and non-liquefied ground. The maximum axial pipe strain corresponding to the value of 0.2 of excess pore water pressure ratio is markedly great. This can be explained as follows: Fig 5.23 shows the magnification ratio of response displacement in a superficial layer. In this analysis, 1/($cT/2$) is less than 1.0; therefore, the magnification ratio increases sharply with an increase in 1/($cT/2$), i.e. with a decrease in c . However, the magnification ratio decreases with a decrease in c when 1/($cT/2$) is greater than 1.0. Effects of the resonance of the liquefied ground are great when excess pore water pressure ratio is equal to 0.2 in this case. Furthermore, Fig. 5.23 suggests that care should also be taken in evaluating the resonance of the liquefied ground for greater width of liquefied ground than that in this analysis. The above results obtained by mathematical analyses suggest that the probability of failure is high

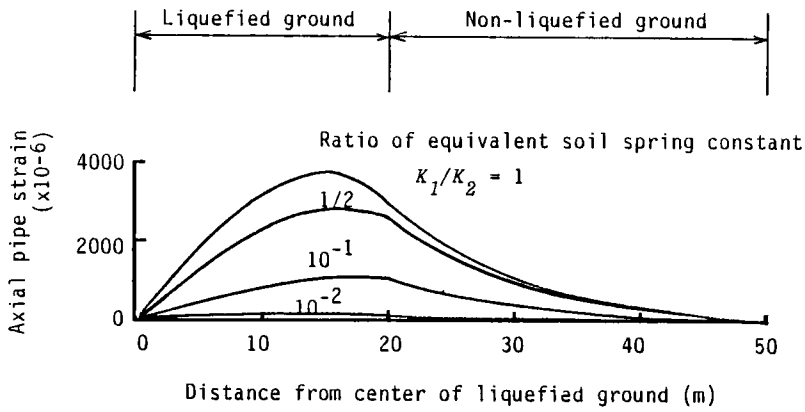

Fig. 5.19 Distribution of axial pipe strain in relation to the ratio of equivalent soil spring constant.

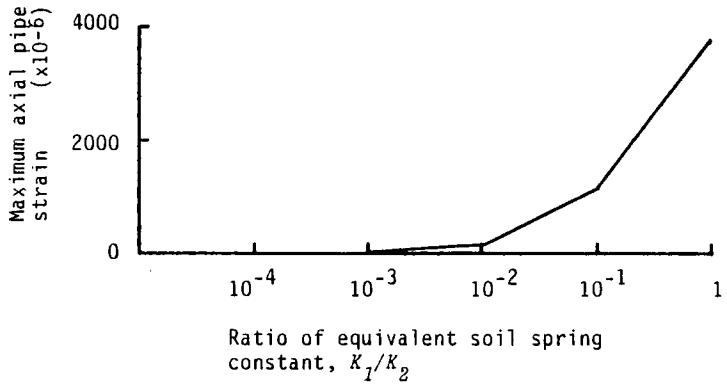

Fig. 5.20 Relationship between maximum axial pipe strain and the ratio of equivalent soil spring constant.

Table 5.2 Conditions of ground and magnitude of earthquake.

Longitudinal wave velocity c	170 (m/s)
Period of shaking T	0.5 (s)
Acceleration in superficial layer α	200 (gal)
Displacement amplitude of non-liquefied superficial layer	$U_{s_0} = (T/2\pi)^2\alpha$

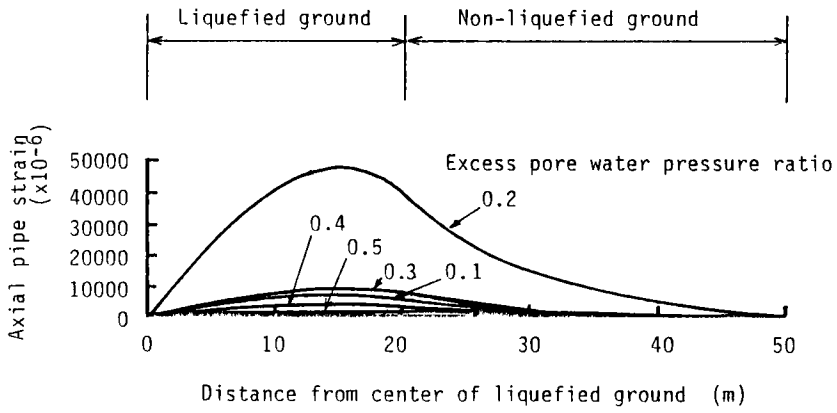

Fig. 5.21 Distribution of axial pipe strain in relation to excess pore water pressure.

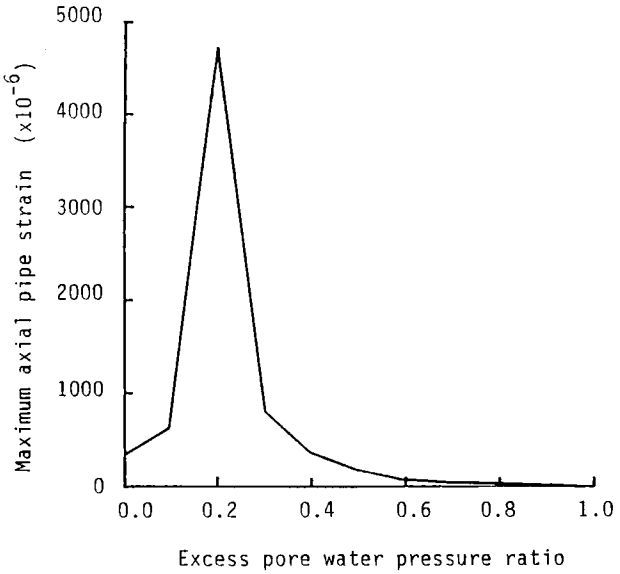

Fig. 5.22 Relationship between maximum axial pipe strain and excess pore water pressure ratio.

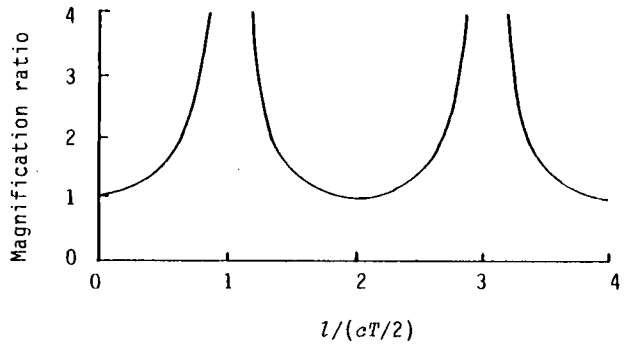

Fig. 5.23 Magnification ratio of response displacement in superficial layer.

at the boundary between the liquefied and non-liquefied ground for each cause of pipe failure. These findings agree with the experimental results presented in Chapter 5.2.

5.4 Conclusions

Response characteristics of pipelines located through both liquefied and non-liquefied ground were clarified based on a model experiment and mathematical analysis. The following can be concluded:

(1) Both the accumulated residual and the vibration-induced strains concentrated near the fixed end and the boundary between liquefied and non-liquefied ground in the model experiments.

(2) The accumulated residual strains were much greater than the vibration induced strains. This finding suggests that the effects of buoyancy dominate in these experiments.

(3) One of the response characteristics of pipelines subjected to subsidence of ground is that the smaller the degree of liquefaction in the superficial ground is, the greater the maximum bending pipe stresses. Moreover, great bending pipe stress occurs in areas of smaller width of the liquefied ground.

(4) The effects of buoyancy on pipe response are great in areas of great width of the liquefied ground and a high degree of liquefaction in the superficial ground.

(5) Resonance of the superficial layer of ground has great influence on the axial pipe strains during liquefaction processes; this result agrees with the findings discussed in Chapter 3. This suggests that great consideration should be given to vibration-induced strains during liquefaction.

References (Publications written in Japanese are so indicated; all others are in English)

1) Kitaura, M. and Miyajima, M.: Dynamic Behaviour of a Model pipe Fixed at One End During Liquefaction, Proceedings of Japan Soc. Civil Eng., No. 336, pp. 31-38, 1983 (in Japanese).
2) Kitaura, M. and Miyajima, M.: Experimental Study on Reduction of Damage to Pipes Buried near Structure Due to Soil Liquefaction, Proceedings of the 6th Symposium on Japan Earthquake Engineering-1982, pp. 1937-1944, 1982 (in Japanese).
3) Kitaura, M. and Miyajima, M.: Experiments on Damage Mitigation of Buried Pipelines Nihonkai to Liquefaction, Proceedings of the 8th World Conference on Earthquake Engineering, Vol. 7, pp. 239-245, 1984.
4) Kitaura, M. and Miyajima, M.: Assessment of Safety of Pipelines Subjected to Soil Liquefaction, Preliminary Report of IABSE Symposium TOKYO 1986, Vol. 51, pp. 133-140, 1986.
5) Miyajima, M., Kitaura, M and Kimura, T.: Mathematical Analysis of Pipelines Located Trough Both Liquefied and Non-Liquefied Ground, Memoirs of the Faculty of Technology, Kanazawa Univ., Vol. 22, No. 1, pp. 21-30, 1989.
6) Nishio, N., Tsukamoto, K. and Hamura, A.: Model Experiment on The Seismic Behavior of Buried Pipeline in Partially Liquefied Ground, Proceedings of Japan Soc. Civil Eng., No. 380, pp. 449-458, 1987 (in Japanese).
7) Yoshimi, Y., Kuwabara, F. and Tokimatsu, K.: One-dimensional Volume Change Characteristics of Sands under Very Low Confining Stresses, Soils and Foundations, Japan Soc. Soil Mecha. Founda. Eng., Vol. 15, No. 3, pp. 51-60, 1975.
8) Lee, K. L. and Albaisa, A.: Earthquake Induced Settlements in Saturated Sands, Proceedings of ASCE, Vol. 100, No. GT4, pp. 387-406, 1974.
9) Yoshida, T. and Uematsu, M.: Dynamic Behavior of a Pile in Liquefaction Sand, Proceedings of the 5th Japan Earthquake Engineering Symposium-1978, pp. 657-663, 1978 (in Japanese).

Appendix 5.1 Presentation of integral constants

The integral constants A_1 - A_9 in chapter 5.3.1 are represented as follows.

$$A_1 = A_3 = \frac{V_0 C_1}{B_1 C_1 - B_2 C_2 + B_3 C_3 - B_4 C_4}$$

$$A_2 = -A_4 = \frac{-V_0 C_5}{-B_5 C_5 + B_6 C_6 - B_7 C_7 + B_8 C_8}$$

$$A_5 = \frac{V_0 C_9}{B_9 C_9 - B_{10} C_{10} + B_{11} C_{11} - B_{12} C_{12}}$$

$$A_6 = \frac{-V_0 C_{13}}{-B_{13} C_{13} + B_{14} C_{14} - B_{15} C_{15} + B_{16} C_{16}}$$

$$A_7 = \frac{G_2}{\lambda_1 \sinh\lambda_1 l - \lambda_2 \frac{G_4}{G_3} \cosh\lambda_1 l \left\{ \frac{2}{cT} \sin G_1 - \lambda_2 \frac{G_4}{G_3} \left(\cos G_1 - \frac{U_2}{G_2} \right) \right\}}$$

$$A_8 = \frac{1}{G_3} (2A_7 \cosh\lambda_1 l + G_2 \cos G_1 - U_2)$$

$$A_9 = A_8 \exp(2\lambda_2 l)$$

$$G_1 = \frac{2\pi l}{cT}$$

$$G_2 = \frac{U_1}{1 + (\frac{2\pi}{\lambda_1 cT})^2}$$

$$G_3 = \exp(\lambda_2 l) + \exp\{\lambda_2 (2L - l)\}$$

$$G_4 = \exp(\lambda_2 l) - \exp\{\lambda_2 (2L - l)\}$$

$$B_1 = \{ \exp(\beta_1 l) + \exp(-\beta_1 l)\} \cos \beta_1 l$$
$$B_2 = D_5 \{D_2 \exp(\beta_1 l) - D_1 \exp(-\beta_1 l)\}$$
$$B_3 = D_5{}^2\{- \exp(\beta_1 l) + \exp(-\beta_1 l)\} \sin \beta_1 l$$
$$B_4 = D_5{}^3\{- D_1 \exp(\beta_1 l) + D_2 \exp(-\beta_1 l)\}$$
$$B_5 = \{ \exp(\beta_1 l) - \exp(-\beta_1 l)\} \sin \beta_1 l$$
$$B_6 = D_5 \{D_1 \exp(\beta_1 l) - D_2 \exp(-\beta_1 l)\}$$
$$B_7 = D_5{}^2\{ \exp(\beta_1 l) + \exp(-\beta_1 l)\} \cos \beta_1 l$$
$$B_8 = D_5{}^3\{ D_2 \exp(\beta_1 l) - D_1 \exp(-\beta_1 l)\}$$
$$B_9 = - B_{15} =- \exp(-\beta_2 l) \cos \beta_2 l$$
$$B_{10} = - B_{16} =D_3 \exp(-\beta_2 l)$$
$$B_{11} = B_{13} =- \exp(-\beta_2 l) \sin \beta_2 l$$
$$B_{12} = B_{14} =- D_4 \exp(-\beta_2 l)$$

$$D_1 = \cos \beta_1 l + \sin \beta_1 l$$
$$D_2 = \cos \beta_1 l - \sin \beta_1 l$$
$$D_3 = \cos \beta_2 l + \sin \beta_2 l$$
$$D_4 = \cos \beta_2 l - \sin \beta_2 l$$
$$D_5 = \frac{\beta_1}{\beta_2}$$

$$C_1=B_6B_{11}B_{16}+B_{10}B_{15}B_8 +B_{14}B_{12}B_7 -B_{14}B_{11}B_8 -B_6B_{12}B_{15} -B_{10}B_7B_{16}$$
$$C_2 =B_5B_{11}B_{16} +B_9B_{15}B_8 +B_{13}B_{12}B_7 -B_{13}B_{11}B_8 -B_5B_{12}B_{15} -B_9B_7B_{16}$$
$$C_3 =B_5B_{10}B_{16} +B_9B_{14}B_8 +B_{13}B_{12}B_6 -B_{13}B_{10}B_8 -B_5B_{12}B_{14} -B_9B_6B_{16}$$
$$C_4 =B_5B_{10}B_{15} +B_9B_{14}B_7 +B_{13}B_{11}B_6 -B_{13}B_{10}B_7 -B_5B_{11}B_{14} -B_9B_6B_{15}$$
$$C_5=B_2B_{11}B_{16}+B_{10}B_{15}B_4 +B_{14}B_{12}B_3 -B_{14}B_{11}B_4 -B_{10}B_3B_{16} -B_2B_{12}B_{15}$$
$$C_6 =B_1B_{11}B_{16} +B_9B_{15}B_4 +B_{13}B_{12}B_3 -B_{13}B_{11}B_4 -B_9B_3B_{16} -B_1B_{12}B_{15}$$
$$C_7 =B_1B_{10}B_{16} +B_9B_{14}B_4 +B_{13}B_{12}B_2 -B_{13}B_{10}B_4 -B_9B_2B_{16} -B_1B_{12}B_{14}$$
$$C_8 =B_1B_{10}B_{15} +B_9B_{14}B_3 +B_{13}B_{11}B_2 -B_{13}B_{10}B_3 -B_9B_2B_{15} -B_1B_{11}B_{14}$$
$$C_9 =B_2B_7B_{16} +B_6B_{15}B_4 +B_{14}B_8B_3 -B_{14}B_7B_4 -B_2B_8B_{15} -B_6B_3B_{16}$$
$$C_{10} =B_1B_7B_{16} +B_5B_{15}B_4 +B_{13}B_8B_3 -B_{13}B_7B_4 -B_1B_8B_{15} -B_5B_3B_{16}$$
$$C_{11} =B_1B_6B_{16} +B_5B_{14}B_4 +B_{13}B_8B_2 -B_{13}B_6B_4 -B_1B_8B_{14} -B_5B_2B_{16}$$
$$C_{12} =B_1B_6B_{15} +B_5B_{14}B_3 +B_{13}B_7B_2 -B_{13}B_6B_3 -B_1B_7B_{14} -B_5B_2B_{15}$$
$$C_{13} =B_2B_7B_{12} +B_{10}B_8B_3 +B_6B_{11}B_4 -B_{10}B_7B_4 -B_2B_8B_{11} -B_6B_3B_{12}$$

$$C_{14} = B_1B_7B_{12} + B_9B_8B_3 + B_5B_{11}B_4 - B_9B_7B_4 - B_1B_8B_{11} - B_5B_3B_{12}$$
$$C_{15} = B_1B_6B_{12} + B_9B_8B_2 + B_5B_{10}B_4 - B_9B_6B_4 - B_1B_8B_{10} - B_5B_2B_{12}$$
$$C_{16} = B_1B_6B_{11} + B_9B_7B_2 + B_5B_{10}B_3 - B_9B_6B_3 - B_1B_7B_{10} - B_5B_2B_{11}$$

6. RESPONSE OF PIPELINES SUBJECTED TO PERMANENT GROUND DISPLACEMENT INDUCED BY SOIL LIQUEFACTION

6.1 General Remarks

Permanent ground displacement induced by soil liquefaction is one of the most serious liquefaction hazards. Using aerial photographs taken before and just after the earthquakes, Hamada et al. measured the permanent ground displacement following the 1964 Niigata Earthquake and the 1983 Nihonkai-Chubu Earthquake. According to their findings, the maximum detected permanent ground displacement was more than 8 m along the Shinano river in Niigata City and more than 5 m in Noshiro City [1]. They also analyzed the quantitative correlations of the magnitude of the permanent ground displacement with the degree of damage to pipelines [2], [3]. Kitaura and Miyajima investigated the relationship between permanent ground displacement and pipeline damage following the 1983 Nihonkai-Chubu Earthquake. The main points of interest were as follows: Most of the permanent ground displacement, exceeding 1 m, occurred in the liquefied areas and the damage ratios of the pipelines were also high in those areas [4]. O'Rourke and Tawfik investigated pipeline response to permanent ground displacement near the Upper Van Norman Reservoir after the 1971 San Fernando Earthquake and related the damage to the patterns of permanent ground movement [5]. These results indicated that buried pipelines were vulnerable to permanent ground deformation. Furthermore, Yasuda et al. carried out model experiments considering the characteristics of permanent ground displacement and discussed the causes of permanent ground displacement [6]. Some research work on the effects of permanent ground displacement on civil engineering structures has been undertaken in recent years [7]-[9]. Little work has been done on the response of pipelines subjected to permanent ground deformation so far, however.

The purposes of this chapter are to clarify the response of pipelines subjected to liquefaction-induced permanent ground displacement and to discuss the subsequent failure of pipelines. In the following Chapter 6.2, characteristics of permanent ground displacement are investigated based on the earthquake damage data during the 1983 Nihonkai-Chubu Earthquake and the results of model experiments. In Chapter 6.3, formulae obtained by a beam theory are described and preliminary analysis is carried out in order to obtain fundamental characteristics of continuous pipelines. Moreover, response simulations are performed by using a modified transfer matrix method and failures of pipelines due to liquefaction-induced permanent ground deformation are discussed. The results obtained from the present study can give us a useful piece of information for determining whether or not countermeasures for the pipeline buried in the ground with high liquefaction potential should be taken, and what countermeasures should be done. The contents of this chapter are based on references 10-13.

6.2 Characteristics of Permanent Ground Displacement Induced by Soil Liquefaction

6.2.1 Permanent Ground Displacement During the 1983 Nihonkai-Chubu Earthquake

Permanent ground displacement caused by the 1983 Nihonkai-Chubu Earthquake was measured in Noshiro City using pre and post-earthquake photographs as mentioned in Chapter 2. Numerous sand volcanoes appeared in the area where the heavy damage was concentrated, showing that the ground was considerably liquefied. In this chapter, the measured areas of the permanent ground displacement described in reference 1 were classified as follows:

(a) Non-liquefied area
(b) Liquefied area without sand volcano
(c) Liquefied area with sand volcanoes

Item(c) means that more than five sand volcanoes were formed in an area 100 m in diameter. Fig. 6.1 shows the relationship between the ground slope and permanent ground displacement in the northern part

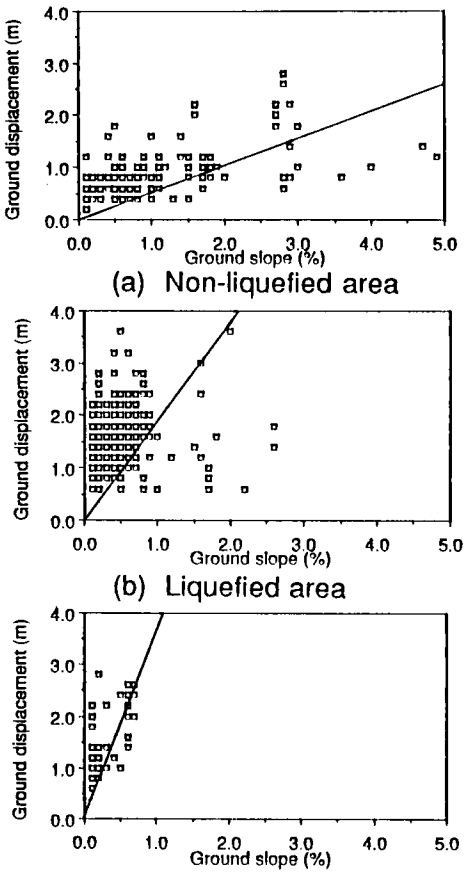

Fig. 6.1 Relationship between ground displacement and ground slope (in the northern part of Noshiro City).

of Noshiro City for each category. The regression straight lines through the origin are also shown in these figures. It can be seen from these figures that most of the permanent ground displacement in the non-liquefied areas was less than 1 m. On the other hand, those in the liquefied areas was more than 1 m. However, differences between the areas with sand volcanoes and without them, are not found in these figures. Moreover, points of the ground slope of greater than 3 % were not obtained in the liquefied areas. This suggests that the liquefaction did not occur at a slope of greater than 3 % because the ground water table was relatively deep in Noshiro City, therefore, permanent ground displacements did not appear.

6.2.2 Experiments on Characteristics of Permanent Ground Displacement

The distribution of permanent ground displacement along pipelines and magnification of the displacement are crucial factors in analysis of pipeline response. According to a distribution map of permanent ground displacement resulting from the 1964 Niigata Earthquake and the 1983 Nihonkai-Chubu Earthquake indicated by Hamada et al. [1], the distribution of permanent ground displacement is affected by local ground conditions such as the slope of the ground surface, the depth of the liquefied ground layer, etc. In this chapter, model experiments are carried out to understand the characteristics of the permanent ground displacement.

The diagram of the experimental apparatus is shown in Fig. 6.2. The sand box was 500 mm in width, 1500 mm in length and 350 mm in height. The model sand deposit had a slope of 2 % to 6 %. The sand deposit was made from loose saturated sand, whose physical properties are shown in Table 6.1. Since the sand stratum was constructed in

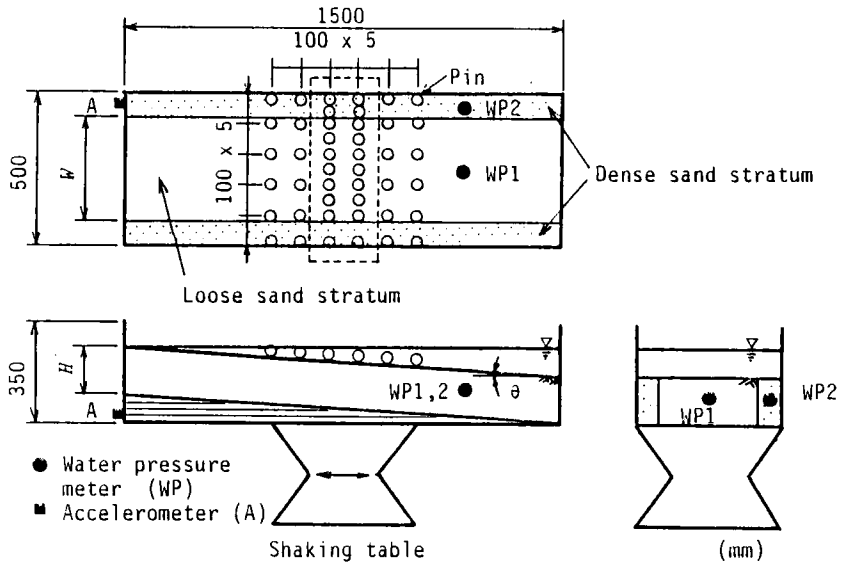

Fig. 6.2 General view of experimental apparatus.

Table 6.1 Physical properties of sand.

Specific gravity	2.67
Uniformity coefficient	2.96
Maximum void ratio	1.030
Minimum void ratio	0.721
50 percent diameter (mm)	0.2
Coefficient of permeability (cm/s)	0.0192

water in these experiments, whole sand stratum was saturated and the ground water table depth did not vary for each case. Therefore the effects of the ground water table depth were negligible in these experiments. Forty six pins were installed at the surface of the sand stratum to measure horizontal deformation of the ground surface. The deformation of the ground surface during excitation was measured by means of a video camera. Pore pressure transducers were buried to a depth of 5 cm to measure an excess pore water pressure in the loose sand stratum and in the more dense one. The model sand stratum was vibrated by a harmonic wave with 5 Hz. Target acceleration of the table was 100 gal and it took about 5 seconds for the table to reach the given acceleration. The duration of the test was 30 seconds.

Fig. 6.3 shows the time histories of input acceleration, excess pore water pressure at the loose sand stratum (WP 1) and displacement at point 7 which is shown in Fig. 6.5 as described later. It is evident from this figure that the model ground deformed in high excess pore water pressure, that is, in a completely liquefied condition. Since the wall of the sand box was against deformation of the sand stratum, the ground displacement in the loose sand stratum near the wall was also little. Therefore, the experiments carried out in the present study corresponded with the permanent ground displacement when liquefaction uniformly occurred in a certain area, which was enclosed with the dense sand stratum and two walls of the sand box in this experiment. Fig. 6.4 shows distribution of the permanent ground

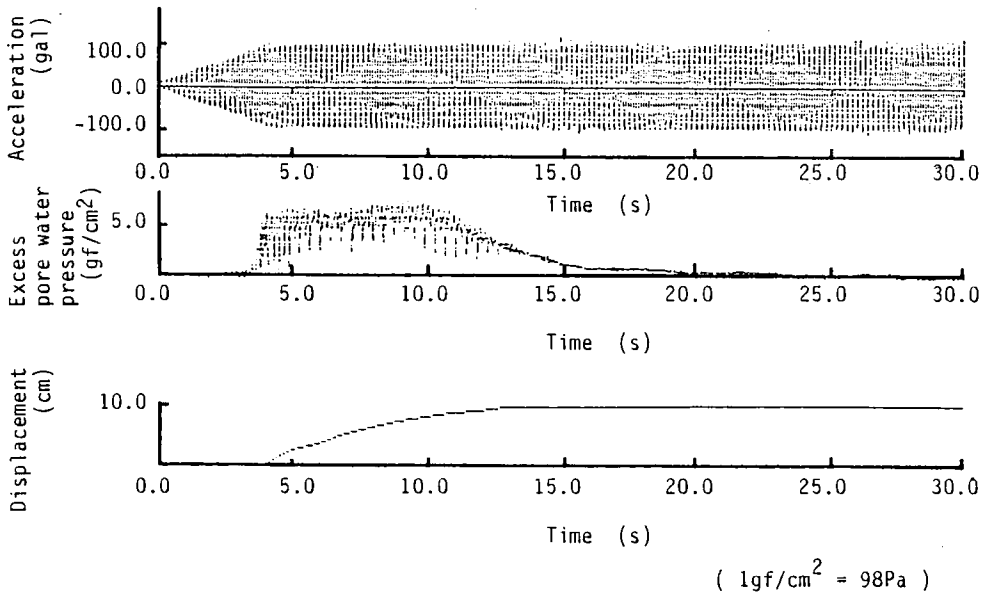

Fig. 6.3 Time histories of acceleration, excess pore water pressure, and permanent ground displacement at point 7.

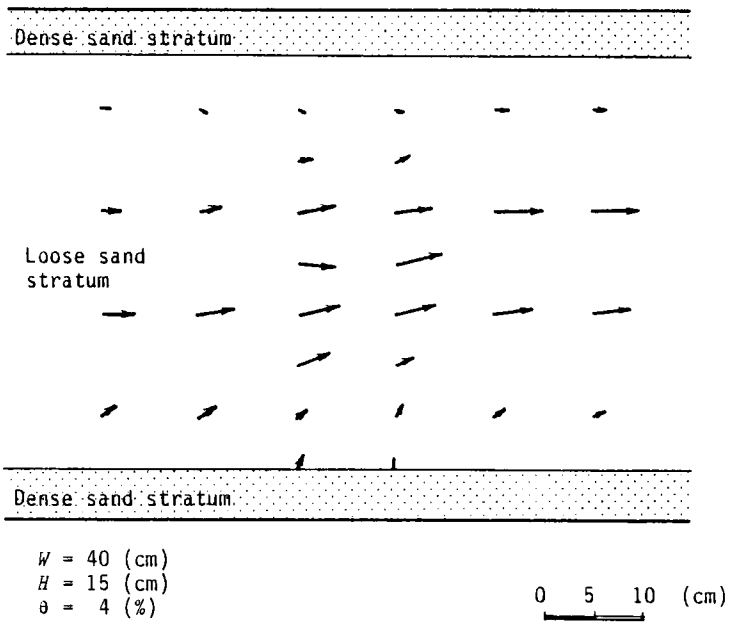

Fig. 6.4 Distribution of permanent ground displacement.

displacement. It is interesting to note that the ground displacement in the middle of the loose sand stratum was greater than that at the sides and the dense sand stratum did not deform. Fig. 6.5 reflects a distribution of residual permanent ground displacement at the middle of the ground surface, shown inside of the dashed area in Fig. 6.2. In this figure, the open circles indicate the initial sites of the pins and the solid circles, squares and triangles show the residual displacement of the pins for each case. This figure suggests that the shape of the distribution of the permanent ground displacement is approximately a sinusoidal curve. Furthermore, the maximum value of the permanent ground displacement is affected by the width of the loose sand deposit, W. Fig. 6.6 shows the relationship between the width of the loose sand stratum and the maximum value of the permanent ground displacement. The maximum value seems to be directly proportional to the width of the loose sand deposit.

Hamada et al. proposed a formula for estimating the magnitude of ground displacement by using the data obtained from the 1964 Niigata, the 1971 San Fernando, and the 1983 Nihonkai-Chubu Earthquakes [2]. In this formula, the ground slope and thickness of the liquefied layer were taken into consideration. The experimental results mentioned above, however, suggest that the width of permanent ground displacement is one of the influential factors determining the magnitude of the ground displacements. Evaluation of the extent of liquefiable areas induced by earthquakes is indispensable for predicting the width of permanent ground displacement. Although several practical methods to evaluate the liquefaction potential of a soil deposit subjected to earthquake loading have been developed [14)-18)], little work has been done on evaluation of the extent of liquefiable areas. Therfore, methods must be sought for predicting the extent of liquefiable areas in the future. Furthermore, the distribution of the permanent ground displacement, which is one of the crucial factors in analysis of pipeline response, displayed a sinusoidal curve.

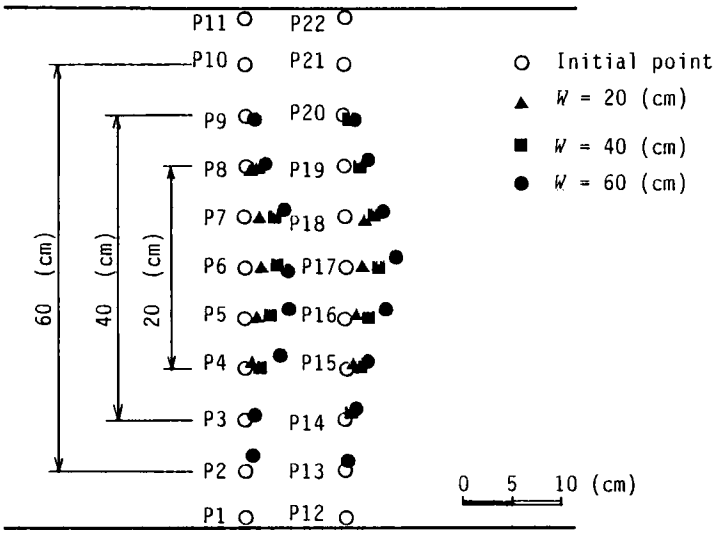

Fig. 6.5 Distribution of residual permanent ground displacement.

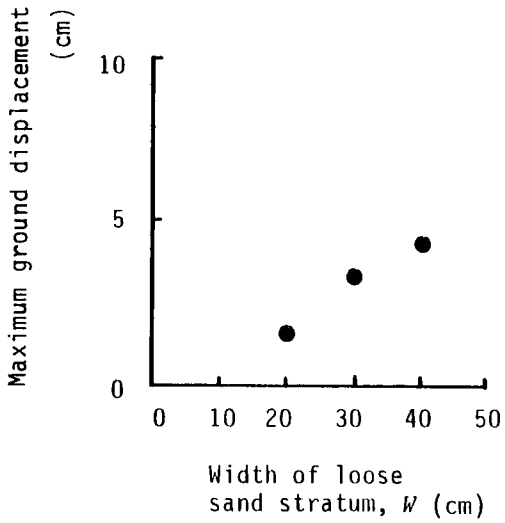

Fig. 6.6 Relationship between width of loose sand stratum and maximum ground displacement

6.3 Mathematical Analysis of Pipelines' Response Due to Permanent Ground Displacement Induced by Soil Liquefaction

6.3.1 A Procedure of Analysis

The distribution of the permanent ground displacement can be assumed to be a sinusoidal curve as mentioned in the previous chapter. Although the results of the experiments indicated one of the displacement patterns which depend on the several ground conditions, this pattern is considered as the basic pattern of the ground displacement. It is because this pattern is shown when liquefaction uniformly occurred in the loose sand stratum on smooth slope of the non-liquefied ground. The displacement pattern in this case is modeled as shown in Fig. 6.7. The basic differential equations governing the motion of a buried pipe can be established as follows:

$$EI \frac{d^4 v_1}{dx^4} + K_{v1} v_1 = K_{v1} d \left(1 - \sin \frac{\pi x}{2l}\right) \qquad (0 < x < l) \quad (6.1)$$

$$EI \frac{d^4 v_2}{dx^4} + K_{v2} v_2 = 0 \qquad (x > l) \quad (6.2)$$

where E = Young's modulus of the pipe material, I = area moment of inertia of the pipe, v_1 , v_2 = displacement of pipeline at

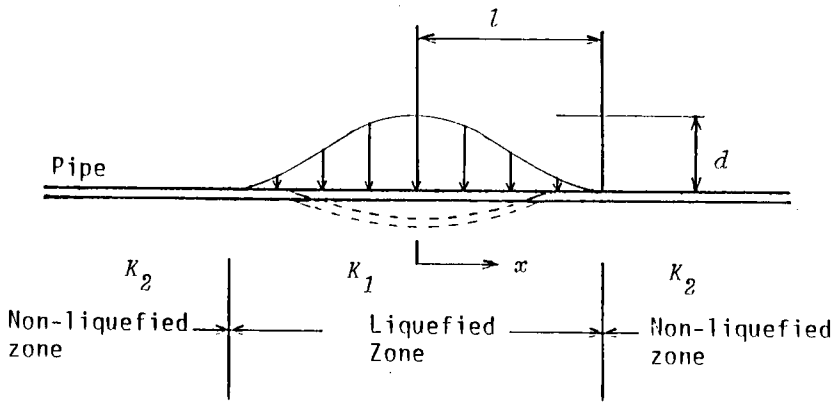

Fig. 6.7 Analytical model (Plane figure).

each zone, K_{v1}, K_{v2} = equivalent soil spring constants for deformed ground and non-deformed ground, which depend on the degree of liquefaction of the soil. d = the maximum magnitude of the permanent ground displacement and l = half of extent of the permanent ground displacement along the pipeline, that is, $2l = W$ Boundary conditions are given as follows:

$$\frac{dv_1}{dx} = 0, \quad \frac{d^3v_1}{dx^3} = 0 \qquad (x = 0) \tag{6.3}$$

$$v_1 = v_2, \quad \frac{dv_1}{dx} = \frac{dv_2}{dx}, \quad \frac{d^2v_1}{dx^2} = \frac{d^2v_2}{dx^2}, \quad \frac{d^3v_1}{dx^3} = \frac{d^3v_2}{dx^3} \qquad (x = l) \tag{6.4}$$

$$v_2, = 0, \quad \frac{dv_2}{dx} = 0 \qquad (x \to \infty) \tag{6.5}$$

Solving the equations by use of the boundary conditions, displacements of the pipe are obtained as follows:

$$v_1(x) = \exp(\beta_1 x)(A_1 \cos \beta_1 x + A_2 \sin \beta_1 x) + \exp(-\beta_1 x)(A_3 \cos \beta_1 x + A_4 \sin \beta_1 x) + v_0 \qquad (0 < x < l) \tag{6.6}$$

$$v_2(x) = \exp(-\beta_2 x)(A_5 \cos \beta_2 x + A_6 \sin \beta_2 x) \qquad (x > l) \tag{6.7}$$

In these equations, v_0 and A_1 - A_6, which are integral constants, are presented in Appendix 6.1, $\beta_1{}^4 = K_1/(4EI)$ and $\beta_2{}^4 = K_2/(4EI)$.

6.3.2 Practical Application of Mathematical Models to Existing Pipelines

Fig. 6.8 shows the relationship between the maximum bending pipe stress and width of the liquefied zone as shown in Fig. 6.7. The maximum magnitude of the permanent ground displacement is 1 m in this case. The pipelines used in this analysis are continuous steel pipelines identical to those used in Chapter 5 and whose dimensions are listed in Table 5.1. It can be seen from this figure that the smaller the

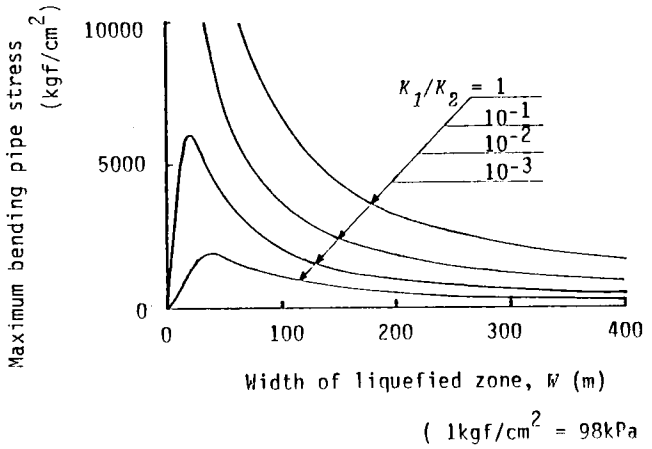

Fig. 6.8 Relationship between width of liquefied zone and maximum bending pipe stress.

ratio of the equivalent spring constant, K_1/K_2 becomes, in other words, the higher the degree of liquefaction, the smaller the maximum bending pipe stress. It can be explained in terms of decrease in the force due to ground deformation acting on the pipelines and the slippage between the pipelines and the liquefied ground. The maximum bending stress for K_1/K_2 =1.0 becomes greater than the allowable bending stress of the steel pipeline, (4200 kgf/cm2 (411.6 MPa)) at a width of the liquefied ground less than about 150 m except for the region near to 0 m of the width in this example; therefore the probability of pipe failure is markedly high in cases of greater ratio of the equivalent soil spring constant. It is also interesting to note that the response of pipelines did not vary remarkably in case of greater than 300 m width of liquefied ground. These findings suggest that the response of pipelines subjected to permanent ground displacement is very sensitive to the equivalent soil spring constant. Although some experimental results are revealed as mentioned at the end of Chapter 4.4, accumulation of experimental data under various conditions is

inevitable before these values are used in the earthquake resistant design. Therefore, the equivalent soil spring constant is regarded as a variable in the present study.

6.4 Simulation of Pipelines' Response Due to Permanent Ground Displacement Induced by Soil Liquefaction

6.4.1 A Procedure of Analysis

This chapter deals with the response of a jointed pipeline subjected to permanent ground displacement. The pipelines used in the analysis were ductile pipelines, whose dimensions are shown in Table 6.2. A modified transfer matrix method mentioned in Chapter 4.3 was also used in this chapter. The differences between the mathematical analysis shown in Chapter 6.3 and the simulation in this chapter are not only the type of pipelines but also the characteristics of equivalent soil spring constants, that is, linear model in Chapter 6.3 and bi-linear model in the present chapter. The bi-linear model was base on reference 19. The model of the permanent ground displacement is the same as that presented in Chapter 6.3. The method described in this chapter is, of course, available for a continuous pipelines and tendency of the results obtained from simulations was similar to that in the preliminary mathematical analyses. Therefore, the only response of a jointed pipeline is discussed in this chapter.

Table 6.2 Dimensions of ductile cast iron pipeline.

Outer diameter	(mm)	425.6
Thickness	(mm)	8.5
Young's modulus	(kgf/cm^2)	1.6×10^6
Specific gravity		7.15

(1 kgf/cm^2 = 98 kPa)

6.4.2 Practical Application of Simulation Models to Existing Pipelines

Figs. 6.9 and 6.10 show the results of the response simulations. These figures display the relationship between the maximum displacement angle at a joint and the width of the liquefied zone as shown in Fig. 6.7. Fig. 6.9 expresses the results for the non-liquefied superficial layer deformation, that is, $K_1/K_2 = 1.0$. It can be seen from Fig. 6.9 that the maximum displacement angle at a joint increases with a decrease in the width of the deformed ground. This tendency is identical to the results obtained in Chapter 6.3. Since the allowable value for displacement angle at a joint is 7°, failure at a joint can be caused by greater than 3 m permanent ground displacement in an area less than 80 m. Pipe failure could also be caused by permanent ground displacement less than 1 m in an area less than 20 m. Fig. 6.10 shows the results for 10^{-3} of the ratio of the equivalent soil spring constants, K_1/K_2. The maximum displacement angle at joints is smaller than that in Fig. 6.9, however, the tendency of lesser pipe response with increasing width of deformed ground is similar.

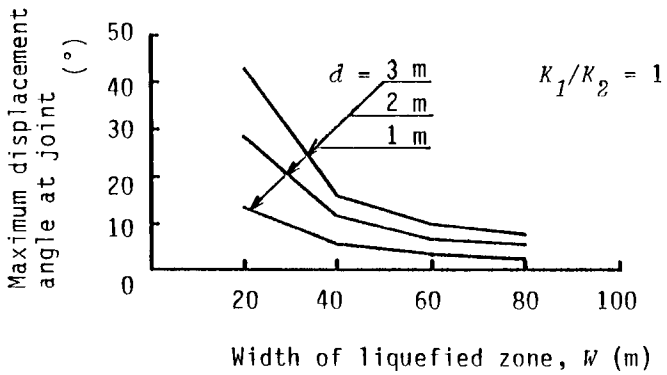

Fig. 6.9 Relationship between width of liquefied zone and maximum displacement angle at joint ($K_1 / k_2 = 1$).

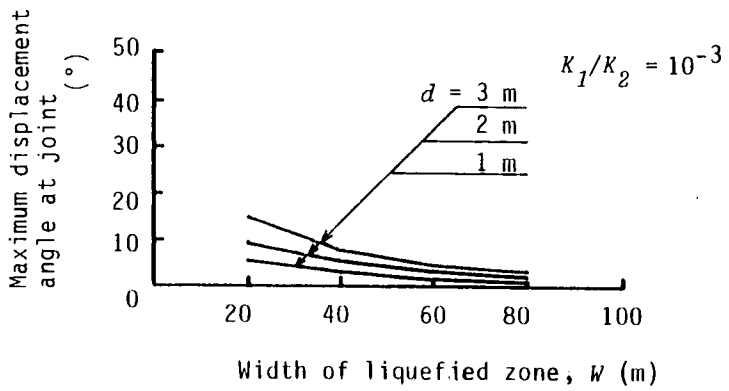

Fig. 6.10 Relationship between width of liquefied zone and maximum displacement angle at joint ($K_1 / k_2 = 10^{-3}$).

Figs. 6.11 and 6.12 express the relationship between the maximum displacement angle at joints and the ratio of equivalent soil spring constant. Fig. 6.11 shows the response of pipelines in case of 1 m of the maximum magnitude of the permanent ground displacement and Fig. 6.12 reflects that in case of 40 m of width of deformed ground. It can be seen from these figures that the maximum displacement angle at a joint decreases with a decrease in the ratio of equivalent soil spring constant, that is, an increase of the degree of liquefaction. As shown in Chapter 6.2, permanent ground displacement in the liquefied ground is greater than that in the non-liquefied ground as shown in Fig. 6.1. This suggests that the greater the degree of liquefaction is, the greater the magnitude of the permanent ground displacement. For example, when the permanent ground displacement of 8 m, which was observed in Niigata City, occurs at the liquefied ground with 80 m width and 10^{-3} of the ratio of the equivalent soil spring constant, the maximum displacement angle at joint becomes 15.1°. Therefore, the failure of pipes at joints could occur with even a relatively small ratio of equivalent soil spring constant, that is, great degree of liquefaction.

Fig. 6.13 reflects the ratio of bending stress to the maximum bending stress of the pipelines at the center of liquefied ground and at

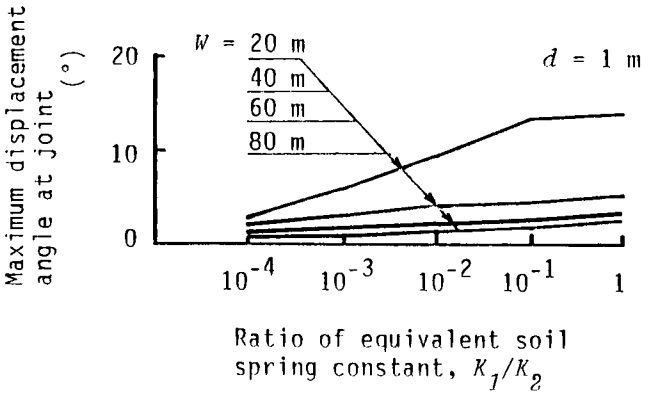

Fig. 6.11 Relationship between ratio of equivalent soil spring constant and maximum displacement angle at joint (d = 1 m).

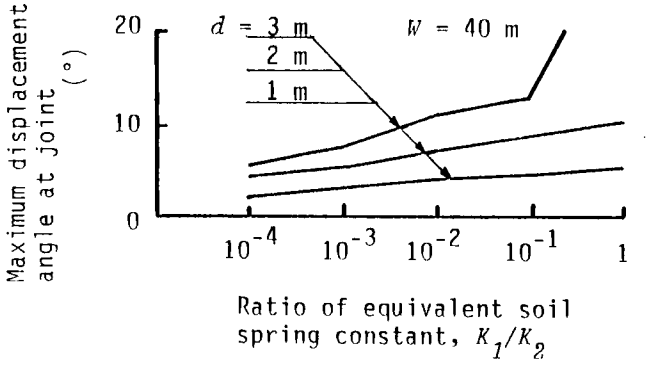

Fig. 6.12 Relationship between ratio of equivalent soil spring constant and maximum displacement angle at joint (W = 40 m).

the boundary between liquefied and non-liquefied ground, respectively. According to this figure, the maximum bending stress occurs at the center of deformed ground in case of high ratio of the equivalent soil spring constant, however, it appears at the boundary between the liquefied and non-liquefied areas in case of low ratio. This is also an interesting point.

The above results obtained by the response simulation seem to show that the probability of failure at joints is high for relatively

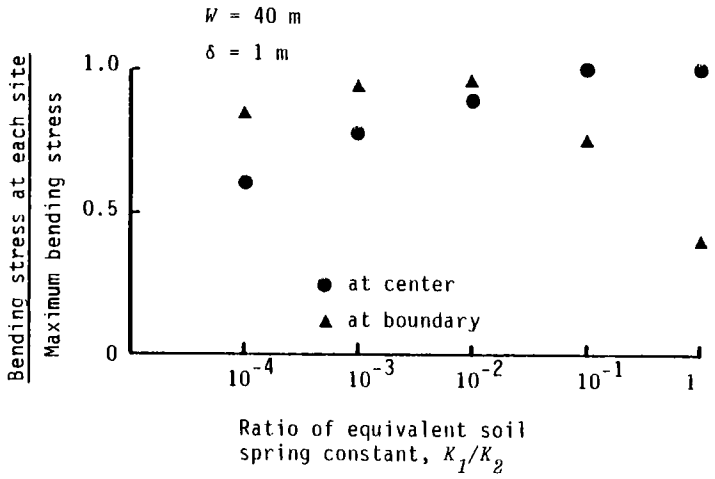

Fig. 6.13 Relationship between ratio of equivalent soil spring constant and ratio of bending stress to maximum bending stress.

narrow width of deformed non-liquefied superficial layer above the liquefied ground. Although we evaluate the response of pipelines subjected to permanent ground deformation, we do not take into consideration the relationship between the magnitude of the maximum ground displacement and the width of deformed ground in these examples. Since the experimental results obtained in Chapter 6.2 suggest that the width of deformed ground is one of the influential factors for the magnitude of the permanent ground displacement, it is crucial point to clarify this relationship between the magnitude of the permanent ground displacement, the degree of liquefaction and the width of deformed ground quantitatively in the future.

6.5 Conclusions

Through the experiments, mathematical analyses and response simulations, the following conclusions have been derived:

(1) From the data of the 1983 Nihonkai-Chubu Earthquake, permanent ground displacement in the liquefied areas are greater than that in the non-liquefied areas.

(2) The shape of the distribution of the permanent ground displacement perpendicular to the slope of ground can be assumed to be a sinusoidal curve in the model experiments. The relationship between the maximum ground displacement and width of the permanent ground displacement is indicated based on the experimental results. The findings suggest that the width of the liquefied area is one of the most influential factors determining the magnitude of the ground displacements.

(3) Formulae for pipeline response due to liquefaction-induced permanent ground displacement are proposed by using a beam theory. Application of the formulae reveals that the probability of failure is high for pipelines in areas with smaller width of the liquefied ground.

(4) The results of the response simulation for jointed pipelines suggest that the probability of failure at joints is high in areas where the deformed non-liquefied superficial layer above liquefied ground is with small width in case of the maximum permanent displacement exceed 1m.

(5) The relationship between the magnitude of permanent ground displacement, degree of liquefaction and width of deformed ground is one of the crucial points for evaluating the failure of pipelines subjected to permanent ground displacement.

(6) It is important to predict the liquefaction potential and generation of ground deformation in the extent smaller than 150 m for evaluating the pipelines' failure induced by permanent ground displacement.

Finally, we focused on only the response of the main distribution pipelines for water service with 400 mm nominal diameter to understand the response characteristics of the pipelines in this study, however, dimensionless parameters should be introduced to discuss the results quantitatively in the future analysis. Although the method for evaluation of pipeline response to permanent ground displacement induced by liquefaction was established in the present study, future study on the mechanisms of generation of permanent ground

displacement is needed in order to clarify the effects of permanent ground displacement on pipelines.

References (Publications written in Japanese are so indicated; all other are in English)

1) Hamada, M., Yasuda, S., Isoyama, R. and Emoto, K.: Observation of Permanent Ground Displacements Induced by Soil Liquefaction, Proceedings of Japan Soc. Civil Eng., No. 376, pp. 211-220, 1986 (in Japanese).
2) Hamada, M., Yasuda, S., Isoyama, R. and Emoto, K.: Study on Liquefaction-Induced Permanent Ground Displacements and Earthquake Damage, Proceedings of Japan Soc. Civil Eng., No. 376, pp. 221-229, 1986 (in Japanese).
3) Hamada, M.: Damage to Buried Pipes and Foundation Piles Due to Liquefaction-Induced Ground Displacement, Proceedings of the 1989 ASME Pressure Vessels and Piping Conference, PVP-Vol. 162, pp. 1-5, 1989.
4) Kitaura, M., Miyajima, M. and Nomura, Y.: Study on Behavior of Buried Pipelines Due to Lateral Spreading Induced by Soil Liquefaction, Journal of Structural Engineering, Japan Soc. Civil Eng., Vol. 33A, pp. 679-686, 1987 (in Japanese).
5) O'Rourke, T. D. and Tawfik, M. S.: Effects of Lateral Spreading on Buried Pipelines During the 1971 San Fernando Earthquake, Proceedings of 1983 International Symposium on Lifeline Earthquake Engineering, PVP-Vol. 77, ASME, pp. 124-132, 1983.
6) Yasuda, S., Tada, H., Fukusaki, S., Nakashima, R. and Yamamoto, Y.: Shaking Table Test of Liquefaction Induced Permanent Ground Displacement, Proceedings of the 22nd Japan National Conference on Soil Mech. and Found. Eng., pp. 731-734, 1987 (in Japanese).
7) Kobayashi, H., Yoshida, N. and Nakamura S.: Investigation of Damage to Pile Foundations During 1964 Niigata Earthquake, Proceedings of the 20th JSCE Earthquake Engineering Symposium-1989, pp. 21-24, 1989 (in Japanese).
8) Mori, S., Shimizu, K., Suzuki, N., Takagi, M. and Nakamura, S.: Damage to Pile Foundations Caused by Liquefaction-Induced Permanent Ground Displacement and Its Analysis, Proceedings of

the 20th JSCE Earthquake Engineering Symposium-1989, pp. 25-28, 1989 (in Japanese).
9) Kawashima, K., Sugita, H., Kano, N., Isoyama, R. and Taguchi, Y.: Relationship Between Damage to Sewerage and Permanent Ground Displacement -in Case of Noshiro City During 1983 Nipponkai-Chubu Earthquake- , Proceedings of the 20th JSCE Earthquake Engineering Symposium-1989, pp. 273-276, 1989 (in Japanese).
10) Kitaura, M. and Miyajima, M.: Effects of Lateral Spreading Due to Soil Liquefaction on Buried Pipelines, Journal of Structural Engineering, Japan Soc. Civil Eng., Vol. 32A, pp.857-864, 1986 (in Japanese).
11) Kitaura, M. and Miyajima, M.: Response of Buried Pipelines Due to Liquefaction-induced Lateral Spreading, Proceedings of the Pacific Conference on Earthquake Engineering, pp. 123-130,1987.
12) Miyajima, M., Kitaura, M. and Nomura, Y.: Characteristics of Permanent Ground Displacement Induced by Soil Liquefaction, Memoirs of the Faculty of Technology, Kanazawa Univ., Vol. 21, No. 1, pp. 1-10, 1988.
13) Miyajima, M., Kitaura, M. and Nomura, Y.: Study on Response of Buried Pipelines Subjected to Liquefaction-induced Permanent Ground Displacement, Proceedings of Japan Soc. Civil Eng., No. 404, pp. 163-172, 1989.
14) Seed, H. B. and Idriss, I. M.: Simplified Procedure for Evaluating Soil Liquefaction Potential, Proceedings of ASCE, Vol. 97, No. SM9, pp. 1249-1273, 1971.
15) Tatsuoka, F., Iwasaki, T., Tokida, K., Yasuda, S., Hirose, M., Imai, T. and Koh-no, M.: Standard Penetration Tests and Soil Liquefaction Potential Evaluation, Soils and Foundations, Japan Soc. Soil Mecha. Founda. Eng., Vol. 20, No. 4. pp. 95-111, 1980.
16) Seed, H. B., Idriss, I. M. and Arango, I.: Evaluation of Liquefaction Potential Using Field Performance Data, Proceedings of ASCE, Vol. 109, No. GE3, pp. 458-482, 1983.
17) Tokimatsu, K. and Yoshimi, Y.: Empirical Correlation of Soil Liquefaction Based on SPT N-value and fines content, Soils and Foundations, Japan Soc. Soil Mecha. Founda. Eng., Vol. 23, No. 4. pp. 56-74, 1983.

18) Shibata, T. and Teparaksa, W.: Evaluation of Liquefaction Potentials of Soils Using Cone Penetration Tests, Soils and Foundations, Japan Soc. Soil Mecha. Founda. Eng., Vol. 28, No. 2. pp. 49-60, 1988.
19) Japan Gas Association: Recommended Practice for Earthquake Resistant Design of Gas Pipelines, pp. 177-182, 1982 (in Japanese).

Appendix 6.1 Presentation of function v_o and integral constants

The function v_0 and integral constants A_1 - A_6 in chapter 6.3.1 are represented as follows.

$$v_0 = d - D_0 \sin \frac{\pi x}{2l}$$

$$A_1 = \frac{B_{17}C_1 - B_{18}C_2 + B_{19}C_3 - B_{20}C_4}{B_1C_1 - B_2C_2 + B_3C_3 - B_4C_4}$$

$$A_2 = \frac{-B_{17}C_5 + B_{18}C_6 - B_{19}C_7 + B_{20}C_8}{-B_5C_5 + B_6C_6 - B_7C_7 + B_8C_8}$$

$$A_3 = F_1 + A_1$$

$$A_4 = F_2 - A_2$$

$$A_5 = \frac{B_{17}C_9 - B_{18}C_{10} + B_{19}C_{11} - B_{20}C_{12}}{B_9C_9 - B_{10}C_{10} + B_{11}C_{11} - B_{12}C_{12}}$$

$$A_6 = \frac{-B_{17}C_{13} + B_{18}C_{14} - B_{19}C_{15} + B_{20}C_{16}}{-B_{13}C_{13} + B_{14}C_{14} - B_{15}C_{15} + B_{16}C_{16}}$$

$$F_1 = -\frac{\pi}{4\beta_1 l}\left\{1+\frac{1}{2\beta_1^2}\left(\frac{\pi}{2l}\right)^2\right\} D_0$$

$$F_2 = \frac{\pi}{4\beta_1 l}\left\{1-\frac{1}{2\beta_1^2}\left(\frac{\pi}{2l}\right)^2\right\} D_0$$

$$B_1 = \{ \exp(\beta_1 l) + \exp(-\beta_1 l)\} \cos \beta_1 l$$

$$B_2 = D_5 \{D_2 \exp(\beta_1 l) - D_1 \exp(-\beta_1 l)\}$$

$$B_3 = D_5{}^2\{- \exp(\beta_1 l) + \exp(-\beta_1 l)\} \sin \beta_1 l$$

$$B_4 = D_5{}^3\{- D_1 \exp(\beta_1 l) + D_2 \exp(-\beta_1 l)\}$$

$$B_5 = \{ \exp(\beta_1 l) - \exp(-\beta_1 l)\} \sin \beta_1 l$$

$$B_6 = D_5 \{D_1 \exp(\beta_1 l) - D_2 \exp(-\beta_1 l)\}$$

$$B_7 = D_5{}^2\{ \exp(\beta_1 l) + \exp(-\beta_1 l)\} \cos \beta_1 l$$

$$B_8 = D_5{}^3\{ D_2 \exp(\beta_1 l) - D_1 \exp(-\beta_1 l)\}$$
$$B_9 = - B_{15} =- \exp(-\beta_2 l) \cos \beta_2 l$$
$$B_{10} = - B_{16} =D_3 \exp(-\beta_2 l)$$
$$B_{11} = B_{13} =- \exp(-\beta_2 l) \sin \beta_2 l$$
$$B_{12} = B_{14} =- D_4 \exp(-\beta_2 l)$$
$$B_{17} = - \exp(-\beta_1 l) (F_1 \cos \beta_1 l + F_2 \sin \beta_1 l) - \frac{EI}{K_1} (\frac{\pi}{2l})^4 D_0$$
$$B_{18} = D_5 \exp(-\beta_1 l) (F_1 D_1 - F_2 D_2)$$
$$B_{19} = D_5{}^2 \exp(-\beta_1 l) (F_1 \sin \beta_1 l + F_2 \cos \beta_1 l) - \frac{1}{2}(\frac{\pi}{2l\beta_2})^2 D_0$$
$$B_{20} = - D_5{}^3 \exp(-\beta_1 l) (F_1 D_2 - F_2 D_1)$$

$$D_1 = \frac{d}{1 + \frac{EI}{K_1} (\frac{\pi}{2l})^4}$$
$$D_1 = \cos \beta_1 l + \sin \beta_1 l$$
$$D_2 = \cos \beta_1 l - \sin \beta_1 l$$
$$D_3 = \cos \beta_2 l + \sin \beta_2 l$$
$$D_4 = \cos \beta_2 l - \sin \beta_2 l$$
$$D_5 = \frac{\beta_1}{\beta_2}$$

$$C_1=B_6B_{11}B_{16}+B_{10}B_{15}B_8 +B_{14}B_{12}B_7 -B_{14}B_{11}B_8 -B_6B_{12}B_{15} -B_{10}B_7B_{16}$$
$$C_2 =B_5B_{11}B_{16} +B_9B_{15}B_8 +B_{13}B_{12}B_7 -B_{13}B_{11}B_8 -B_5B_{12}B_{15} -B_9B_7B_{16}$$
$$C_3 =B_5B_{10}B_{16} +B_9B_{14}B_8 +B_{13}B_{12}B_6 -B_{13}B_{10}B_8 -B_5B_{12}B_{14} -B_9B_6B_{16}$$
$$C_4 =B_5B_{10}B_{15} +B_9B_{14}B_7 +B_{13}B_{11}B_6 -B_{13}B_{10}B_7 -B_5B_{11}B_{14} -B_9B_6B_{15}$$
$$C_5=B_2B_{11}B_{16}+B_{10}B_{15}B_4 +B_{14}B_{12}B_3 -B_{14}B_{11}B_4 -B_{10}B_3B_{16} -B_2B_{12}B_{15}$$
$$C_6 =B_1B_{11}B_{16} +B_9B_{15}B_4 +B_{13}B_{12}B_3 -B_{13}B_{11}B_4 -B_9B_3B_{16} -B_1B_{12}B_{15}$$
$$C_7 =B_1B_{10}B_{16} +B_9B_{14}B_4 +B_{13}B_{12}B_2 -B_{13}B_{10}B_4 -B_9B_2B_{16} -B_1B_{12}B_{14}$$
$$C_8 =B_1B_{10}B_{15} +B_9B_{14}B_3 +B_{13}B_{11}B_2 -B_{13}B_{10}B_3 -B_9B_2B_{15} -B_1B_{11}B_{14}$$
$$C_9 =B_2B_7B_{16} +B_6B_{15}B_4 +B_{14}B_8B_3 -B_{14}B_7B_4 -B_2B_8B_{15} -B_6B_3B_{16}$$
$$C_{10} =B_1B_7B_{16} +B_5B_{15}B_4 +B_{13}B_8B_3 -B_{13}B_7B_4 -B_1B_8B_{15} -B_5B_3B_{16}$$
$$C_{11} =B_1B_6B_{16} +B_5B_{14}B_4 +B_{13}B_8B_2 -B_{13}B_6B_4 -B_1B_8B_{14} -B_5B_2B_{16}$$
$$C_{12} =B_1B_6B_{15} +B_5B_{14}B_3 +B_{13}B_7B_2 -B_{13}B_6B_3 -B_1B_7B_{14} -B_5B_2B_{15}$$

$$C_{13} = B_2B_7B_{12} + B_{10}B_8B_3 + B_6B_{11}B_4 - B_{10}B_7B_4 - B_2B_8B_{11} - B_6B_3B_{12}$$
$$C_{14} = B_1B_7B_{12} + B_9B_8B_3 + B_5B_{11}B_4 - B_9B_7B_4 - B_1B_8B_{11} - B_5B_3B_{12}$$
$$C_{15} = B_1B_6B_{12} + B_9B_8B_2 + B_5B_{10}B_4 - B_9B_6B_4 - B_1B_8B_{10} - B_5B_2B_{12}$$
$$C_{16} = B_1B_6B_{11} + B_9B_7B_2 + B_5B_{10}B_3 - B_9B_6B_3 - B_1B_7B_{10} - B_5B_2B_{11}$$

7. CONCLUDING REMARKS

This dissertation has presented effective methods to analyze the response of pipelines subjected to soil liquefaction. In this study, mathematical methods and simulations have been applied to existing pipelines and ground and some aspects of damage to water supply pipelines due to soil liquefaction have been discussed. The main results have been briefly summarized and recommendations given for earthquake-resistant design of water pipeline systems, along with proposals for future studies.

In Chapter 1, the general scope of this dissertation, and a review of past studies on seismic response of pipelines were presented.

In Chapter 2, statistical analysis was conducted using actual earthquake damage to water supply pipelines in order to clarify failure modes of buried pipelines. According to earthquake damage caused by the 1964 Niigata Earthquake and the 1983 Nihonkai-Chubu Earthquake, markedly high damage ratios to pipes with a large diameter of 400 mm and 450 mm were presented. It was noted that these pipes were located at liquefied sites near the boundary between the liquefied and non-liquefied sites. This fact was investigated in detail in Chapter 5 as mentioned below. The results of multivariate analysis revealed that liquefaction was the most influential factor leading to the pipe damage. Although the multiple correlation coefficients obtained by the analyses were too low to establish an equation for prediction of earthquake damage to pipelines, the results suggested that liquefaction was more significant in evaluating pipe damage than such ground characteristics as SPT blow count, ground water table, etc. Furthermore, it was pointed out that permanent ground deformation induced by liquefaction was one of the most serious liquefaction hazards. This was studied in Chapter 6 described below. In establishing an equation for prediction of earthquake damage to pipelines using actual earthquake damage data, it is necessary to accumulate more detailed data of earthquake damage to pipelines and ground conditions.

In Chapter 3, vibration tests using model pipes were conducted to identify the characteristics of pipe behavior during liquefaction processes. Pipe strains should be classified according to the mechanism of generation: i.e. vibration strains which indicate pipe vibration, and accumulated residual strains which indicate pipe bending due to uplift. Mode of pipe failure induced by the former is different from the latter. A conceptual model of the generation factors of vibration strains was proposed. This model includes not only the resonance of the system exerted by an external exciting force, but also the degree of transmission of the input waves through the model ground, the degree of transmission of ground strain to the pipe, and flexibility of the entire system. Under the assumption that the degree of vibration strain during liquefaction could be obtained as the product of these factors, the experimental results in Chapter 3 can be well accounted for.

In Chapter 4, a hybrid procedure was proposed to analyze the behavior of buried pipelines during the liquefaction process. This procedure consists of a ground response evaluation using the finite element method and a pipe response analysis using the transfer matrix method. These methods can properly evaluate the rise of the ground water table due to liquefaction. The response of the pipelines can also be investigated when the unsaturated sand layer around the pipelines liquefies, by considering the rise of the ground water table and subsequent accumulation of excess pore water pressure. The application of this method to existing pipelines and ground revealed that the response characteristics of buried pipelines change during liquefaction processes; when the excess pore water pressure is low, the effect of the ground motion on the pipelines is predominant and the higher the excess pore water pressure, the greater the buoyancy effect.

In Chapter 5, characteristics of the failures of pipelines through a boundary between liquefied and non-liquefied sites were focused on. Two vibration tests were conducted; one was an experiment using a model, simulating a pipeline connected to a building and the other used a model pipeline located through both liquefiable and non-liquefiable sandy grounds. The experimental results indicated that both accumulated residual and vibration strains concentrated near the fixed end and at the boundary between liquefied and non-liquefied ground. The accumulated residual strains were much greater than the vibration

strains in these experiments. Furthermore formulae for pipeline response due to buoyancy effects, subsidence and seismic motion in the liquefied ground, which were different from that of the neighboring ground, were presented and mathematical analyses for existing pipelines and ground were conducted.

In Chapter 6, liquefaction-induced permanent ground displacement and subsequent failure of pipelines were dealt with. Characteristics of permanent ground displacement were investigated based on actual earthquake damage data and model experiments. From the data of the 1983 Nihonkai-Chubu Earthquake, it was found that permanent ground displacement in the liquefied areas was greater than that in the non-liquefied ground. The experimental results revealed that the shape of the distribution of the permanent ground displacement was assumed to be a sinusoidal curve. The results also suggested that the width of permanent ground displacement along pipelines was one of the most influential factors determining the magnitude of the permanent ground displacement. Formulae for pipeline response due to permanent ground displacement were proposed and mathematical analyses using these formulae were conducted. The results shows that the probability of failure was high for pipelines located in area of 150 m or less of the deformed ground were obtained by the mathematical analyses. Based on the results of the mathematical analyses, a simulated response of jointed pipelines was accomplished. It was clarified that the probability of failure at joints was great as non-liquefied superficial layer above liquefied ground deformed with in area of 100 m or less.

Design formulae for pipelines subjected to liquefaction were proposed and results obtained from the model experiments, mathematical analyses and response simulation for pipelines were given. Nevertheless, there still exists certain unsolved problems before earthquake resistant systems can be designed. First, forces acting on pipelines during liquefaction processes, namely, the magnitude of subsidence and permanent ground displacement, and equivalent soil spring constants, should be estimated more quantitatively because pipeline responses are very sensitive to the magnitude of such forces. Secondly, since the effects of liquefaction on pipelines are crucial, countermeasures for not only pipelines themselves but also the adjacent ground are indispensable. Economic aspects of the countermeasures

may be also important because of the extensive length of pipelines. Finally, methods must be sought for predicting the extent of liquefiable areas induced by earthquakes. Although the present aseismic design codes for lifelines describe methods for evaluating the liquefaction potential at a given site, it is necessary that the liquefaction potential in area of 100 m or less along pipelines be evaluated in order that effective countermeasures can be taken.